SYNTHESIS AND CHARACTERIZATION OF ANTIMONY CYANOXIMATES FOR MICROBIOLOGICAL STUDIES

A Master's Thesis

Presented to

The Graduate College of

Missouri State University

In Partial Fulfillment

Of the Requirements for the Degree

Master of Science, Chemistry

By

Seth Adu Amankrah

May 2022

SYNTHESIS AND CHARACTERIZATION OF ANTIMONY CYANOXIMATES FOR MICROBIOLOGICAL STUDIES

Chemistry

Missouri State University, May 2022

Master of Science

Seth Adu Amankrah

ABSTRACT

Antibiotic-resistant pathogenic microorganisms (such as MRSA and alike) represent a real and significant threat to the health and wellbeing of the general population. The search for new compounds of non-antibiotic nature that act as antimicrobial agents is an important task with obvious practical applications in the biomedical field. Metal-based coordination and organometallic compounds that demonstrate antimicrobial activity was found to exhibit a completely different mode of action compared to antibiotics. That suggests the absence of the mechanism of developing tolerance to these types of compounds at least for 30 - 40 years. Thus, there are numerous organotin (IV), silver (I), copper (II) and arsenic (III) compounds that have been extensively studied with that goal in the past. However, most of them are toxic to biological species. On the contrary, organoantimony (III, V) compounds possess much lower general toxicity but demonstrate appreciable antimicrobial properties and better body clearance. Unfortunately, there is still an insufficient amount of information regarding the latter class of compounds. Our research group's previous experience clearly identified cyanoximes – compounds with the general formula NC-C(=NOH)-R, with R being an electron-withdrawing group – as potent biologically active compounds. These small molecules also act as very good ligands binding a variety of metal ions and metalloids with many compounds showing a good potential for biomedical applications. Except for one publication in 2000, there are no investigations of any kind of Sb-based compounds with oxime-bearing ligands. Therefore, the goal of the proposed research is to synthesize and characterize a series of antimony complexes with some specifically selected biologically active cyanoximes structures. All the synthesized novel compounds were characterized by elemental analysis (C,H,N), IR & NMR spectroscopy, thermal analysis (TG/DSC), and x-ray crystallography. The biological activity of the synthesized compounds was tested against bacterial strains MRSA, PAO1, and *E. coli.* Optical density (OD) was used to measure microbial cell growth, at a wavelength of 600 nm (OD600).

KEYWORDS: cyanoximates, MRSA, biologically active, organoantimony, cytotoxicity, toxicity, antimicrobial activity, cell growth, thermal analysis, diastereomers.

SYNTHESIS AND CHARACTERIZATION OF ANTIMONY CYANOXIMATES FOR MICROBIOLOGICAL STUDIES

By

Seth Adu Amankrah

Master of Science, Chemistry

A Master's Thesis
Submitted to the Graduate College
Of Missouri State University
In Partial Fulfillment of the Requirements
For the Degree of Master of Science, Chemistry

May 2022

Approved:

Nikolay N. Gerasimchuk, Ph.D., Thesis Committee Chair

Reza Sedaghat-Herati, Ph.D., Committee Member

Keiichi Yoshimatsu, Ph.D., Committee Member

Marianna Patrauchan, Ph.D., Committee Member

Julie Masterson, Ph.D., Dean of the Graduate College

ACKNOWLEDGEMENTS

I would like to thank the following people for their support during my graduate studies.

1. My research advisor Dr. Nikolay N. Gerasimchuk. I cannot express enough gratitude for his patience and eagerness to teach me how to be a chemist.

2. Professor Olexander Hietsoi, Murfreesboro, Department of Chemistry, Middle Tennessee State University, for helping with X-ray work (data collection when our instrument stopped working.)

3. Dr. Sergiy Tyukhtenko, Northeastern University, Boston, for ^{1}H, ^{13}C NMR spectra studies.

4. Mr. Kevin Pinks, my former lab partner and the first student to start the Sb- Chemistry project.

5. Prof. Marianna Patrauchan, Oklahoma State University, Oklahoma, for being our microbiological consultant on this project and performing biological activity tests on our compounds.

6. Prof. Karen Wozniak, Oklahoma State University, Oklahoma, for being our microbiological consultant on this project and performing biological activity tests on our compounds.

7. Ms. Tarosha Salpadoru, Oklahoma State University, Oklahoma, for biological activity tests performed on my synthesized compounds.

I dedicate this thesis to Mr. Daniel Adu Amankrah and Mrs. Veronica Asantewaa for their unwavering support and prayers to get me through my graduate education. To my wife, Abigail, a huge thank you for the constant push to do my best and for being my support system. Finally, to the many friends made, thank you for making this experience enjoyable and worthwhile.

TABLE OF CONTENTS

LIST OF TABLES

LIST OF FIGURES

I. INTRODUCTION

I. 1. Antimicrobials

Antimicrobial compounds are one of the most important drugs in modern medicine because they are used to treat numerous infections. There is a distinction between antibiotics and antimicrobials: Antibiotics have an effect only on bacteria, while antimicrobial reagents affect all microorganisms including bacteria, fungi, and viruses. Antimicrobials have a very large impact on the treatment of infectious diseases amongst other classes of drugs used in medicine. Although most of our exposure to antimicrobials is attributed to the 1900s with the emergence of the modern era of antibiotics, traces of tetracycline – an antibiotic – found in the human skeletal remains from ancient Sudanese Nubia dating back to 305-550 CE suggest that some were already in use.[1] Paul Ehrlich is known widely as the father of antimicrobial chemotherapy and bioinorganic chemistry because with the help of his Japanese assistant Sahachiro Hata, they were able to find the "magic bullet" (compound 606) capable of treating infectious microbes without also killing the host.[2] This compound is an arsenic-based chemical ($C_{12}H_{13}As_2ClN_2O_2$), was used to successfully treat syphilis and was later marketed as Salvarsan, meaning "Lifesaving". Ehrlich designed methods in search of this effective compound, and such strategy is currently still being used.[1]

The accidental discovery of Penicillin in 1928 by Alexander Fleming is the first of many natural antibiotics found by scientists. Penicillin was monumental around the time of its discovery as it was effective against streptococci, meningococci, and *Corynebacterium diphtheriae*, the causative agent of diphtheria.[3,4,5] Thus, increasing the life expectancy and reducing the mortality rate. A few years later, German scientists Josef Klarer, Fritz Mietzsch, and Gerhard Domagk discovered antibacterial activity of a synthetic dye, prontosil which is a

sulfanilamide drug. Sulfanilamide became the first synthetic antimicrobial drug created and its success led to the synthesis of a wide variety of other synthetic antimicrobials like quinolines that do not occur in nature.[5] Antibacterial drugs can either work by killing off the bacteria (bactericidal) or reversibly inhibiting the growth of the bacteria (bacteriostatic). These drugs can also be narrow-spectrum or broad-spectrum substances. Narrow-spectrum ones have specific antimicrobial targets that they affect like only gram-positive bacteria, or gram-negative bacteria while broad-spectrum drugs have a wide range of target, attacking microbes with no respect to their value to the body.[6] That is one of the issues with broad-spectrum antimicrobials as they also attack normal healthy microbiota within the body that keeps some harmful microorganisms in check. This increases the possibility of antimicrobial resistance to antimicrobial drugs.[7]

I. 2. Antimicrobial Resistance

Antimicrobial resistance (AMR) occurs when microorganisms are not affected anymore by the drugs designed to kill or arrest their growth. This is one of the greatest global public health challenges we are currently facing. According to the Center for Disease Control and Prevention's (CDC) report on antibiotic/antimicrobial resistance conducted in 2019, annually, there are more than 2.8 million antibiotic-resistant (AR) infectious cases of which more than 35,000 people die.[8, 72] Aside that, the economic impacts due to treating these infections as well as from the loss of productivity is astronomical – about $4.6 billion annually.[9] With modern medicine's reliance on antimicrobials especially antibiotics in treating diseases such as pneumonia, tuberculosis, sexually transmitted diseases. The problem with AR/AMR is that we will have no effective treatment soon. The world is headed toward a very dangerous place where minor infections could once again be detrimental. Various organizations like the World Health

Organization (WHO), CDC and World Economic Forum have shown great concern and deemed antibiotic resistance as a "global public health concern".[10]

I. 3. Causes of Antimicrobial Resistance

An overuse of antibiotics is one of the paramount reasons for the rapid evolution of resistance within bacteria. Other causes include inappropriate prescribing which goes hand in hand with the inability of patients to follow through with the full dose of the drug. Extensive use of antibiotics in agricultural settings, as well as wide availability of few antibiotics are also important factors causing the rapid increase in resistance to various antibiotics by bacteria.[4] Therefore, we now have a multiple-drug resistance (MDR) phenomenon.[11] This situation led to the appearance of antibiotic resistant bacterial infections such as Methicillin-Resistant *Staphylococcus Aureus* (MRSA), and Vancomycin-Resistant Enterococci (VRE) which are increasingly becoming difficult to treat with the current range of available antibiotics.[10, 11] Resistance can come by natural process, which is intrinsically present and always expressed in the species or induced. That is when the resistance is present but expressed only when exposed to antibiotics. Also, it can be acquired through transformation, transduction, or conjugation.[14] All the aforementioned factors are selection pressures that fuel the rapid evolution of drug resistance that would not have happened naturally that fast. Once the genes encoding antibiotic resistance arises through various mutations in bacteria, they are exchanged among other bacteria. With gene transfer through transformation, pieces of DNA are taken from the environment and incorporated into the genome of the bacterium. With gene transfer through transduction, bacteriophages containing the favorable AMR genes are used to infect other bacteria and with conjugation, transfer of genes is done through mating with other bacteria.[10,12]

I. 4. Mechanism of Antimicrobial Drug Resistance

Antimicrobial drug resistant genes acquired by microbes can work by either modifying or inactivating the drug, preventing cellular uptake, or increasing efflux pumps, drug target site modifications and enzymatic bypass.[10, 13]

Drug Modification or Inactivation. With this mechanism, the genes acquired by the microorganism encode for enzymes that can modify the antimicrobial compound making it ineffective against their drug targets. These enzymes can transfer a chemical group onto the drug which makes it usable for metabolism. Another mode of action is the degradation of the drug by breaking down bonds within the drug molecule. This is seen in the activity of β-lactamases hydrolyzing β-lactam bond within the β-lactam ring of drug molecules and inactivating them or in the acetylation, phosphorylation and adenylation of aminoglycosides as a form of resistance against these drugs.[1,13,14]

Increase of Efflux Pumps or Prevention of Cellular Drug Uptake. Naturally, the composition of the bacterial cell wall makes it difficult of certain antimicrobials to penetrate and affect the bacteria. This intrinsically provides resistance to bacteria that lack a cell wall against drugs that target the cell wall.[14] Some antimicrobial compounds are hydrophilic and larger in size and, hence, need bigger porins to enter the cell. The mechanism here involves the modification of the selectivity of these porins to prevent the uptake of these antimicrobials or reducing the number of porins present within the cell walls and therefore increasing the resistance towards those antimicrobials.[13,14] An example is the carbapenem resistance in *Pseudomonas aeruginosa* where the abundance of OprD porin, the main entry point of carbapenems, is decreased on the outer membrane of the microbe.[13] Another way to increase resistance is through the increase in the abundance of efflux pumps that actively pump out the antimicrobial out of the cell, preventing it from ever reaching the threshold dose required for an effect. This can be achieved

through the overexpression of genes encoding these transporters under certain environmental stimuli such as the presence of antimicrobial compounds.[14] The presence of biofilms also increased the expression of genes required for resistance. These genes can then be shared by cell conjugation among the bacteria community[14] and allows for cross-resistance against other antimicrobials.

Drug Target Site Modification. Bacteria have a variety of target sites that antimicrobials target and so the modification of these sites can render the antimicrobial ineffective when administered. Some target sites where mutations were observed include metabolic enzymes, DNA gyrases or topoisomerases, ribosomal subunits, lipopolysaccharide (LPS) structures and peptidoglycan subunit peptide chains.[13,14] *Streptococcus pneumoniae* alters the penicillin-binding-proteins' (PBPs) active site (competitive binding) to prevent the binding of β-lactam drugs, making it resistant to those drugs.[13] *Staphylococcus aureus,* widely known for its resistance to methicillin, developed this through the acquisition of *mecA* gene responsible for changing the structure of PBP2a and decreasing its affinity for PBPs and in effect inhibiting drug binding.[13,14] This provides resistance against β-lactam drugs as seen with Methicillin-resistant Staphylococcus aureus (MRSA).

I. 5. Strategies for Discovery of New Antimicrobial Drugs

With the rampant global issue of AMR showing no signs of slowing down, there is a need for some novelty to the drugs or targets they affect in bacteria. Pharmaceutical companies are steering clear of research into antimicrobials[15] because they do not get high returns on such investments compared to development of drugs for most chronic, life-threatening non-infectious diseases such as hypertension. Additionally, approval times by the Food and Drug Administration (FDA) board is about 6.2 years, making it difficult to for researchers to work on

novel antimicrobials. Such problems could be remedied with the provision incentives to pharmaceutical companies to encourage more research into antimicrobials. Strategies that have been tried to remedy the issue of AMR include improvement of currently used antimicrobials, or preventing and reducing dependence on antimicrobial[1] because bacteria will develop resistance naturally against antibiotics, but it is the rampant use of antibiotics that is ushering in the spread of AMR across the globe.

With MDR microorganisms, synthetic antimicrobials may be the way out as specific drugs can be synthesized to affect specific drug target sites. Elementorganic compounds like organoarsenic and organotin have a great history in the search for antibiotics to treat various diseases.[1] While there is a plethora of information on arsenic, other inorganic compounds may offer antimicrobial properties that have not yet been explored. Coordination compounds of silver (I),[16] mercury (I),[17] copper (II)[18] and zinc (II)[19] have been studied and shown that only the silver (I) complexes possess antimicrobial properties.[71] Henceforth, they have been used in colloidal solutions for topical applications, coatings for various implants and as fabric for wound treatment.[20 - 22] With addition of a variety of organometallic complexes to research, the possibility of finding novel antimicrobials is practically endless.

I. 6. Element of Choice: Antimony

Antimony is in the main Group 15 (pnictogens) in the periodic table along with Nitrogen, Phosphorus, Arsenic and Bismuth. Antimony has atomic number 51, atomic weight 121.760 g/mol with melting point (m.p.) and boiling point (b.p.) of 630.63 °C and of 1,587 °C respectively.[30] The pnictogens display varying properties despite being in the same group. Nitrogen and Phosphorus are non-metals, Arsenic and Antimony are metalloids, and Bismuth demonstrates metallic properties. Antimony comes from the Greek words anti and monos,

meaning “enemy of solitude”, but its symbol (Sb) is derived from its Latin name, stibium.[68] Antimony has four oxidation states: -3, 0, +3 and +5, with the most common oxidation states being +3 and +5 because of their stability. The H_3SbO_3 and H_3SbO_4 are acids corresponding to those oxidation states. Sb is a poor conductor of heat and electricity.[23, 30] Stibine (SbH_3) is a gaseous antimony compound with an oxidation state of -3, and forms in reaction of acids on metal Zn/Sb alloys through the reduction of antimony. Stibine is toxic and poses a danger since it can be released when some lead batteries are overcharged because Pb is used in alloys with Antimony.[24]

I. 7. Uses of Antimony

Antimony’s use can be dated back to the early Egyptians. It has been used as coatings for other metals, or for cosmetic purposes – even as an eyeliner.[25] Other uses of antimony are in flame retardants, in semi-conductor devices, and in alloys for batteries and bullets.[26] In the modern era, the biological aspect of antimony has been explored and applied. Main group compounds like Arsenic and Bismuth in group 5 have wide pharmacological applications like salvarsan being used back in the day for treating syphilis. Bismuth subsalicylate being the active ingredient in Pepto-Bismol, is a very important drug of choice in many households for most digestive issues like indigestion, heartburn, and diarrhoea.[27, 69] Antimony derivatives or organoantimony compounds have been used to treat diseases such as trypanosomiasis and leishmaniasis because they exhibit appreciable effect as biocides, fungicides, antitumor and antioxidants. [28]

Medicinal uses. Antimony compound, $NaSbO_3$ - meta antimonate, has been used as an emetic up until the late 1700s. A compound with tartaric acid and Sb (III), was used as a

treatment drug for leishmaniasis, but had numerous side effects such as coughs and depression and even death due to its high toxicity.[29] One of the successful uses of antimony is in the treatment of Leishmaniasis. Leishmaniasis is caused by a protozoan parasite of genus *Leishmania*, transmitted through the bite of infected sandflies. This results in either cutaneous leishmaniasis (CL) or visceral leishmaniasis (VL), with the latter being most severe.[29] The spread of Leishmaniasis in South and Central America, Bangladesh, southern Europe, and North Africa led to the reliance on organoantimonial compounds for drug therapy. Antimonials contain this element in trivalent and pentavalent forms. Trivalent antimonials (those having Sb (III)) effectively killed parasitic cells, but unfortunately, eventually killed the human host too. This fact initiated the discovery of pentavalent antimonials, which are less toxic than their trivalent counterparts. Pentavalent antimonials (having Sb(V)) such as sodium antimony gluconate (Pentostam)[31] and meglumine antimonate (Glucantime)[32] have been in use for more than six decades to treat Leishmaniasis and Indian kala-azar disease.[29, 70] Additionally, organoantimony compounds have been studied to show antimicrobial, antifungal, and antitumor activity.[33-38, 70] The latter was seen in some diphenylorganoantimony (V) thiophosphates such as $Ph_2Sb\{S_2\text{-}PR_2\}$ ($Ph = C_6H_5$, R = Ph, *i*-OC_3H_7)[39, 40] and methylantimony (III) complexes like $(CH_3)SbL$ where L are derivatives of meta-substituted salicylic acid.[41] Observed organoantimony's antitumor activity is similar in mechanism and effect to cisplatin with cytotoxicity levels lower than that for Palladium (Pd) and Platinum (Pt).[27]

I. 8. Mechanism of action of antimonials

Testing that has been done on amastigote cells showed that the pentavalent antimony was taken up by the cell and reduced to the more active and toxic trivalent form which kills the cell.[42, 43] This reduction requires thiol compounds to provide the reducing power, higher pHs and

slightly elevated temperatures. The trivalent form on antimony *in vivo* targets zinc finger containing proteins and trypanothione reductase (TR) in the leishmania parasite.[29] The TR prevents the cells from damage by oxidative stress and toxic heavy metals. Zinc fingers are also involved in DNA recognition, RNA packaging, transcriptional activation, regulation of apoptosis, protein folding and assembly, and that the apoptosis of amastigotes is due to influx of calcium ions and increased oxidative stress.[29, 43] This is the pro-drug mechanism of action model (Figure 1) for the pentavalent antimonials. The other two proposed models are the intrinsic antileishmanial activity and host immune activation model.[29, 32] The intrinsic antileishmanial activity model proposes that pentavalent antimonials do not have to be reduced to the trivalent forms to exact an effect. Studies into this model were carried out on amastigotes has suggested intrinsic antileishmanial activity is achieved through interruptions in the macromolecular biosynthesis through inhibition of glycolysis and fatty acid β-oxidation. Finally, the host immune activation model depicts that the action of the pentavalent antimonial is that of immune system activation to not only clear the Leishmania parasites but also offer immunity against future infections. [29] The prodrug model (Figure 1) is currently the most widely accepted mechanism.[44] Ulamina (an experimental drug containing antimony pentachloride and N-methyl-glucamine), showed that when injected, only 23% of the pentavalent is reduced to trivalent antimony.[45] Studies with monkeys also supported the prodrug model in that when meglumine antimoniate (Sb V) was administered, the amount of trivalent antimony in the plasma rose from 5% on day one of exposure to about 50% on day nine.[46]

I. 9. Toxicity of Antimony and its Excretion

Excretion of antimony from the body is reliant on the form of antimony (+3 or +5) absorbed in the gastrointestinal tract. Pentavalent is excreted more rapidly than trivalent antimony, with over 50% of pentavalent being excreted in urine within 6 hours after intravenous administration compared to 25% of trivalent after 24 hours of administration.[23] Analysis of data from treatment of patients suffering from Leishmaniasis with antimonials have shown the primary targets of antimony are the heart, gastrointestinal tract, musculoskeletal system, liver, pancreas, and the nervous system. Symptoms that manifest include dizziness, nausea, abdominal pain, diarrhea, anorexia, and myalgia. [47-49]

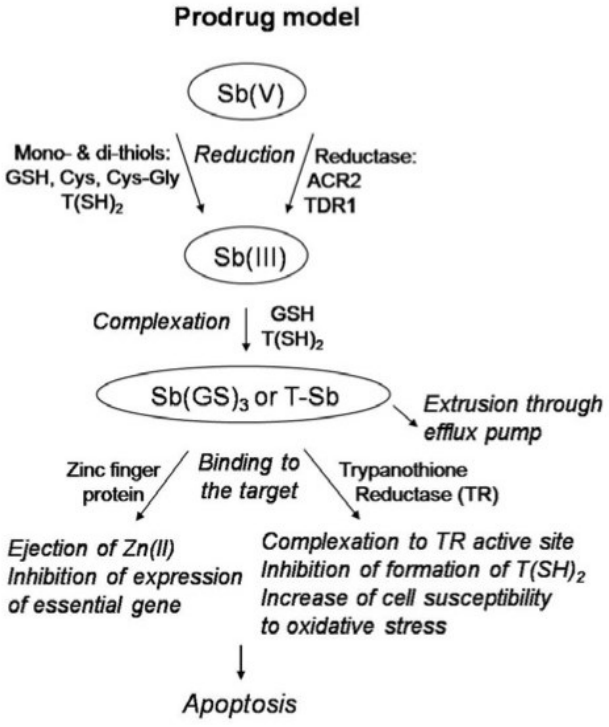

Figure 1. Prodrug model showing apoptosis inducing mechanism of antimony *in vivo* [reproduced from Reference 29]

I. 10. Coordination compounds

Coordination complexes of the Werner type are products of Lewis acid-base reactions where neutral molecules or negatively charged ions (anions) – ligands – bind to a central atom, normally a metallic ion or atom.[51-53] The ligands are Lewis bases which contain at least one pair of electrons to donate to the metal ion or atom, forming a dative covalent bond in which the base donates both electrons for the formation of the bond. The metal atom or ion is the Lewis acid which accepts the electrons from the Lewis base. The coordination number refers to ligands that are classified as monodentate (binding to the metal ion or atom at one place and donating a pair of electrons), or polydentate (binding to the metal ion or atom at more than one place). Some of the ligands exists as ambidentate ligands, which contain two or more donor atoms and can bind to the central metal atom or ion via either donor atom. Examples of such ligands are nitrite ions, linear pseudohalide ions.[53] The coordination number refers to the number of bases or donor atoms, groups attached to the central metal atom or ion. There are bi- and polydentate ligands, which bind tightly to metal ions with many of them being chelating agents used for separation of and extracting metals.[51] Numerous chelating organic compounds are used in treating metal poisoning since they bind stronger to the metal ions than molecules in human tissue.[51] An example is ethylenediaminetetraacetic acid (EDTA), or mercaptopropanol, HS-CH_2-CH_2-CH_2-OH. There are also naturally occurring powerful chelates and macrocycles containing metal ions such as chlorophyll, hemoglobin, cyancobalamin, and others.[54]

I. 11. Cyanoximes: Ligands for Coordination Compounds

Cyanoximes are a new class of oximes that can form a variety of coordination compounds. The general structure for cyanoximes is HO-N=C(CN)-R, where R represents the

varying electron withdrawing group, typically O, N, or S (Figure 2). The nitrile group (CN) makes the cyanoxime 10000 times more acidic and a better ligand when compared to other oximes.[55] It also makes it easier for deprotonation to happen in both aqueous and polar organic solvents which yields a color change due to the transition from $n \rightarrow \pi^*$ in the nitroso chromophore.[56-59] The linear and polar nitrile group provides rigidity to the cyanoximes which helps in crystallization of both ligands and their metal complexes.[55] These cyanoximes are also ampolydentate in nature as demonstrated by one of them, 2-oximino-2-cyanoacetamide, called ACO^- anion, demonstrating different modes of binding to various metals (Figure 5). Cyanoximes also show rich coordination chemistry.[55] For synthesis of cyanoxime three main routes exist (Figure 7), with the general mechanism of formation of cyanoximes shown in Figure 3, along with the two possible diastereomers - *syn* and *anti*. The process of diastereomers formation is purely kinetic driven since thermodynamic of the oximination reaction is the same. Thus, different groups attached to the >C=N-O fragment due to their varied bulkiness and electronic structure are affecting the ratio of diastereomers. This was confirmed by X-ray analysis and NMR spectroscopy The illustrations in Figures 3 and 4 also explain the possibility of the four different experimentally found geometrical isomerism present within cyanoximes (Figure 6). Figure 4 shows the delocalization of the negative charge in aryl-cyanoxime anions such as in Ag (I), and Tl (I) salts. It is evident that the free rotation about the single bond (N-C) allows for the O=N- fragment to rotate, forming two out of the three resonance forms possible within the cyanoxime. There are 44 known cyanoximes today (Figure 8) that have been characterized thus far with many found to have significant biological activity. It ranges from growth regulation, detoxification, to antimicrobial applications.[60-67] Antimicrobial activity has been seen in silver (I) cyanoximates and in compounds containing the sulfur thioamide-cyanoxime, HO-N=C(CN)

C(S)NH_2, (later TCO)[73, 74] Currently, there are new antiviral oxime-containing compounds being developed that affect HIV, SARS-CoV-2, and MERS-CoV-2, all of which are now in different stages of clinical trials.[75]

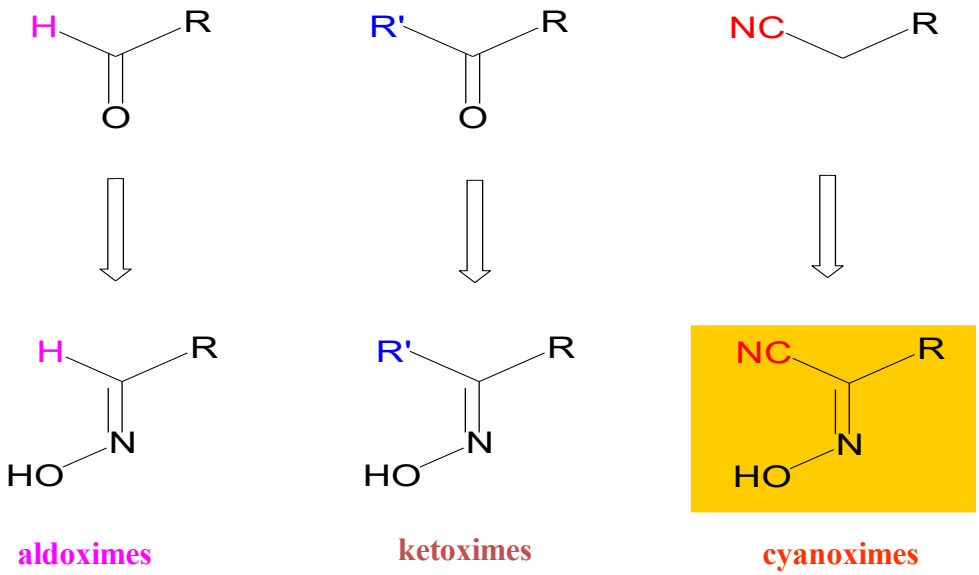

Figure 2. Types of oximes and their precursors.

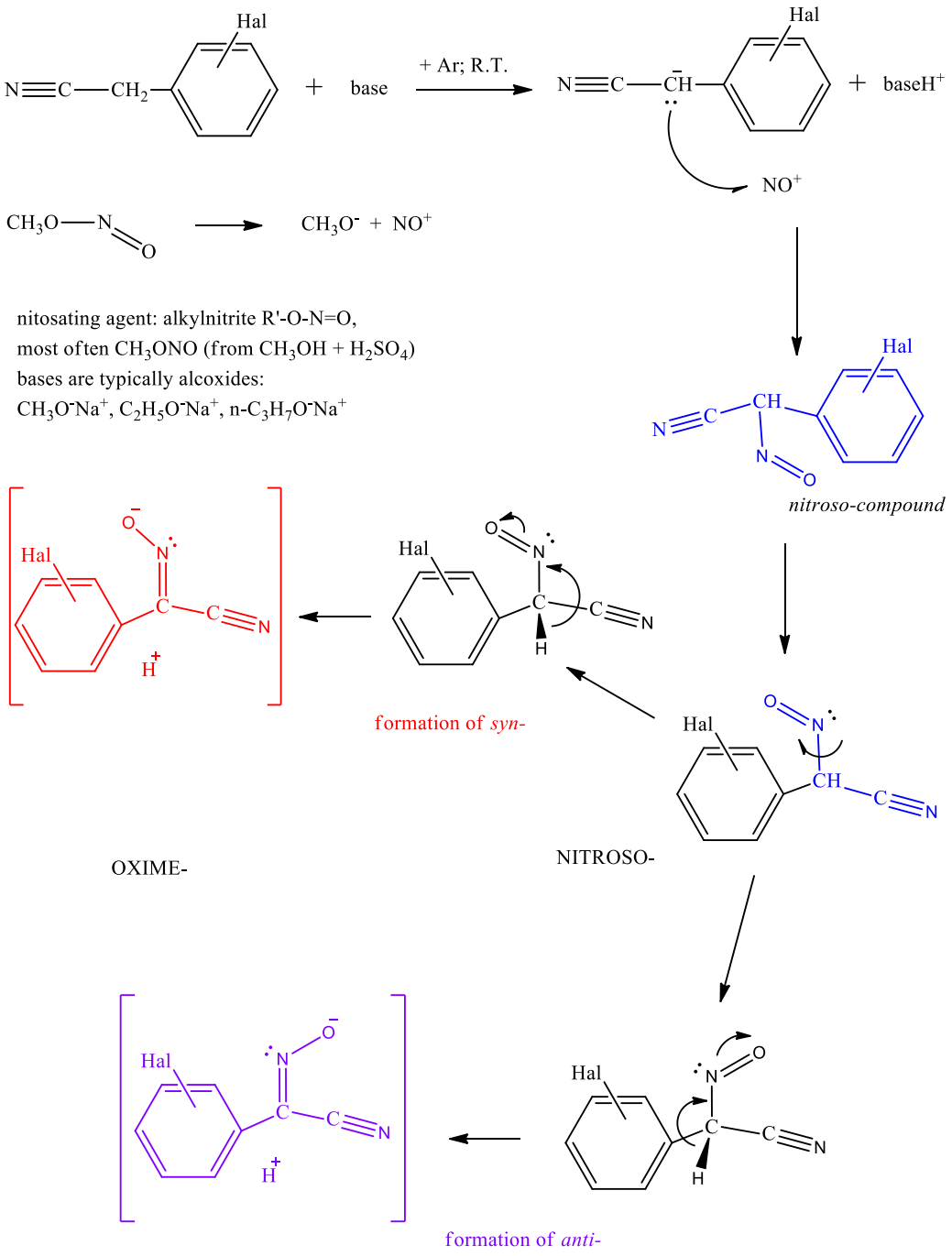

Figure 3. Mechanism of formation of two diastereomers – syn and anti – during synthesis of cyanoximes.

In previous research carried out by my colleague Kevin Pinks, tetraphenyl antimony was complexed with cyanoxime ligand to test for the presence of any antimicrobial activity.[60] The

$SbPh_4Br$ as initial compound is available commercially. The cyanoxime ligands were chosen for their partial water solubility, polarity as well as earlier demonstrated biological activity. Tetraphenyl antimony has considerable lipophilicity and hence was a good baseline to start in the quest for new synthetic non-antibiotic antimicrobial compounds using the antimony cyanoximates. The higher the lipophilicity of a compound, the better it binds to its proteins *in vivo* and the greater its distribution.[97] With the help of collaborative group in the Department of Microbiology and Molecular Genetics at Oklahoma State University, Pinks tested his compounds against bacterial strains -Methicillin-resistant *Staphylococcus aureus* strain NRS70, *Escherichia coli* strain S17, and *Pseudomonas aeruginosa* strain PAO1 – and fungal strains – *Candida albicans, Cryptococcus neoformans.* His research showed that, of the five antimony (V) cyanoximates tested for antimicrobial activity, $Sb(Ph)_4(ACO)$, and $Sb(Ph)_4(ECO)$, had significant antimicrobial effect against all three bacterial strains used: two gram-negative *E. coli* strain S17 and *P. aeruginosa* strain PAO1, alongside a single gram-positive Methicillin-resistant *Staphylococcus aureus* strain NRS70. The $Sb(Ph)_4(TCO)$ and $Sb(Ph)_4(TDCO)$, containing the thioamides, had significant effects on the gram- positive MRSA strain NRS70 only. Antifungal studies showed that $Sb(Ph)_4(ECO)$ was effective against *Cryptococcus neoformans* and *Candida albicans* in a positive trend. The $Sb(Ph)_4(TCO)$ was the next contributor towards antifungal activity against both strains. The $Sb(Ph)_4(ACO)$ and $Sb(Ph)_4(TDCO)$ were only effective at inhibition of *Cryptococcus neoformans*, while those compounds did not contribute to any inhibition towards *Candida albicans.* Finally, testing of free cyanoximes against both the bacterial and fungal strains yielded no effect showing that they had to be complexed with antimony for there to be an effect.[60]

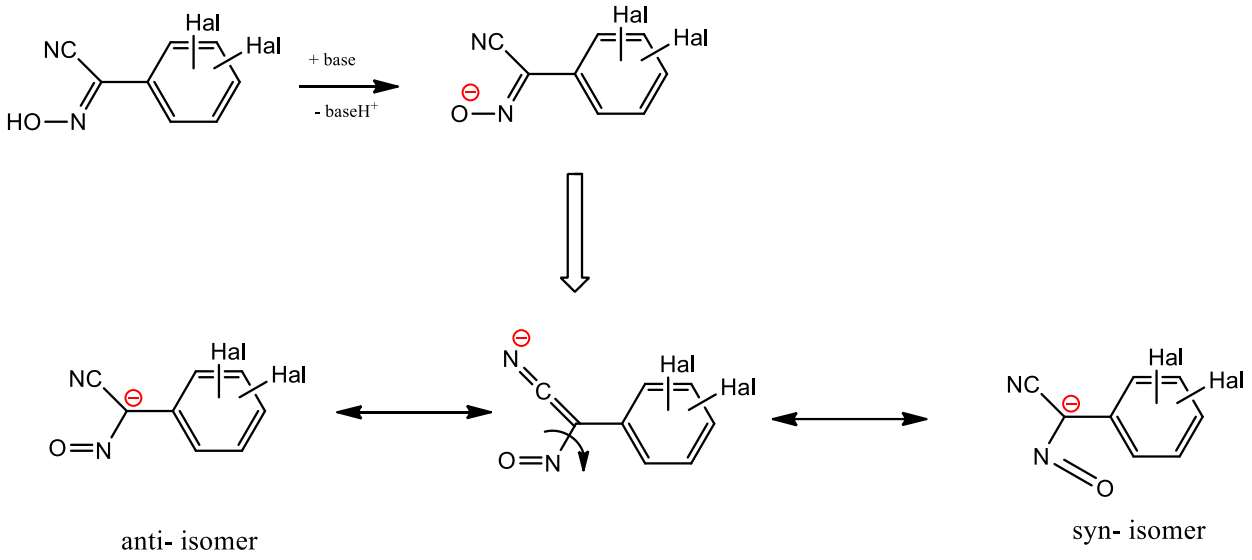

Figure 4. Schematic representation of delocalization of negative charge in aryl-cyanoxime anions (such as in Ag, Tl-salts) showing that two out of three isomeric forms represent anions in the nitroso form where the rotation of the O=N- fragment around N-C bond is possible.

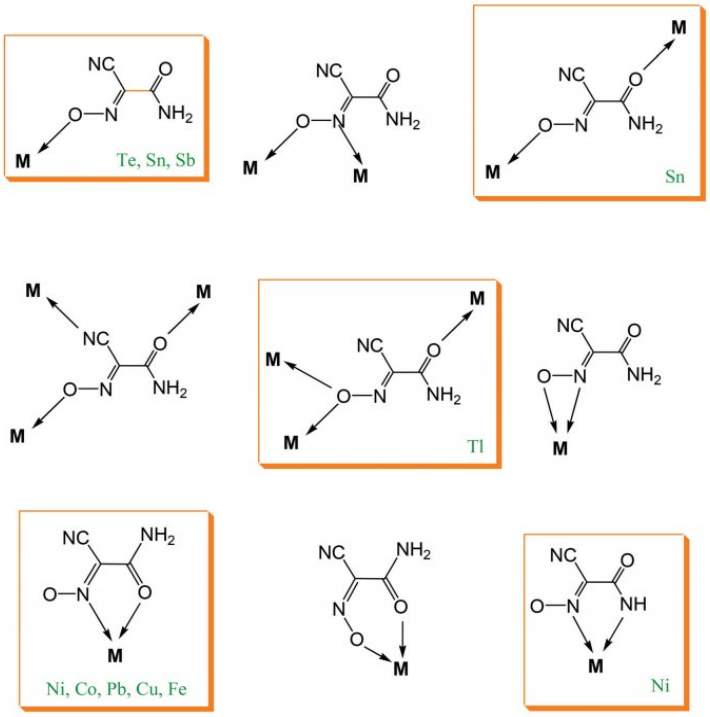

Figure 5. Ampolydentate character of cyanoxime anions for ACO- anion. Binding modes enclosed in boxes were confirmed by crystallographic studies.

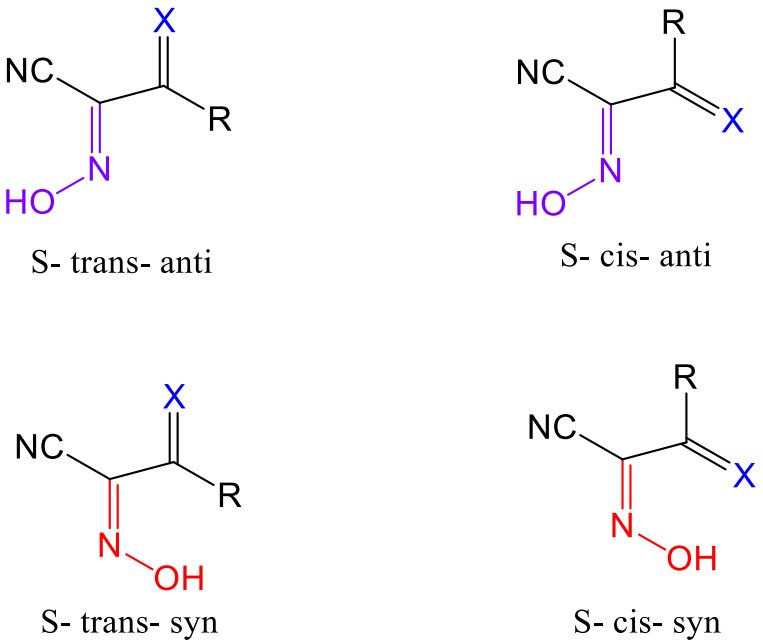

Figure 6. Experimentally found geometrical isomers of cyanoximes. (X=O, S; R= alkyl, aryl groups).

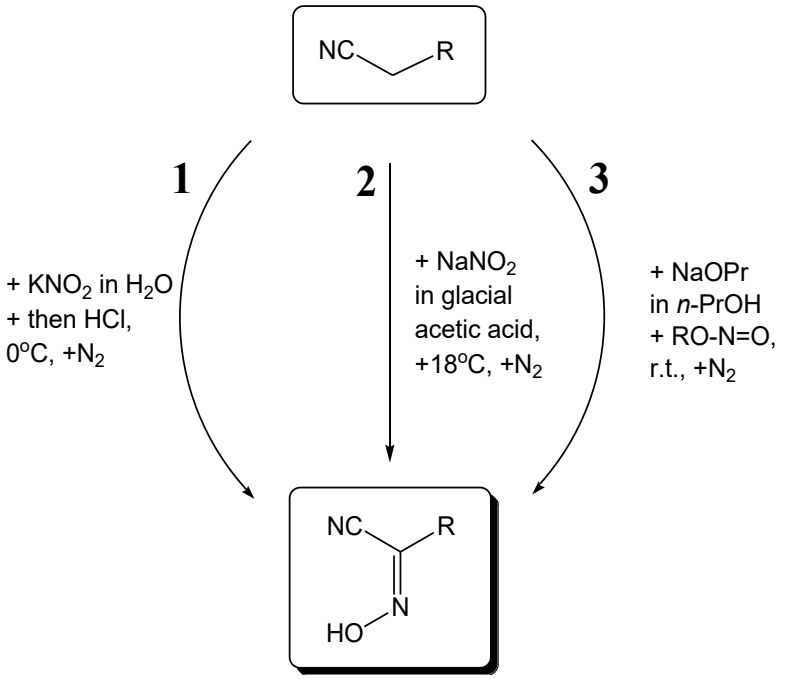

Figure 7. Routes for cyanoxime synthesis.

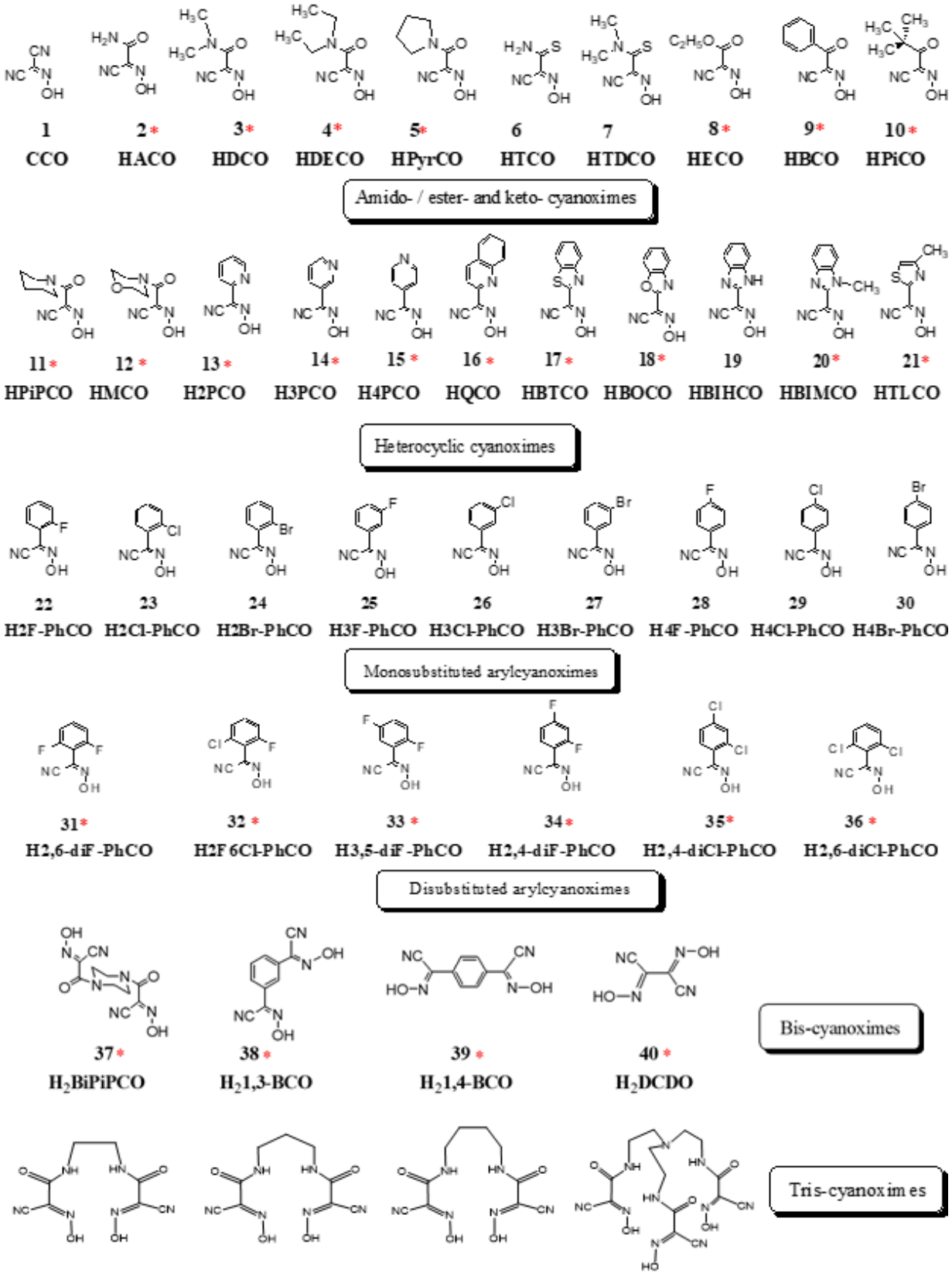

Figure 8. List of known cyanoxime ligands. * Compounds with determined crystal structures.

II. RESEARCH GOAL

My research goal was to prepare a series of new organoantimony (V) compounds and characterize them. The ligands used were previously identified cyanoximes that had biological activity.[55] The choice of metalloid fragment was $SbMe_3$, with the source of antimony obtained from lab-synthesized trimethylantimony dibromide ($SbMe_3Br_2$). Compared to the previously used tetraphenyl (V) antimony, trimethylantimony (V) is less lipophilic and bulky as well as being able to bind two cyanoxime ligands instead of one. This increased overall solubility in organic solvents, and cyanoxime "double" load is proposed to increase the antimicrobial effect previously witnessed with the tetraphenyl (V) antimony cyanoximates obtained by Pinks. The choice of anionic ligands for this research was disubstituted arylcyanoximes which have proven biological activity.[55] These will be novel antimony cyanoximates that will be tested for their antimicrobial activity. For good comparison on the effect of decreased lipophilicity and bulkiness, I synthesized antimony cyanoximates with the ligands used in previous research for antimicrobial studies by Kevin Pinks (Figure 9).

Due to limited research on these compounds, I synthesized the antimony cyanoximates, and submit them for testing on bacterial and fungal strains to assess for antimicrobial properties at our collaborative institution – Department of Microbiology and Molecular Genetics at Oklahoma State University. There are two research groups led by Professor Marianna Patrauchan and Professor Karen Wozniak. The goal was to compare the effect of adding one more cyanoxime moiety to the antimony complex as compared to Pinks' molecules. My hypothesis therefore will be that increasing the number of cyanoxime groups attached to the Sb(V) center should increase its microbial properties compared to not having any cyanoximes attached. My ligands of choice are shown in Figure 9 – which includes both the new aryl

cyanoximes and the old, tested cyanoximes that Kevin Pinks worked with. The new halogenated aryl cyanoximes have already established biological activity.

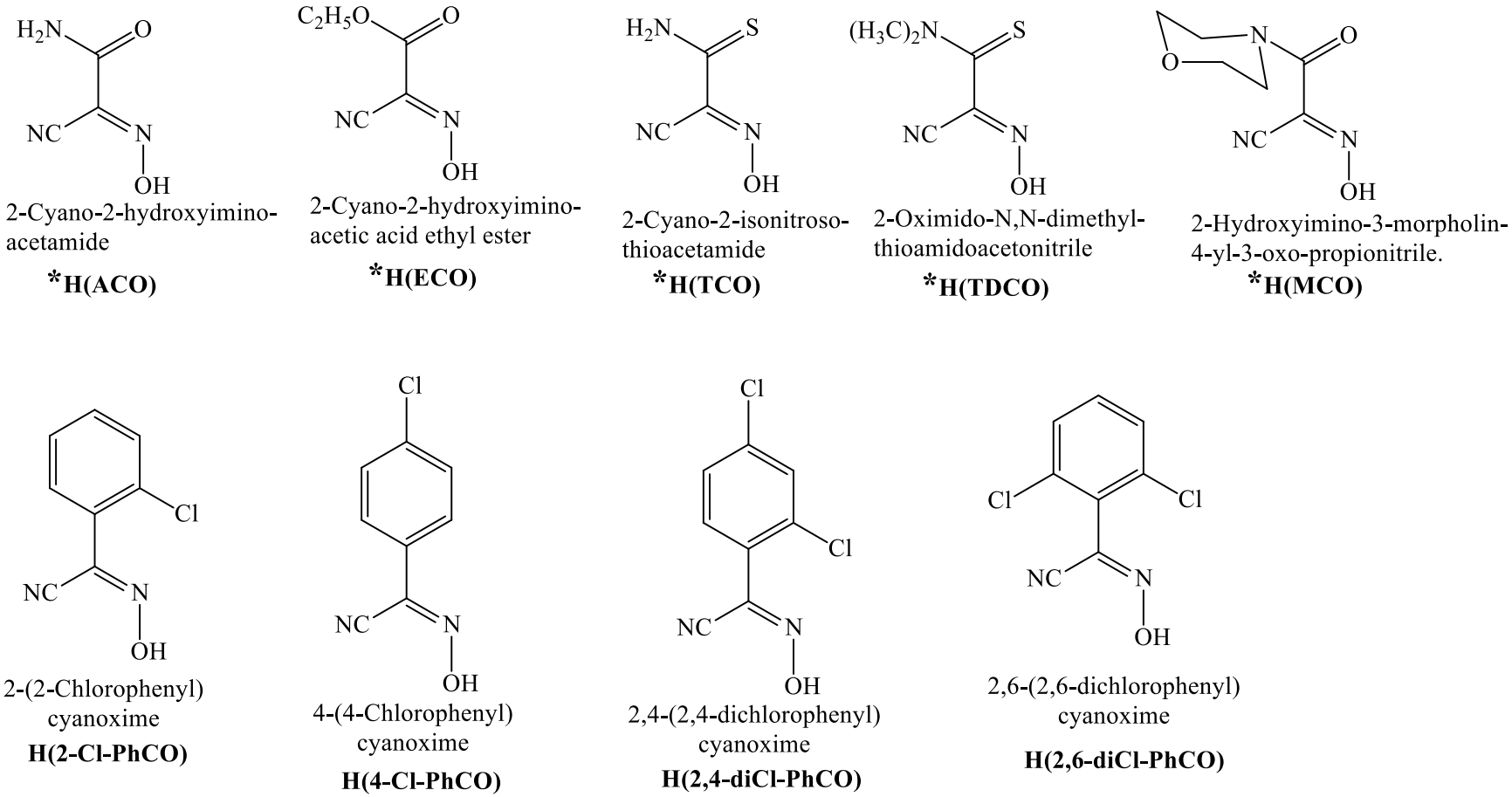

Figure 9. Choice of ligands for antimicrobial studies. * Indicate Ligands used by Kevin Pinks in his work.

III. EXPERIMENTAL PART

III. 1. Reagents and General Considerations

Solvents used for carrying out reactions and crystallizations were HPLC grade and employed without further purification. The inorganic compounds (Na metal, NaCl and Na_2SO_4 anhydrous) were obtained from Mallinckrodt. Reagent grade ethyl cyanoacetate ($C_5H_7NO_2$), chloroform ($CHCI_3$), and Antimony (III) chloride (99.0%) were purchased from Sigma Aldrich for my synthesis. All other chemicals and organic solvents - isopropyl alcohol (i-PrOH), acetonitrile (CH_3CN), diethyl ether sodium nitrite ($NaNO_2$), concentrated sulfuric acid (H_2SO4), and concentrated hydrochloric acid (HCI) from Fisher Scientific. Cyanoximes and their silver (1) derivatives selected for current studies were either taken from a bank of ligands in Dr. Gerasimchuk's research laboratory or obtained using published procedures from starting substituted acetonitriles.[60,71,76,77,82] The arylcyanoximes were synthesized through the same process. Therefore, compounds such as Ag(MCO), Ag(ACO) and Ag(ECO), were used for syntheses of organoantimony(V) cyanoximates from previous investigations'. The thioamides-based cyanoximes H(TCO), H(TDCO) as well as all TI(I) cyanoximates were prepared by Dr. Gerasimchuk to avoid graduate students' exposure to stench or toxic chemical compounds. Melting points were determined with the use of pre-calibrated apparatus with urea and naphthalene standards Digi-Melt (MPA106 SRS) in open melting point capillaries and reported without correction. Elemental analysis on C, H, N (and S with thioamide-based cyanoximes) content was conducted at the Atlantic Microlab (Norcross, GA). Elemental analysis was not conducted on compounds that had their crystal structures already determined since the crystal structure confirms the elemental composition of the compound being studied.

III. 2. Vibrational spectroscopy

The IR-spectra of all compounds reported herein were studied by using Bruker ATR FT spectrophotometer. The resolution was set to be 4 cm^{-1} with 64 scans in the range of 400-4000 cm. An atmospheric compensation and baseline correction were applied for data treatment.

III. 3. NMR spectra

Some spectra were obtained on a Varian INova-400 MHz spectrometer at room temperature in DMSO-d_6 and $CDCl_2$ solutions for ^{1}H and ^{13}C, respectively. Spectra of halogenated ligands and organoantimony (V) complexes were recorded at Northeastern University, (NEU) in Boston, MA.

III. 4. X-ray crystallography

Suitable single crystals of organoantimony(V) cyanoximates were grown at +4 °C exclusively using the vapor diffusion method: acetonitrile solutions of compounds were placed into the inner tube and vapors of anhydrous ether were used as crystallizing agent from the outer tube with a screw cap. Normally within 2-3 weeks after setting up, transparent, well-shaped crystals appeared on the walls in the inner tube suitable for crystallographic studies. All crystals selected for studies were placed on plastic MiTeGen holders attached to the copper-pin on the goniometer head of the Bruker APEX-2 diffractometer, equipped with a SMART CCD area detector. The intensity data were collected at low temperature. Data collection was done in ω scan mode using the Mo tube (Kα radiation; λ = 0.71073 Å) with a highly oriented graphite monochromator. Intensities were integrated from 4 series of 364 exposures, each covering 0.5 °

steps in ω at 20 - 60 seconds of exposure time depending on the crystal diffracting power, with the total data set being a sphere. The space group determination was done with the aid of the XPREP software. The absorption correction was performed by a crystal face indexing procedure with use of a video microscope followed by numerical input into the SADABS program. Both cited programs are included in the Bruker AXS software package. All structures were solved by direct methods and refined by least squares on weighted F^2 values for all reflections with $I > 3\sigma(I)$ using the SHELXTL program. In several structures it was possible to identify all H-atoms on the electron density map due to the high quality of crystals. However, in some structures H-atoms were placed in calculated positions in accordance with the hybridization state of a hosting carbon atom and were refined isotropically. No apparent problems or complications were encountered during the structures' solutions and refinement as evident from very positive PLATON checkCIF reports. Values of selected bond lengths and valence angles are presented in respective Tables following the discussion of crystal structures. A representative drawing of the crystal structures and packing diagrams was done using the ORTEP 3v2 and Mercury software packages. All determined crystal structures have been deposited at CCDC (England), with PLATON checkCIF reports.

III. 5. Thermal stability studies

Thermal stability of the obtained metal complexes was assessed using Q-600 TG/DSC analyzer (TA Instruments, Delaware, USA) under UHP Ar flow of 100 mL/min at 10 °/min heat rate. Heating of samples was carried out to 800 °C at which the samples' complete decomposition was attained.

IV. PREPARATION OF COMPOUNDS

IV. 1. Synthesis of Initial Trimethylantimony (V) Dibromide ($SbMe_3Br_2$), Metalloid Source

Due to the unavailability of trimethylantimony dibromide commercially, it was synthesized in the lab. The reaction is shown in Figure 10. The procedure followed was that of G. O. Doak et. al[1] submitted in *Inorganic Syntheses, Volume IX.*[78,79] Methylmagnesium iodide solution, CH_3MgI, 3 M in diethyl ether, was purchased from Sigma Aldrich; (#25,436-3). This allowed for bypassing the initial reaction (1) in Figure 10. A dry ice/acetone bath was made in a Dewar. With a syringe, 30 mL of the Grignard reagent (CH_3MgI) was transferred into a 3-necked round-bottomed flask under Argon flow. A solution of 6.845 g of Antimony (III) chloride ($SbCl_3$) in 17.7 mL ether was made and added dropwise to the flask via an addition funnel.

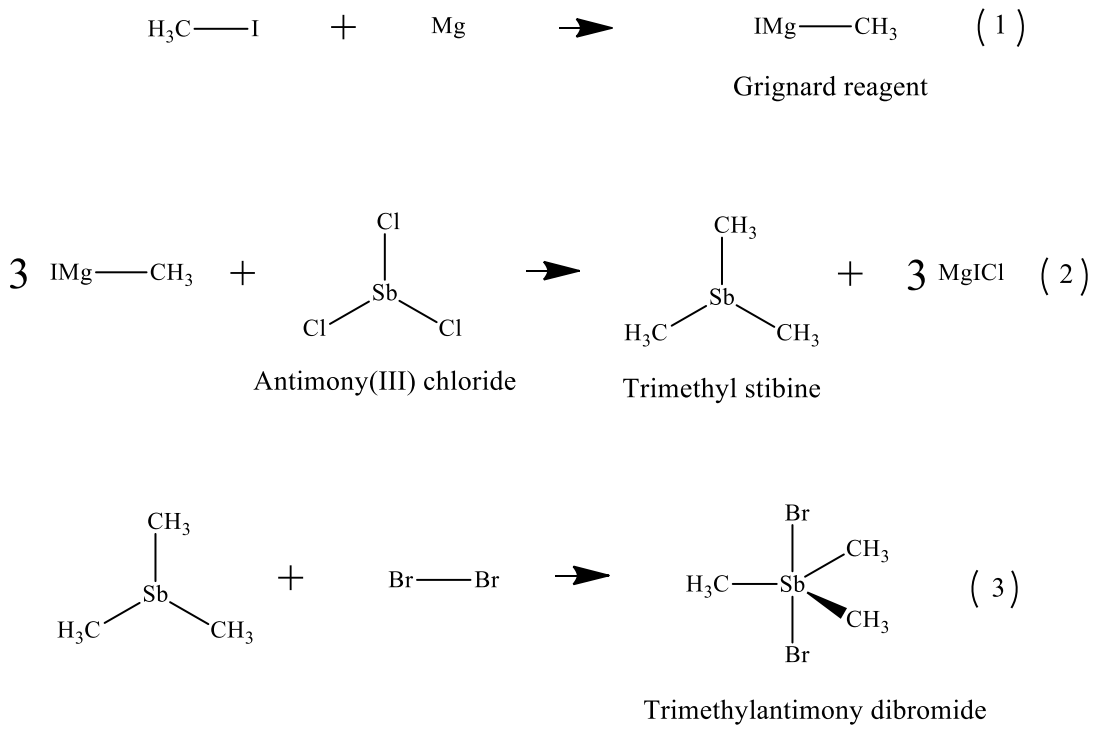

Figure 10. Synthesis of Trimethylantimony (V) Dibromide.

With a mechanical stirrer to facilitate stirring, the reaction progressively turned grey. The stirrer was disconnected once the reaction reached completion and a distillation apparatus was connected to the reaction flask with the receiving flask chilled in an ice bath. A slurry white mixture of trimethylstibine and ether was collected in the receiving flask and brominated with a solution of 0.5 mL bromine in 7.8 mL carbon tetrachloride (CCl_4). The product turned a consistent yellow color and was dried overnight. The crude product was recrystallized in hot ethanol into a white crystalline product. The yield of the purified product was 1. 152 g to 1.763 g (23% to 35%) based upon $SbCl_3$. The melting point was 183.2 – 183.5 °C. IR spectrum, cm^{-1}: 3004^{as}, 2919^{s} ν(C-H); 1386^{as} δ(C-H); 865 ρ(C-H); 567^{as} ν(C-Sb). Some physical properties and yield of all the compounds synthesized in this project are summarized in Table 1.

IV. 2. Synthesis of arylcyanoxime ligands (HL)

General Considerations. Arylcyanoximes were synthesized by the Meyer reaction shown in Figures 11 and 12. The initial compounds for these reactions are commercially available from Aldrich. These reagents were used by my previous colleagues in the lab for the synthesis of their compounds, like oximino (2,4-dichlorophenyl) acetonitrile, H(2,4-diCl-PhCO) and 2-cyano-2-isonitrosothioacetamide, H(TCO).[60,82.]

In an Erlenmeyer flask, 0.404g (0.0176 mol) of sodium metal was dissolved in 60mL of propanol under argon flow. This solution was transferred to an Erlenmeyer flask with a solution of the starting acetonitrile NC-CH_2-R, compound (2.65 g; 0.0175 mol for monosubstituted, 0.0142 mol for disubstituted) dissolved in 100mL propanol. Cold sulfuric acid was then added dropwise to a solution 22 g (0.319 mol) of sodium nitrite ($NaNO_3$) dissolved in 50:50 mL of water and methanol in a round-bottomed flask to create the gaseous methylnitrite, CH_3-ONO that bubbled through the Erlenmeyer flask with the initial acetonitrile. Passing gaseous methylnitrite

immediately changes color of solution to yellow and after ~15 min the reaction mixture was purged with N_2 gas and left in the cold (+4 °C) overnight. TLC was ran on the solution against the initial compounds before the experiment was continued to confirm the formation of the product. The solvent was removed from the solution using rotary evaporator and the yielding yellow solid of Na-Ligand was dissolved in about 20 mL of water and acidified with a 1:5 solution of water and sulfuric acid (H_2SO_4) until pH~4. The protonated oxime was then washed with ether and brine solution to extract the organic (ether) layer with the oxime. The ether layer was dried and stored in the fridge overnight. Then the ether was removed with Rotovap, and the white solid cyanoxime was dried in a desiccator over H_2SO_4.

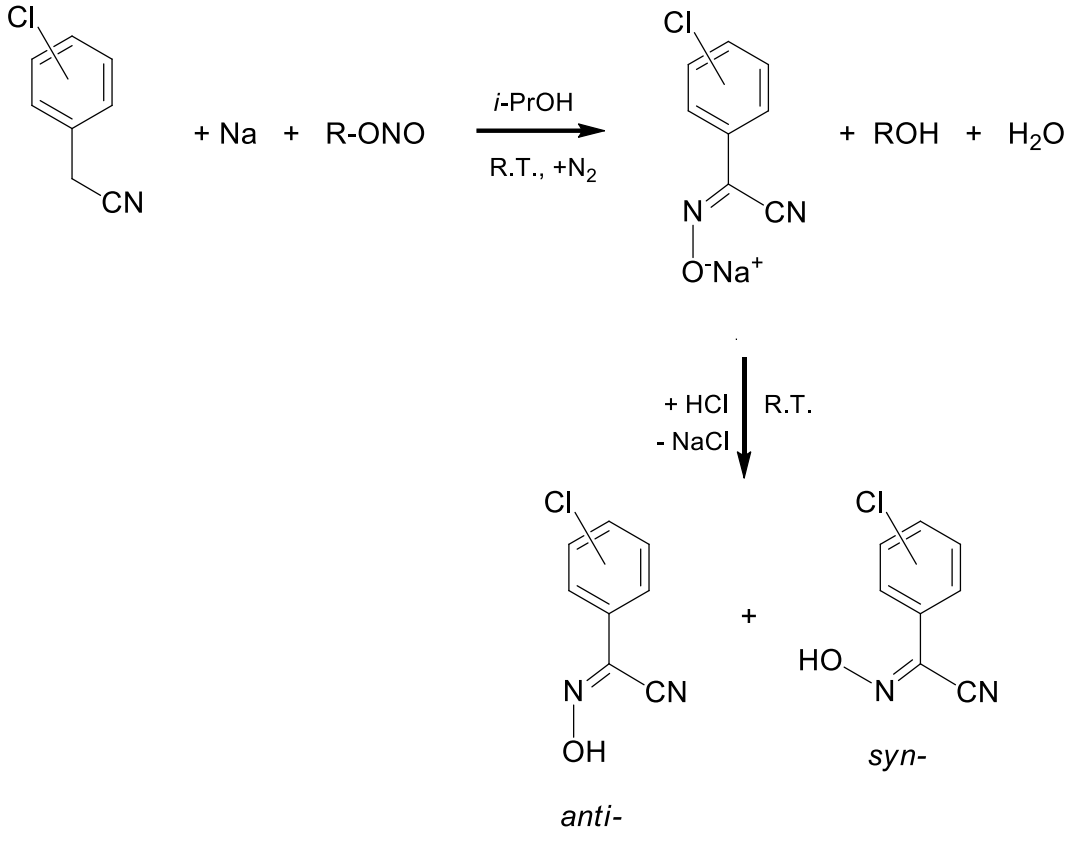

Figure 11. The general reaction used preparation of monosubstituted arylcyanoximes.

Synthesis of Oximino (2-chlorophenyl) Acetonitrile, H(2-Cl-PhCO). The initial compound used was 2-chlorobenzyl cyanide (97%), purchased from Sigma Aldrich, #18,849-2. Figure 11 illustrates the procedure for the synthesis of the compound. The melting point of the target compound was 124.43 °C. The yield of the product was 0.944 g (30%), R_f value of 0.29 (EtOAc/hexane = 1:4). The ^{1}H NMR spectrum in dmso-d_6, ppm: 14.08 (1H, singlet, oxime group), 7.65 (1H, doublet), 7.63 (1H, multiplet, Ar H), 7.59 (1H, multiplet, Ar H), 7.50 (1H, multiplet, Ar H). IR spectrum, cm^{-1}: 3334 ν(O-H); 3075 ν(C-H); 2236 ν(C≡N); 1670 ν(C=N); 1581 ν(C=C); 965 ν(N-O); 756 δ(C-H); 700 - 500 ν(C-Cl).

Synthesis of Oximino (4-chlorophenyl) Acetonitrile, H(4-Cl-PhCO). The initial compound used for this synthesis was 4-chlorobenzyl cyanide (97%), purchased from Sigma Aldrich, #C2, 800-6. The melting point was 95 °C.[10] The yield of the product, H(4Cl-PhCO) was 0.692 g (22%), R_f value of 0.32 (EtOAc/hexane = 1:4). The IR spectrum, cm^{-1}: 3281 ν(O-H); 2972 ν^s(C-H); 2251 ν(C≡N); 1594 ν(C=N); 1488 ν(C=C); 964 ν(N-O); 826 δ(C-H); 487 ν(C-Cl).

Synthesis of Oximino (2,4-dichlorophenyl) Acetonitrile, H(2,4-diCl-PhCO). The initial compound used was 2,4-dichlorophenyl acetonitrile[81] purchased from Sigma Aldrich, #17-846-2, while the reaction is displayed in Figure 12. The melting point was 133.51°C. The yield of the product was 2.3 g (73%), R_f value of 0.37 (EtOAc/hexane = 1:4). IR spectrum, cm^{-1}: 3277 ν(O-H); 3155 ν(C-H); 2245 ν(C≡N); 1583, 1474 ν(C=C); 1421 ν(C=N); 1090, 632 ν(C-Cl); 1034, 969 ν(N-O); 818, 755 δ(C-H).

Synthesis of oximino (2,6-dichlorophenyl) acetonitrile, H(2,6-diCl-PhCO). The initial compound used was 2,6-dichlorophenyl acetonitrile[82] purchased from Sigma Aldrich, #12,601-2. The melting point was 99.61 °C. The yield of the product was 0.283 g (60%), R_f value of 0.32 (EtOAc/hexane = 1:4). The ^{1}H NMR, ppm: 14.41 (1H, s, oxime group), 7.68 (2H, multiplet),

7.59 (1H, multiplet). ^{13}C NMR, ppm: 135.26 (carbons at *2,6*-positions), 133.26 (carbons at *3,5*-positions), 129.07 (carbon at *4*-position), 127.27 (carbon at 1-position), 129.64 (oxime carbon), 114.29 (CN-group). IR spectrum, cm^{-1}: 3420 ν(O-H); 3171, 3083 ν(C-H); 2250 ν(C≡N); 1577, 1559 ν(C=C); 1431 ν(C=C) - Ph-group pulsing; 725, 783, 794 δ(C-H) - 1,2,3-Ph-group pattern; 1411 ν(C=N); 1047 ν(N-O); 1126^{as}, 1083^{s} ν(C-Cl).

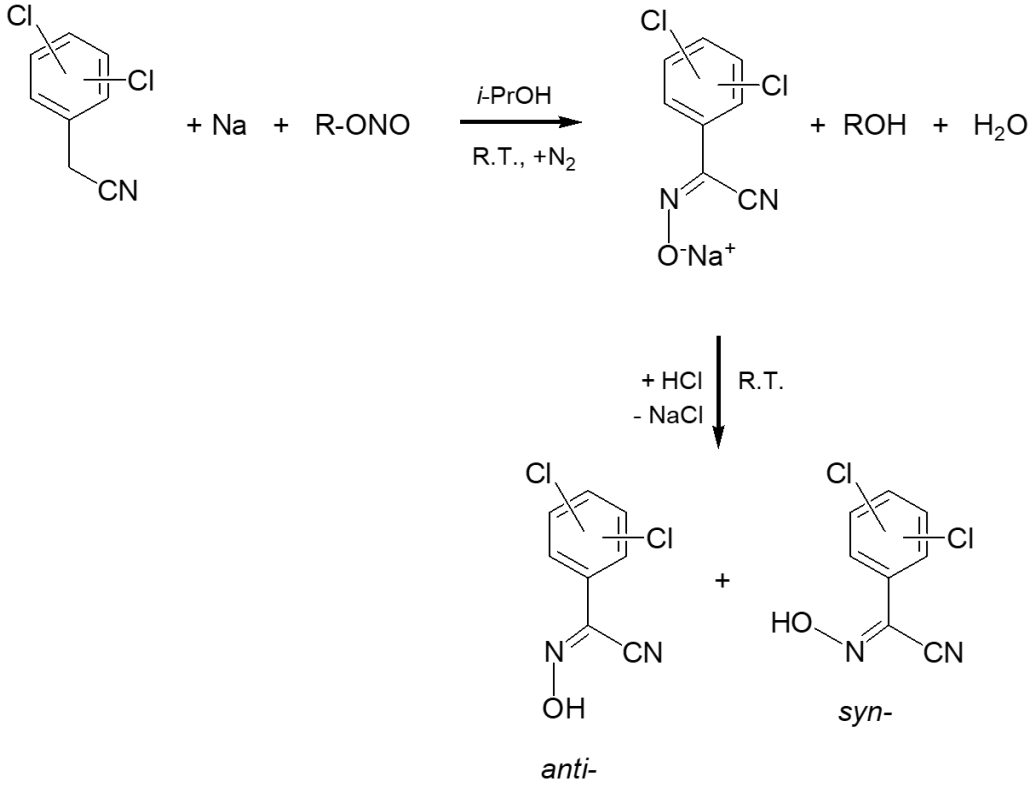

Figure 12. Scheme for making disubstituted arylcyanoximes.

For the preparation of trimethylantimony (V) cyanoximates, it was necessary to make either Ag(I) or Tl(I) cyanoximates. Some ligands with Ag(I) do not form stable complexes – thioamides and aryl cyanoximes. These complexes were highly light sensitive compared to other complexes of Ag(I) synthesized in the lab. Therefore, Tl(I) was necessary to be able to form

stable complexes for the metathesis reaction to proceed. Tl(I) also shares a lot of similarities with Ag(I), making it a successful replacement for our reactions.

IV. 3. Synthesis of Silver (I) and Thallium (I) Complexes from HL

There were several silver (I) cyanoximates already prepared in our laboratory by previous colleagues and their synthesis was unnecessary because they were available. The Ag-Ligand form chosen for the metathesis reactions with $SbMe_3Br_2$ were Ag(MCO), Ag(ECO) and Ag(ACO). Other cyanoximes, such as thioamides and haloaryl, do not form stable Ag(I) compounds and for the organoantimony (V) compounds, Tl(I) were necessary. Thioamide based cyanoximes, H(TCO) and H(TDCO) were also available in the laboratory, but their thallium cyanoximates Tl(TCO) and Tl(TDCO)) were synthesized by Dr. Gerasimchuk to prevent graduate students' exposure to toxic thallium salts.[7] The other TlL syntheses with halogenated cyanoximes were performed by Dr. Gerasimchuk as well.

The reaction is carried out on a hot plate, where a hot solution of thallium carbonate (Tl_2CO_3) is made by dissolving it in 13 mL of water. In small portions, the HL is added, and carbon dioxide is evolved. A yellow solution is formed is filtered while hot in a large-mouthed test tube already submerged into hot water (about 55 °C) in a large Dewar flask. The thallium solution is then left to slowly crystallize over several days. One example of the synthesis is illustrated in Figure 13. Thus, Thallium (I) salts; Tl(2-Cl-PhCO) had a yield of 0.2690 g (36.6%) based on 0.346 g of H(2-Cl-PhCO). The Tl(4-Cl-PhCO) had a yield of 0.5551 g (64.62%) based on 0.404 g of H(4-Cl-PhCO). The Tl(2,4-diCl-PhCO) had a yield of 0.8242 g (64.4%) based on 0.658 g of H(2,4-diCl-PhCO). The Tl(2,6-diCl-PhCO) had a yield of 0.2809 g (19.2%) based on 0.7511 g of H(2,6-diCl-PhCO).

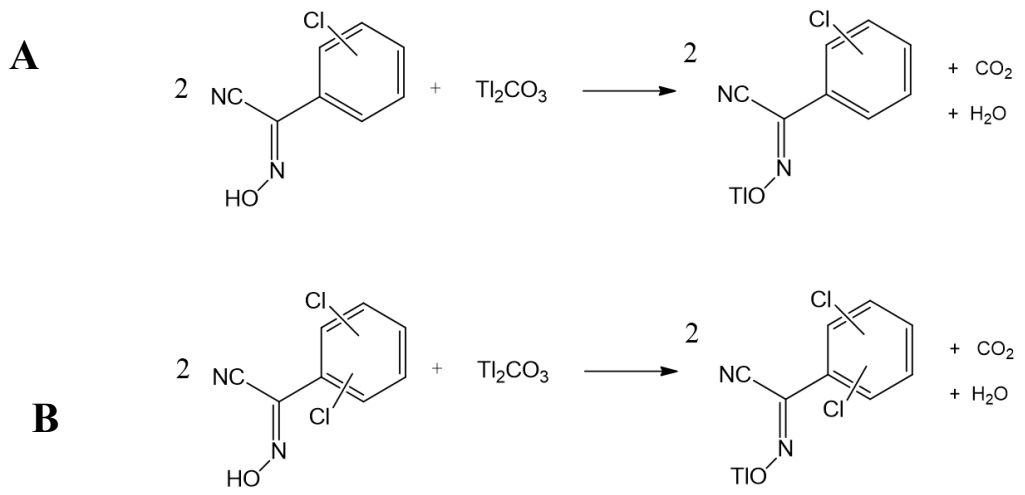

Figure 13. General scheme for synthesis of Tl-Ligand salts from H-Ligands for **(A)** mono- and **(B)** disubstituted arylcyanoximes.

IV. 4. Synthesis of Antimony Cyanoximates ($SbMe_3L_2$): The Metathesis Reaction

Trimethylantimony (V) cyanoximates were prepared via metathesis reaction shown in Figure 14. Trimethylantimony (V) dibromide is dissolved in about 5 mL of acetonitrile or propionitrile with the help of a sonicator. The Tl(L) is then added carefully to the solution under stirring. There is a color change from yellow to colorless/clear for all cyanoximes except TCO^- and $TDCO^-$. The reaction is fast and after~10 mins, the precipitate of AgBr or TlBr was separated via centrifuge. Complete separation required 3 mins using the Thermo-Scientific Sorvall Legends Micro 17 at 10,000 rpm (Figure 16). After centrifugation, the liquid, now containing trimethylantimony (V) cyanoximate was transferred into a small beaker crystallization[80] in a desiccator charged with paraffin. The general pictorial sequence of the procedure is shown in Figure 15. For metathesis reaction with AgL, this procedure was carried out under a red-light lamp to prevent the decomposition of the light-sensitive silver salts.[60,80]

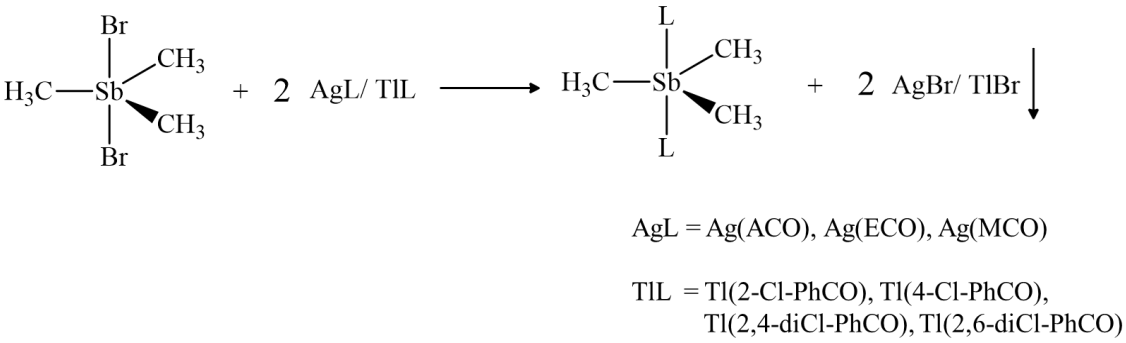

Figure 14. General scheme for antimony cyanoximate metathesis reaction. **L** represent the ligands used in the synthesis.

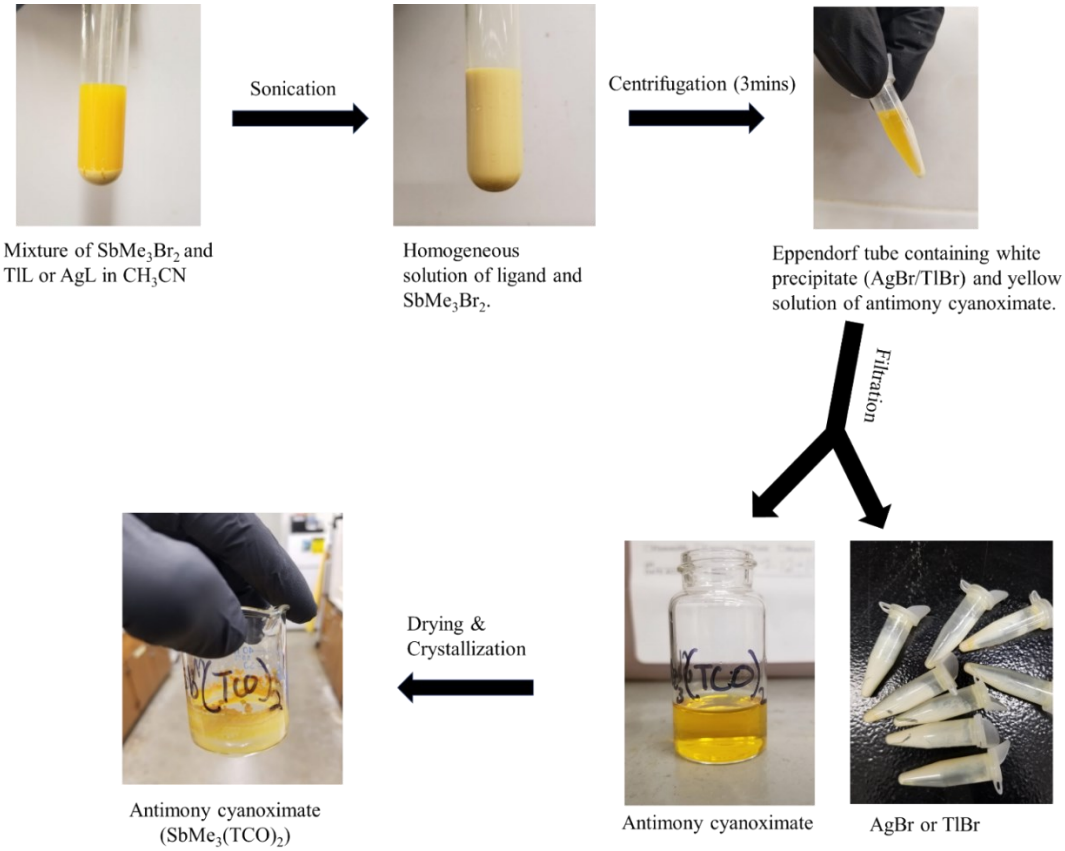

Figure 15. General sequence of procedures for the metathesis reaction shown in Figure 5.

Synthesis of $SbMe_3(2\text{-Cl-PhCO})_2$. The 0.08507g (0.2604 mmol) of $SbMe_3Br_2$ and 0.2000g (0.5209 mmol) of Tl(2-Cl-PhCO) was used in the metathesis reaction (Figure 5). The

yield of the dry product was 0.1100 g (80.3%) based on $SbMe_3Br_2$. The melting point was 128.78°C. The IR spectrum, cm^{-1}: 3067, 3029, 2921 ν(C-H); 2219 ν(C≡N); 1590 ν(C=N); 1518, 1479 ν(C=C); 1470, 755 δ(C-H); 974 ν(N-O); 651 ν(C-Cl); 586 $\nu(C\text{-}Sb)^{as}$.

Synthesis of $SbMe_3(4\text{-}Cl\text{-}PhCO)_2$. The 0.1700 g (0.5204 mmol) of $SbMe_3Br_2$ and 0.4000g (1.042 mmol) of Tl(4-Cl-PhCO) was used in the metathesis reaction (Figure 14). The yield of the dry product was 0.1211g (44.2%) based on $SbMe_3Br_2$. The melting point was 162.27°C. The IR spectrum, cm^{-1}: 3072, 2966, 2932 ν(C-H); 2220 ν(C≡N); 1594 ν(C=N); 1489 ν(C=C); 1489, 1397, 821 δ(C-H); 972 ν(N-O); 710 ν(C-Cl); 544 $\nu(C\text{-}Sb)^{as}$.

Synthesis of $SbMe_3(2,4\text{-}diCl\text{-}PhCO)_2$. The 0.1570 g (04806 mmol) of $SbMe_3Br_2$ and 0.4000 g (0.9560 mmol) of Tl(2,4-diCl-PhCO) was used in the metathesis reaction (Figure 14). The yield of the dry product was 0.2130 g (74.0%) based on $SbMe_3Br_2$. The melting point was 129.18°C. The IR spectrum, cm^{-1}: 3087 ν(C-H); 2219 ν(C≡N); 1585 ν(C=N); 1498 ν(C=C); 1379, 851 δ(C-H); 979 ν(N-O); 821 ν(C-Cl); 570 $\nu(C\text{-}Sb)^{as}$.

Synthesis of $SbMe_3(2,6\text{-}diCl\text{-}PhCO)_2$. The 0.07807 g (0.2390 mmol) of $SbMe_3Br_2$ and 0.2000 g (0.4870 mmol) of Tl(2,6-diCl-PhCO) was used in the metathesis reaction (Figure 14). The yield of the dry product was 0.1010 g (71.0%) based on $SbMe_3Br_2$. The melting point was 184.35 °C. The IR spectrum, cm^{-1}: 3089, 3077, 2933 ν(C-H); 2217 ν(C≡N); 1583 ν(C=N); 1561, 1526 ν(C=C); 1430, 777, 725 δ(C-H); 972 ν(N-O); 632 ν(C-Cl); 561 $\nu(C\text{-}Sb)^{as}$.

Synthesis of $SbMe_3(TCO)_2$. The 0.1956 g (0.5988 mmol) of $SbMe_3Br_2$ and 0.4000 g (1.203 mmol) of Tl(TCO) was used in the metathesis reaction (Figure 14). The yield of the dry product was 0.03100 g (12.2%) based on $SbMe_3Br_2$. The melting point was from 186.9 - 189.6 °C. The ^1H NMR spectrum in DMSO-d_6, ppm: 14.34, 10.5 (NH_2 group in syn-); 9.98, 9.53 (NH_2 group in anti-). $^{13}C\{^1H\}$ NMR spectrum in dmso-d_6, ppm: 186.51 (thioamide, anti-), 185.91

(thioamide, syn-), 133.36 (oxime group, syn-), 131.79 (oxime group, anti-), 109.47 (CN group, syn-), 108.83 (CN group, anti-). The IR spectrum, cm^{-1}: 3440, 3389 $\rho(NH_2)$; 2922 ν(C-H); 2236 ν(C≡N); 1693 ν(C=N); 1472, 1331 δ(C-H); 1180, 1068 $\nu(C=S)^a$ 981 ν(N-O); 591 $\nu(C\text{-}Sb)^{as}$.

Synthesis of $SbMe_3(TDCO)_2$. The 0.1168 g (0.3575 mmol) of $SbMe_3Br_2$ and 0.2579g (0.7153 mmol) of Tl(TDCO) was used in the metathesis reaction (Figure 14). The yield of the dry product was 0.1023 g (41.5%) based on $SbMe_3Br_2$. The melting point was 175.27 °C. ^1H NMR spectrum in DMSO-d_6, ppm: 3.45, 3.40 (6H, singlet, CH_3- groups tertiary amine-accidental overlap), 3.35, 3.17 (3H singlet, CH_3- groups tertiary amine), 1.79, 1.77, 1.75 (3H, singlet, CH_3 - group Sb). $^{13}C\{^1H\}$ NMR spectrum in dmso-d_6, ppm: 183.72 (thioamide, anti-), 182.67 (thioamide, syn-), 133.96 (oxime group, syn-), 132.15 (oxime group, anti-), 114.55 (CN group, syn-), 110.09 (CN group, anti-). The IR spectrum, cm^{-1}: 2932 ν(C-H); 2225 ν(C≡N); 1531 ν(C=N); 1449, 1394 δ(C-H); 1141, 1078, 1050 $\nu(C=S)^a$, 969 ν(N-O); 568 $\nu(C\text{-}Sb)^{as}$.

Synthesis of $SbMe_3(ACO)_2$. The 0.2000 g (0.6122 mmol) of $SbMe_3Br_2$ and 0.2693 g (1.224 mmol) of Ag(ECO)was used in the metathesis reaction (Figure 14). The yield of the dry product was 0.0250 g (10.4%) based on $SbMe_3Br_2$. The IR spectrum, cm^{-1}: 3406 $\rho(NH_2)$; 2935 ν(C-H); 2228 ν(C≡N); 1684 $\nu(C=O)^a$, 1600 ν(C=N); 1423, 1312 δ(C-H); 981 ν(N-O); 587 $\nu(C\text{-}Sb)^{as}$.

Synthesis of $SbMe_3(ECO)_2$. The 0.2000 g (0.6122 mmol) of $SbMe_3Br_2$ and 0.3049 g (1.225 mmol) of Ag(ECO)was used in the metathesis reaction (Figure 14). The yield of the dry product was 0.2220 g (80.8%) based on $SbMe_3Br_2$. The melting point was 140.52 °C. ^1H NMR spectrum in DMSO-d_6, ppm: 4.31 (2H, multiplet, CH_2-group ECO^-), 1.89, 1.71 and 1.67 (3H, singlet, CH_3-group Sb), 1.28 (3H, multiplet, CH_3-group ECO^-). $^{13}C\{^1H\}$ NMR spectrum in dmso-d_6, ppm: 159, 127 (oxime carbons), 109.59 (CN-group), 62.08 (CH_2- group ECO^-), 14.47

(CH_3- group ECO^-), 8.33, 7.10, 6.63 (CH_3- group Sb). The IR spectrum, cm^{-1}: 2996, 2967, 2940 ν(C-H); 2230 ν(C≡N); 1716 ν(C=O)^a; 1465, 1372 δ(C-H); 1060 ν(N-O); 583 ν(C-Sb)^{as}.

Synthesis of $SbMe_3(MCO)_2$. The 0.1636 g (0.5008 mmol) of $SbMe_3Br_2$ and 0.2922 g (1.008 mmol) of Ag(MCO)was used in the metathesis reaction (Figure 14). The yield of the dry product was 0.1023 g (77.3%) based on $SbMe_3Br_2$. The melting point range was from 118.5 - 120.9 °C. The IR spectrum, cm^{-1}: 2965, 2935 ν(C-H); 2224 ν(C≡N); 1634 ν(C=O)^a; 1460, 1390 δ(C-H); 930 ν(N-O); 589 ν(C-Sb)^{as}.

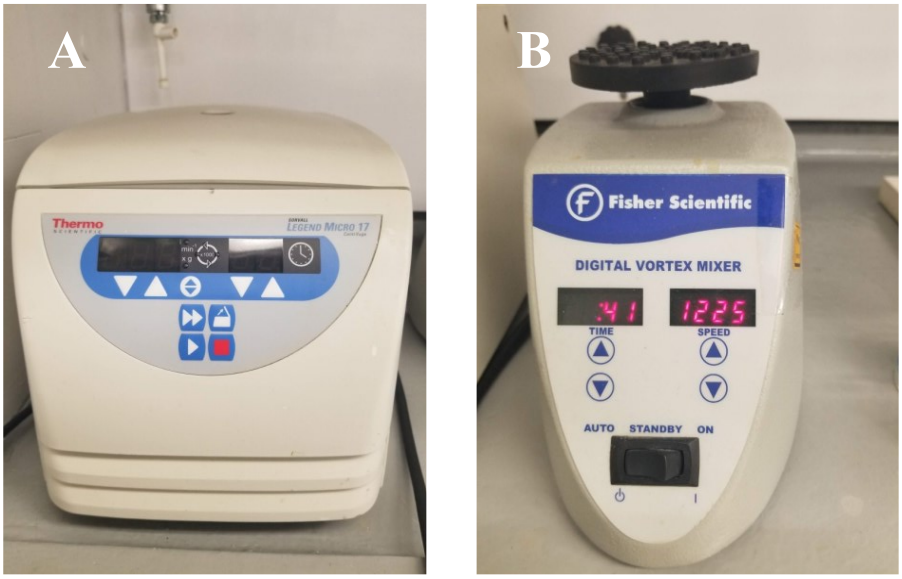

Figure 16. Instrumentation used in synthesis. **A)** Thermo Scientific Sorvall Legends Micro 17 and **B)** Fisher Scientific Vortex.

Table 1. Elemental analysis, yield and color of initial compounds, ligands, and antimony cyanoximates

Compound	Melting point (°C)	Yield (%)	Elemental Analysis, Element %		
			C, % Calc. (Found)	H, % Calc. (Found)	N, % Calc. (Found)
$SbMe_3Br_2$	183.2 - 183.5	23-25	N/A	N/A	N/A
H(2-Cl-PhCO)	124.43	30	N/A	N/A	N/A
H(4-Cl-PhCO)	95[83]	22	N/A	N/A	N/A
H(2,4-diCl-PhCO)	133.51	73	N/A	N/A	N/A
H(2,6-diCl-PhCO)	99.61	60	44.68 (44.75)	1.87 (1.94)	13.03 (13.12)
Tl(2-Cl-PhCO)	N/A	36.6	25.02 (25.30)	1.05 (0.88)	7.30 (7.18)
Tl(4-Cl-PhCO)	N/A	64.6	25.02 (25.91)	1.05 (0.92)	7.30 (7.26)
Tl(2,4-diCl-PhCO)	N/A	64.4	22.96 (24.66)	0.72 (0.67)	6.70 (6.86)
Tl(2,6-diCl-PhCO)	N/A	19.2	22.96 (22.19)	0.72 (0.64)	6.70 (6.36)
$SbMe_3(2\text{-}Cl\text{-}PhCO)_2$	128.78	80.3	N/A	N/A	N/A
$SbMe_3(4\text{-}Cl\text{-}PhCO)_2$	162.27	44.2	43.38 (43.33)	3.26 (3.35)	10.65 (10.39)
$SbMe_3(2,4\text{-}diCl\text{-}PhCO)_2$	129.18	74.0	38.36 (38.07)	2.54 (2.43)	9.42 (9.35)
$SbMe_3(2,6\text{-}diCl\text{-}PhCO)_2$	184.35	71.0	N/A	N/A	N/A
$SbMe_3(TCO)_2$	186.9 - 189.6	10.4	N/A	N/A	N/A
$SbMe_3(TDCO)_2$	175.27	41.5	32.58 (32.77)	4.42 (4.36)	17.54 (17.47)
$SbMe_3(ACO)_2$	N/A	8.0	N/A	N/A	N/A
$SbMe_3(ECO)_2$	140.52	80.8	N/A	N/A	N/A
$SbMe_3(MCO)_2$	118.5 - 120.9	77.3	N/A	N/A	N/A

***** N/A = sample data was not recorded.

V. RESULTS & DISCUSSIONS

X-ray Single Crystal Analysis

Block-type single crystals, suitable for the X-ray analysis, were obtained in two ways: 1) during an overlay of pentane over ether solution of the cyanoxime within ~2 weeks at +4 °C in the thin tube in the refrigerator; 2) using vapor diffusion (ether) method into acetonitrile solution of the compound. All synthesized compounds in this work were characterized via X-ray diffraction by Dr. Nikolay Gerasimchuk. That is: a) initial cyanoximes, b) their Tl-derivatives, c) trimethylantimony(V) dibromide and d) cyanoximates of the latter Sb-source. Total number of determined crystal structures in this project is 17. Crystallographic output was in a form of the RES and CIF files that were later used by me for plotting the most representative pictures. Also, some of the datasets were reprocessed by me (meaning step-by-step structure solution and refinement) for gaining proficiency in the method and educational purposes. All structures were solved using direct methods incorporated into the SHELXS - 2013 and refined using the Bruker SHELXTL Software Packages. [60,84,85] In the case of crystal twins, application of the detwinning procedure with the help of CELL_NOW followed by absorption correction was accomplished with the help of TWINABS.[84-86] Some of the drawings of molecular structures were done with ORTEP 3v2, [84, 87] while the other molecular structures and packing diagrams for structures were performed using the Mercury Program. [57,84,88] The ORTEP drawings (abbreviated from: *Oak-Ridge Thermal Ellipsoids Plots*) is done at 50% probability.

In this thesis we follow typical way of presentation of crystal structures of chemical compounds showing I) the ASU first, which is the asymmetric unit; II) GROW mode, which is actual molecular structure; III) table of the crystal and refinement data; IV) details of the

structure with emphasis on H-bonding (if present), geometrical features such as stereochemistry; V) crystal packing diagrams if necessary for comprehension and discussion.

V. 1. Structure and Properties of The Initial Sb-Source Compound

The Crystal Structure of $SbMe_3Br_2$. All the antimony cyanoximates were made from $SbMe_3Br_2$ which has pentacoordinated pnictogen atom in formal oxidation state +5. This compound was prepared using methods previously described[78] without modification. Compound represents white crystalline substance soluble in common organic solvents and hydrolyzes in water to a mixture of hydrated products including polynuclear species. Covalently attached bromine atoms are prone to replacement by better nucleophiles and that makes $SbMe_3Br_2$ excellent starting compound for making new trimethyl-antimony(V) organometallic compounds. Despite the fact of earlier determination of the crystal structure in the '70s, we performed re-determination of its structure using modern hardware and processing software. Obtained data are much better than previously reported. Crystallographic community encourages chemists to improve quality of old deposited into Cambridge Crystal Structures Datacenter by deposition better structures into the database.

The crystallographic data for $SbMe_3Br_2$ is shown in Table 2. In solid state this compound adopts the trigonal bipyramid geometry with equal bond lengths from the metal Sb core to both bromine atoms (Sb1–Br1) and the three carbon atoms (Sb1–C1) bonded to it. This can be seen on the ASU unit in Figure 17A. The distances are 2.653 Å and 2.103 Å, respectively. The measured valence angles are as follows: Br1-Sb1-Br1 = 180 °, Br1-Sb1-C1 = 90 °, and C1-Sb1-C1 = 120 ° (Figure 18). The $SbMe_3Br_2$ represents a compound with D3h point group symmetry of non-H atoms with a 3-fold principal axis, 2-fold axes and a set of mirror planes. Figure 17B shows multiple positions for H-atoms originated from their Site Occupancy Factor (SOF) for

each H-atom is 0.25 because of their hosting C-atom occupying the mirror plane. For each hydrogen to have SOF = 1, there must be 4 H-atoms with SOF 0.25. Thus, there are 3 hydrogen atoms distributed between four positions totaling in occupancy to 1 and attached to the hosting single carbon atom generating 12 H-atoms in total on the methyl carbon. Figure 18 shows bond lengths and valence angles in the structure of this important precursor for the rest of reported here trimethylantimony(V) cyanoximates.

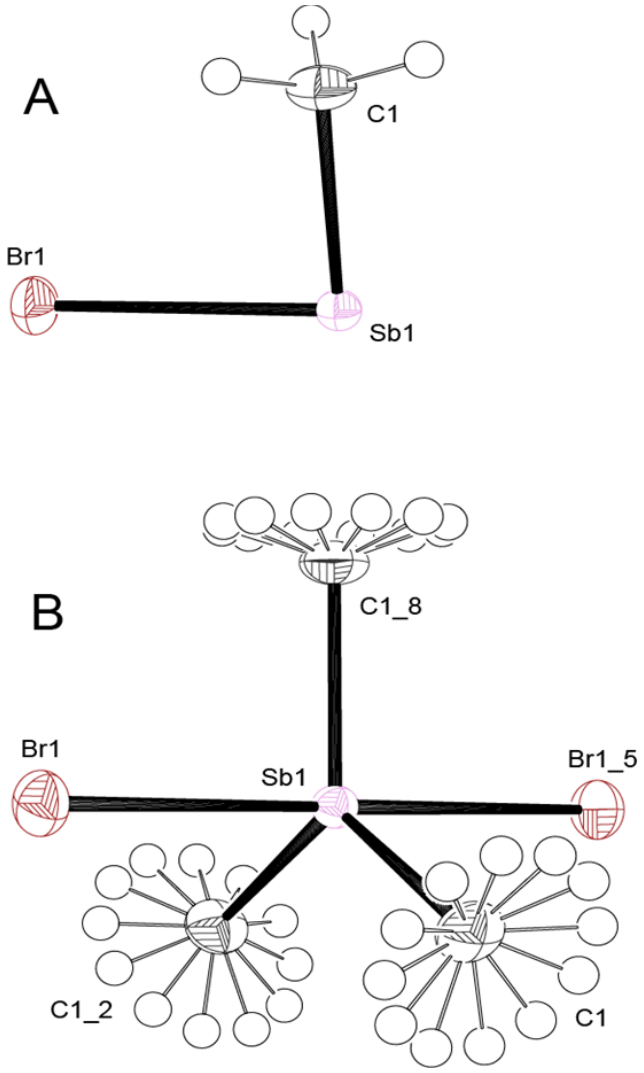

Figure 17. The molecular structure and numbering scheme for $SbMe_3Br_2$. The ASU in the structure **(A),** and the GROW fragment **(B).** Symmetry operations for positions : _2: -y, x-y, z; _5: y, -x-y, z+1/2; and _8: x-y, -y, -z.

Table 2. Crystal and refinement data for $SbMe_3Br_2$.

Parameter	**$SbMe_3Br_2$**	
Empirical formula	$C_2H_6Br_{1.33}Sb$	
Formula weight, g/mol	258.36	
Temperature, K	120(2)	
Wavelength, Å	0.71073	
Crystal size, mm	0.142×0.09×0.08	
Color	colorless needle	
Crystal system	hexagonal	
Space group	*P 6₃/mmc*	
Unit cell dimensions, Å, °	a = 7.298(2)	α = 90
	b = 7.298(2)	β = 90
	c = 8.842(3)	γ = 120
Unit cell volume, $Å^3$	407.8(3)	
Z	3	
Density (calculated), g/cm^3	3.156	
Absorption coefficient, mm^{-1}	14.700	
F (000)	347	
Θ range, °	3.22 to 27.00	
Index ranges	$-9 \leq h \leq 9$	
	$-9 \leq k \leq 9$	
	$-11 \leq l \leq 11$	
Reflections collected	4422	
Independent reflections	200 [R_{int} = 0.0250]	
Transmission (max and min)	0.7465 and 0.4474	
Data / restraints / parameters	200 / 0 / 11	
Goodness-of-fit on F^2	1.091	
Final R indices [I>2σ(I)]	162 data;	R1 = 0.0141
		wR2 = 0.0362
R indices [all data]		R1 = 0.0186
		wR2 = 0.0381
Largest diff. peak and hole, $eÅ^{-3}$	0.795 and -0.294	

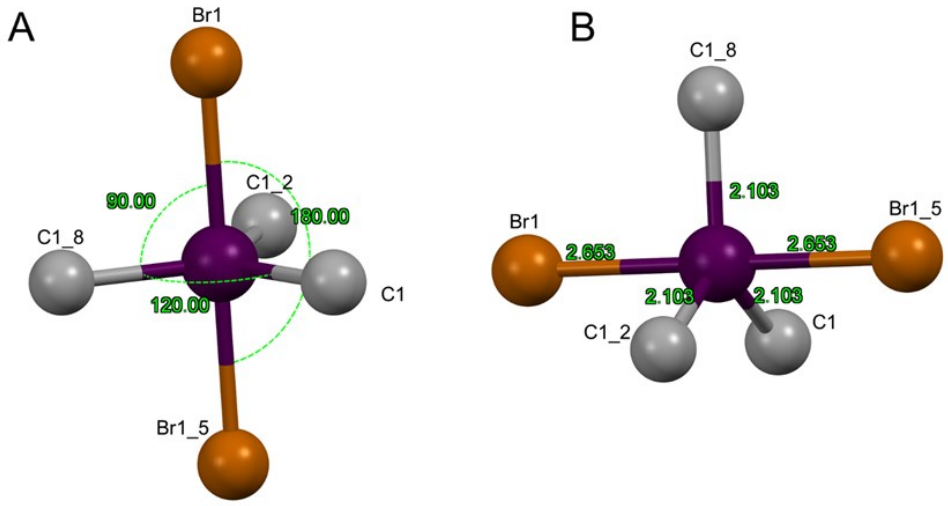

Figure 18. Trigonal bipyramid geometry of $SbMe_3Br_2$ showing valence angles **(A)** and bond lengths **(B)** in the molecule.

V. 2. Crystal Structures of Organic Ligands Used for The Preparation of Sb(V) Compounds

Previously we observed formation of mixtures of two diastereomers of cyanoximes – *syn* and *anti* – as the result of the nitrosation reaction,[89] and both are kinetic products since overall reaction is thermodynamically facile and typically affords desired compound in high yield.[67,90] Rotation of the NO-group around N-C bond during the nitrosation reaction leads to the formation of the *syn*-diastereomer. Most of the time we observed crystallization of just one, more favorable *anti*-diastereomer. However, isolation of pure individual *syn*-diastereomers was accomplished prior to this work in only two cases in work by the former student Leon Goeden.[82] Thus, a series of halogenated both monosubstituted[83] and disubstituted-arylcyanoximes[83,91] have been synthesized and initially characterized in Dr. Gerasimchuk's laboratory some time ago. Crystal structures of some of them have been reported earlier[57,91] including the *anti*-isomer of the H(2,6-

diCl-PhCO).[67] This diastereomer crystallizes in rare tetragonal non-centrosymmetric space group $P4_32_12$ with unit cell parameters a = b = 7.804 Å, c = 31.713 Å; V = 1931.8 Å^3.

In general, being weak organic acids families of both groups of both monosubstituted and disubstituted-arylcyanoximes undergo deprotonation in aqueous and non-aqueous solutions with the formation of yellow-colored anions due to $n \rightarrow \pi^*$ transition in the >C-N-O fragment. Their electronic structure can be described as an average between several resonance forms with charge delocalization among functional groups.[93] There is a significant contribution of the *nitroso-* form of the anion. Ionic cyanoximates in their alkali metal salts[67,89] adopt planar structures in which bond lengths indicate conjugation between functional groups in the molecule. This conjugation, for instance, can be seen from the shift to low wavenumbers and significant intensity increase for the ν(C≡N) vibration in the IR-spectra of Cat^+L^- as compared to HL (Cat^+ = Na, K, Cs; L^- = cyanoxime anion). It should be noted in context of this study that both mono- and di-halogenated arylcyanoximes form Werner-type complexes with metal ions such as Pd, Pt,[67] and especially Tl.[57.67,83]

The Crystal Structure of syn-H(2,6-diCl-PhCO). This compound was found to be able to crystallize as separate diastereomers: *anti-* and *syn-*, depending on the solvent and crystallization conditions. A rare case of pure *syn-* diastereomer is described here. Thus, looking back at previous studies the *anti*-isomer was obtained upon slow crystallization of the ether/acetone solution, while *syn*-isomer crystallized from a long tube containing overlaid with hexane ether/acetonitrile solution. Grown in the latter case, large crystals on the tube wall were harvested and used for structure determination. Molecular structure of this diastereomer is displayed in Figure 19. Crystal and refinement data are presented in Table 3, while the most important bonds and valence angles are summarized in Table 4. Similarly, to its *anti*-isomer this

compound has highly non-planar structure with a large dihedral angle α=74.29 º between two planar fragments: chloro-aryl and cyanoxime (Figure 19). In the crystal structure of *anti*-H(2,6-diCl-PhCO) this angle has surprisingly (and counterintuitively) slightly larger value of: α=77.1 º.[59,67]

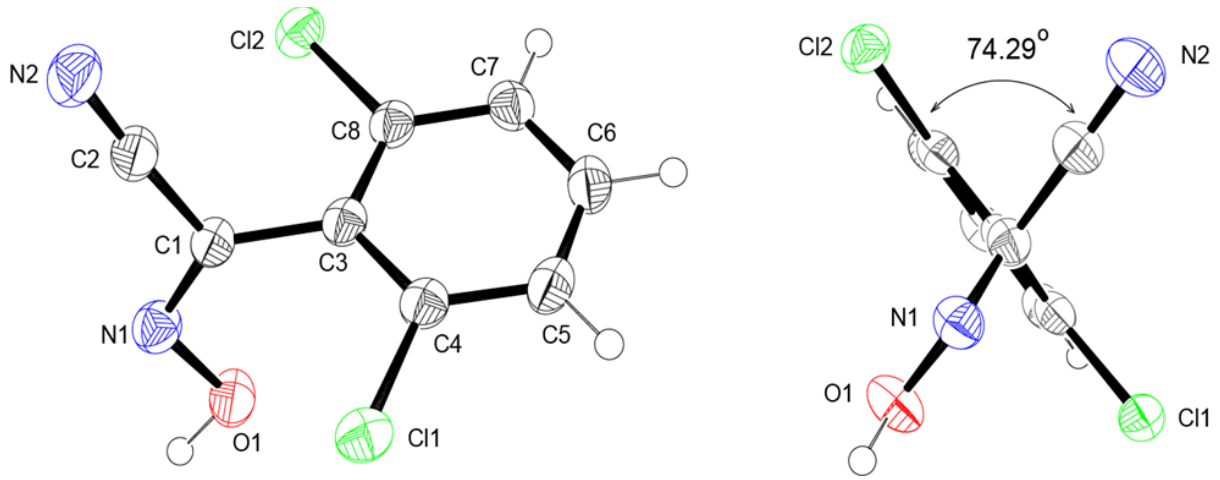

Figure 19. Molecular structure and numbering scheme for *syn*-H(2,6-diCl-PhCO) (in ORTEP representation drawn at 50% thermal ellipsoids probability level) showing two orthogonal views and a large dihedral angle between two planar fragments.

Molecules in the structure of the *syn*-H(2,6-diCl-PhCO) diastereomer in the crystal form rarely observed H-bonding via OH-group and N-atom of the nitrile group forming zigzag chain running along *c*-direction (Figure 20). Overall structure is columnar with π–π stacking interactions between neighboring di-chloroaryl fragments where inside the column there are alternating coplanar and angled at ~18.6 º arrangements (Figure 21A). Aside of H-bonding there are other short intermolecular van-der-Waals and electrostatic contacts ranging from 3.27 to 3.44

Å highlighted in Figure 21B. Those include phenyl-group centroid to Cl atom and C-H---C-H interactions between slipped parallel π-systems.

Table 3. Crystal and refinement data for *syn*-H(2,6-diCl-PhCO).

Parameter	***syn*-H(2,6-diCl-PhCO)**	
Empirical formula	$C_8H_4Cl_2N_2O$	
Formula weight, g/mol	215.03	
Temperature, K	100.6(7)	
Wavelength, Å	1.54184	
Crystal size, mm	0.24×0.15×0.12	
Color	colorless	
Crystal system	Monoclinic	
Space group	*P2/c (#13)*	
Unit cell dimensions, Å, °	a = 8.1720(2)	α = 90
	b = 8.8013(3)	β = 102.546(3)
	c = 13.0146(4)	γ = 90
Unit cell volume, $Å^3$	913.71(5)	
Z	3	
Density (calculated), g/cm^3	1.563	
Absorption coefficient, mm^{-1}	6.064	
F (000)	347	
Θ range, °	5.025 to 76.592	
Index ranges	$-9 \le h \le 9$	
	$-9 \le k \le 9$	
	$-11 \le l \le 11$	
Reflections collected	8213	
Independent reflections	1877 [R_{int} = 0.0348]	
Transmission (max and min)	N/A	
Data / restraints / parameters	1877 / 0 / 122	
Goodness-of-fit on F^2	1.107	
Final R indices [I>2σ(I)]	162 data;	R1 = 0.0459
		wR2 = 0.1268
R indices [all data]		R1 = 0.0471
		wR2 = 0.1280
Largest diff. peak and hole, $eÅ^{-3}$	0.795 and -0.294	

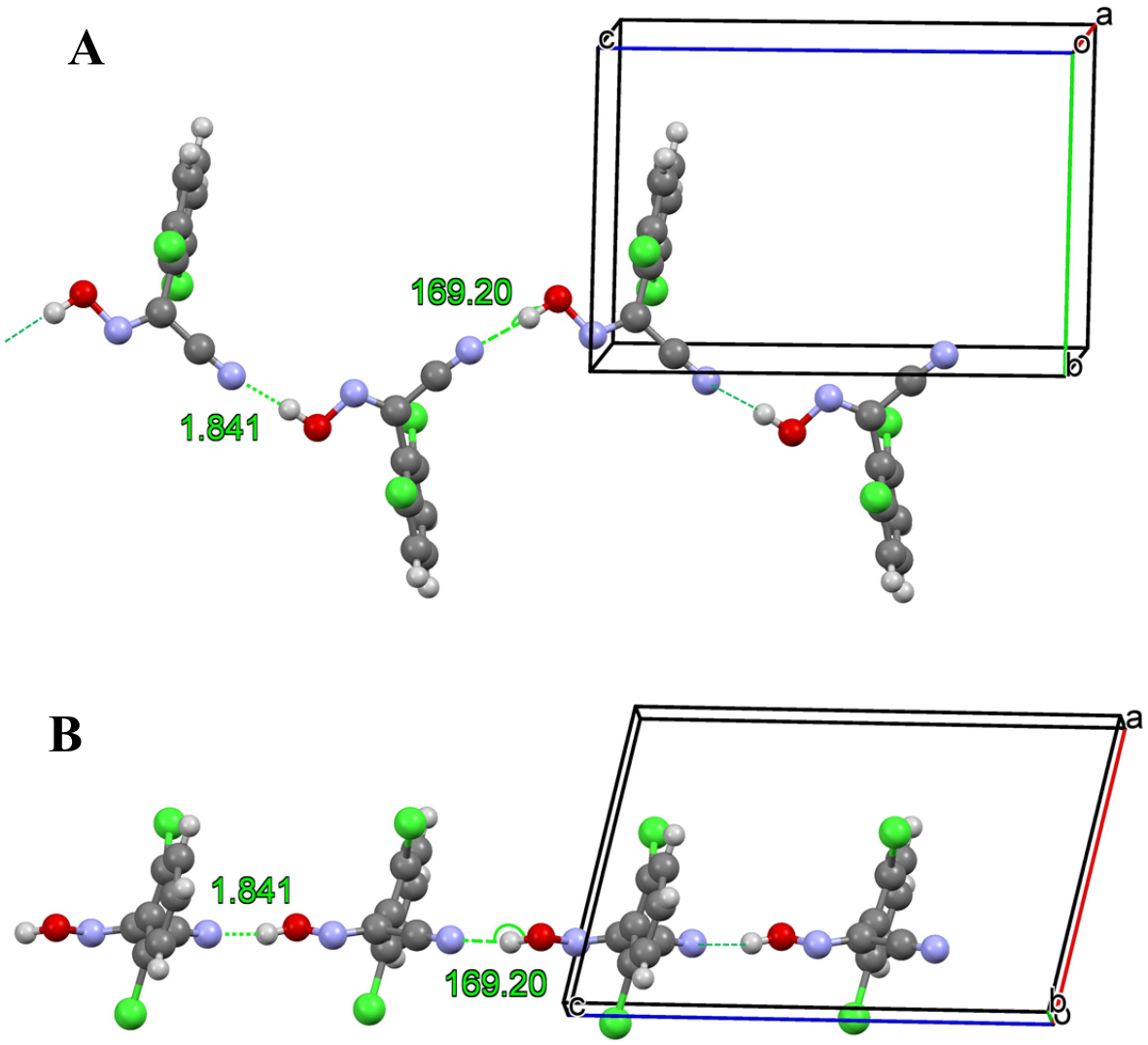

Figure 20. Geometry of H-bonding in the structure of *syn*-H(2,6-diCl-PhCO) showing bond and angle in C≡N---H-O fragment: **A** – pruned view of the chain along *a*-direction; **B** – along *b*-direction.

Comparison of crystal structures of two diastereomers intuitively suggests that the *syn*-isomer is more compact due to an inward orientation of the oxime fragment. Indeed this is the case: density of the *syn*-isomer is greater (d=1.5631 g/cm^3) as for the *anti*-isomer (d=1.479

g/cm^3), and the structure of discussed in this work *syn*-diastereomer occupies 62.5% of the unit cell volume (Table 3) as compared for the 58.1% value in the *anti*-diastereomer.[67]

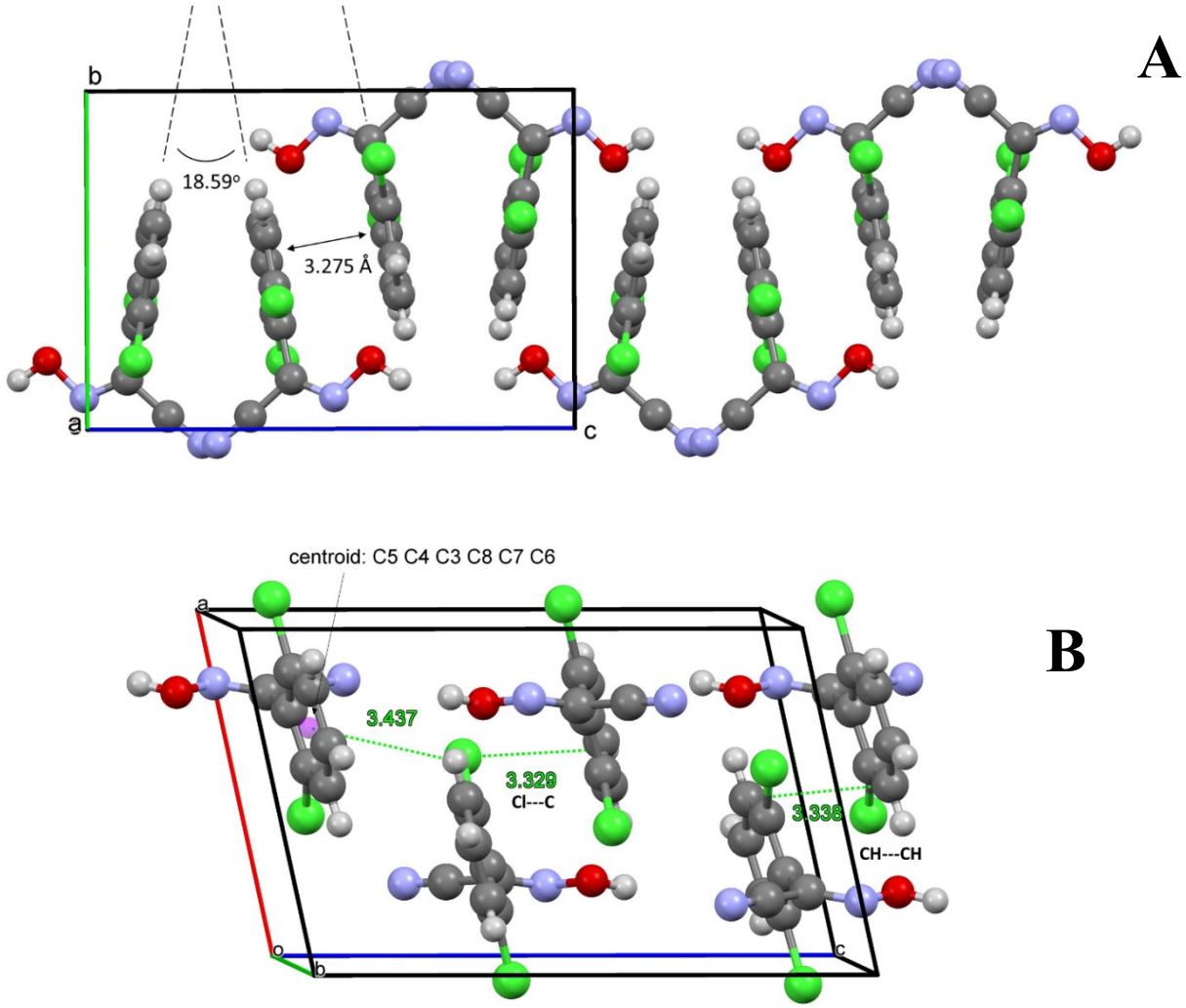

Figure 21. Organization of crystal packing in the columnar structure of *syn*-H(2,6-diCl-PhCO): **A** – formation of zigzag column running along *c*-direction showing parallel *c*-direction; **B** – all short intermolecular contacts in the structure.

Table 4. Selected* bond lengths and valence angles (degrees) for the cyanoxime fragment in two structurally characterized *anti*- and *syn*-(bis-chlorinated) arylcyanoximes.

anti- & *syn*-H(2,6-diCl-PhCO)			
anti-H(2,6-diCl-PhCO) [data from ref. 67]		*syn*-H(2,6-diCl-PhCO)	
Bond length, Å			
O(1)-N(1)	1.352	O(1)-N(1)	1.368(3)
N(1)-C(7)	1.323	N(1)-C(1)	1.292(3)
N(2)-C(8)	1.134	N(2)-C(2)	1.145(3)
C(1)-C(7)	1.474	C(1)-C(2)	1.442(3)
C(7)-C(8)	1.439	C(1)-C(3)	1.485(3)
Valence angle,°			
C(7)-N(1)-O(1)	108.1	C(7)-N(1)-O(1)	111.3(2)
N(1)-C(7)-C(8)	124.0	N(1)-C(7)-C(8)	127.3(2)
N(1)-C(7)-C(1)	116.2	N(1)-C(7)-C(1)	114.4(2)
C(8)-C(7)-C(1)	119.8	C(8)-C(7)-C(1)	118.2(2)
N(2)-C(8)-C(7)	177.2	N(2)-C(8)-C(7)	176.4(3)

* - geometry of the phenyl group with attached halogen atoms is normal and not shown.

The Crystal Structure of H(TDCO). This compound was obtained first time in 1992 by Konstantin Domasevitch,[93] who was working in Prof. Gerasimchuk research group, but was never crystallographically characterized. The only available structure for this thioamide-cyanoxime is in its Tl-complex: Tl(TDCO).[94] The crystal and refinement data are shown in Table 5. The asymmetric unit (ASU) in the structure of this thioamide-cyanoxime H(TDCO) is presented in Figure 22. Important bonds/angles are shown in Figure 23. In this structure the cyanoxime adopts *trans-anti* geometry. The molecule is highly non-planar with dihedral angle between the cyanoxime and the thioamide groups being 60.80° as shown in Figure 24. Hydrogen bonding leads to the formation of chains within the crystal structure of H(TDCO). This can be seen in Figure 25 along this the hydrogen bond lengths. The parameters for this rare hydrogen bond between sulfur and the oxime hydrogen are O1-H1O1---S1 = 2.24(4) Å, H1O1---S1 =

3.154(2) Å with <DHA = 152(3). This is very rare case of the S---H-O- hydrogen bonding. Other intermolecular forces such as electrostatic and van-der-Waal further stabilize the crystal structure. This thioamide-cyanoxime H(TDCO) is the only precursor for synthesis of complexes based on this ligand. Using protonated cyanoxime it was possible to prepare its Cs^+ and then Tl^+ salts with the latter being the most important starting compound for preparation of trimethyl-antimony(V) cyanoximates.

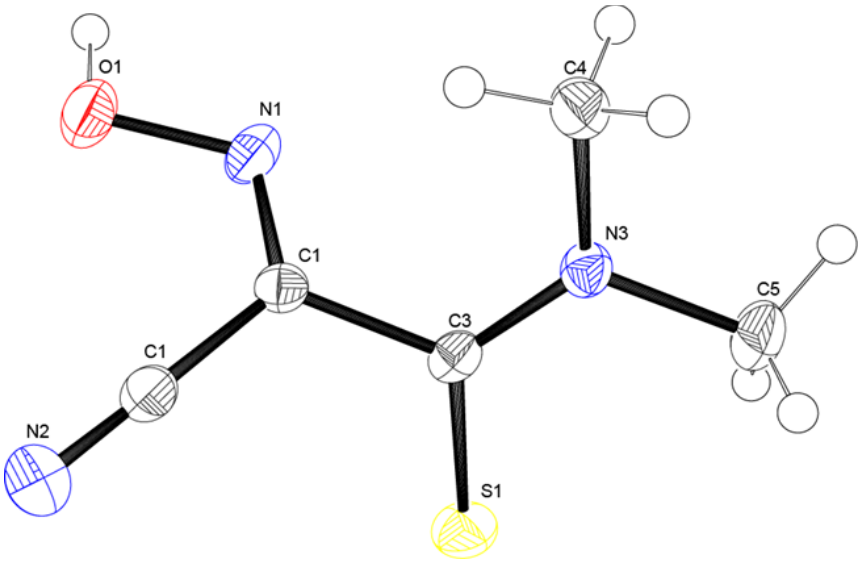

Figure 22. The ASU in the structure of one of the initial compounds H(TDCO) showing atomic numbering scheme.

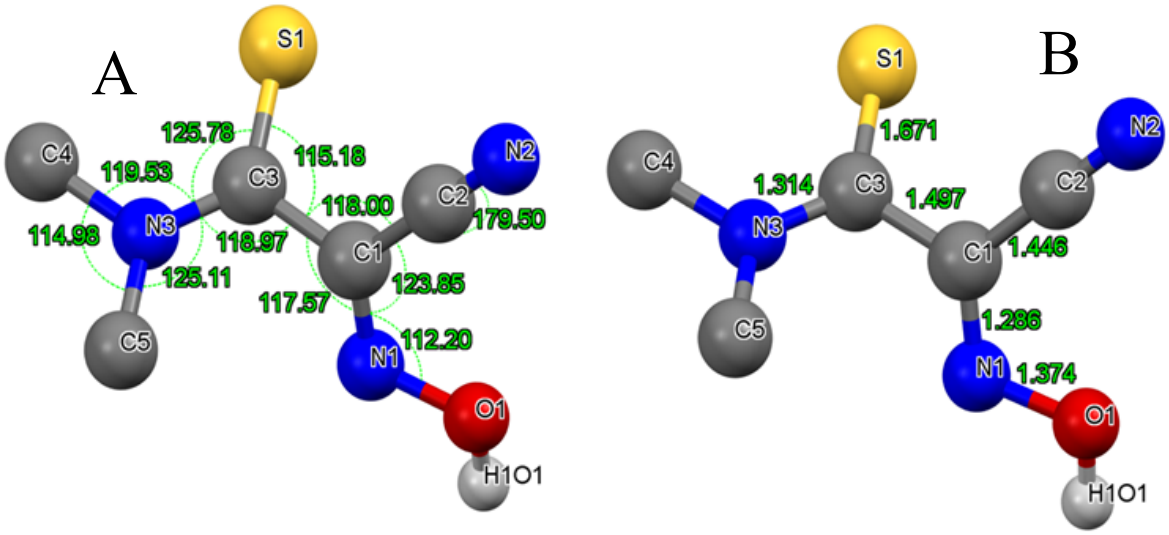

Figure 23. Some geometrical details in the structure of H(TDCO): **A** – valence angles; **B** – selected bond lengths. H-atoms are omitted for clarity.

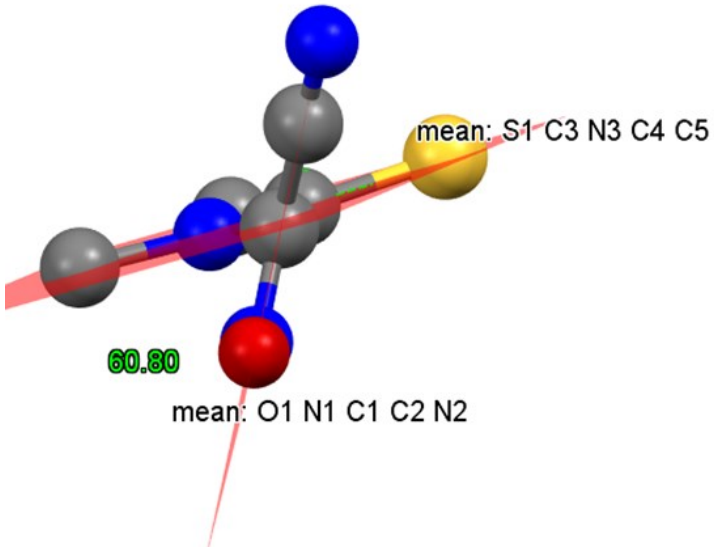

Figure 24. Dihedral angle between mean planes for the thioamide and the cyanoxime groups.

Table 5. Crystal and refinement data for H(TDCO).

Parameter	**H(TDCO)**
Empirical formula	$C_5H_7N_3OS$
Formula weight, g/mol	157.20
Temperature, K	100(2)
Wavelength, Å	0.71073
Crystal size, mm	0.217×0.183×0.165
Color	yellow
Crystal system	monoclinic
Space group	$P2_1/c$
Unit cell dimensions, Å, °	a = 9.9455(11) α = 90 b = 6.5012(8) β = 106.840(2) c = 12.0927(14) γ = 90
Unit cell volume, $Å^3$	748.36(15)
Z	4
Density (calculated), g/cm^3	1.395
Absorption coefficient, mm^{-1}	0.366
F (000)	328
Θ range, °	2.14 to 26.00
Index ranges	-12 ≤ h ≤ 12 -8 ≤ k ≤ 8 -14 ≤ l ≤ 14
Reflections collected	7407
Independent reflections	1461 [$R_{(int)}$ = 0.0617]
Transmission (max and min)	0.745 and 0.615
Data / restraints / parameters	1461 / 0 / 119
Goodness-of-fit on F^2	1.076
Final R indices [I>2σ(I)]	1215 data; R1 = 0.0469 wR2 = 0.1233
R indices [all data]	R1 = 0.0562 wR2 = 0.1289
Largest diff. peak and hole, $eÅ^{-3}$	0.682 and -0.230

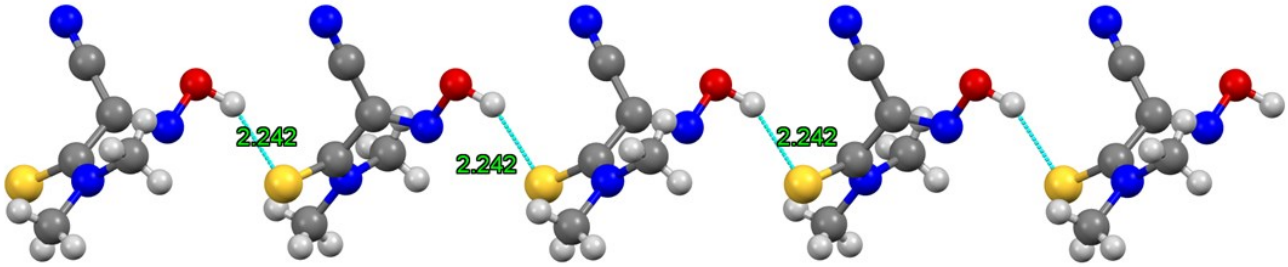

Figure 25. H-bonding distances viewed along *b* - axis.

The Crystal Structure of "Cs(TDCO)". The Cs-salt was obtained using Cs_2CO_3 and H(TDCO) at room temperature. Block-type crystals grew from aqueous solution in plastic vial dark within ~2 months under inert conditions (Ar). It turned out that after structure solution, the compound had formula Cs(TDCO)×H(TDCO) representing an acid salt of monoxime.[95] There are two types of those salts: one with equidistant position of the bridging H-atom between two identical anions (somewhat like HF_2^- anions), and the second one with practically co-crystallized in one lattice protonated oxime HL and its CatL salt (Cat = NH_4^+, Na^+, K^+). Cases of formation of this type of compounds are known, but very rare.

Crystal and refinement data for this salt are shown in Table 6. The asymmetric unit (ASU) in the structure of Cs(TDCO)×H(TDCO) is shown in Figure 26. Selected bond lengths and valence angles are presented in Table 7. The structure is rare case of an acid salt[89], but not of Cat{HL_2} type previously observed for Na^+ and K^+ salts.[82,96] In this case, however, this acid salt has a distinctive anion and a distinctive protonated ligand contrary to many of those with equidistant position of the hydrogen atom between the cyanoximes.[89] The cesium atom is not bound to any specific atom of the cyanoximes moieties as depicted in Figure 26. It rather has a highly distorted environment with multiple atoms surrounding it with multiple angles as for the

typical *ionic compound*. This compound is heavily non-planar due to the bulkiness of the dimethylamine $N(Me)_2$ fragment in the ligand. The dihedral angle between the cyanoxime group and the thioamide fragment is 61.61 ° for the anion and 69.21 ° for the protonated oxime. Both values are much larger than the other complexes of TDCO anion due to the presence of Cs^+ ion. The cyanoxime in both moieties adopt exceedingly rare pure *trans-anti-* geometry. Their bond lengths for the cyanoxime group are all acceptable and within the expected range. Hydrogen bonding helps secure the lattice structure as well as electrostatic and van-der-Waal forces.[89] Hydrogen bonding is made possible by the protonated ligand within the structure (Figure 26).

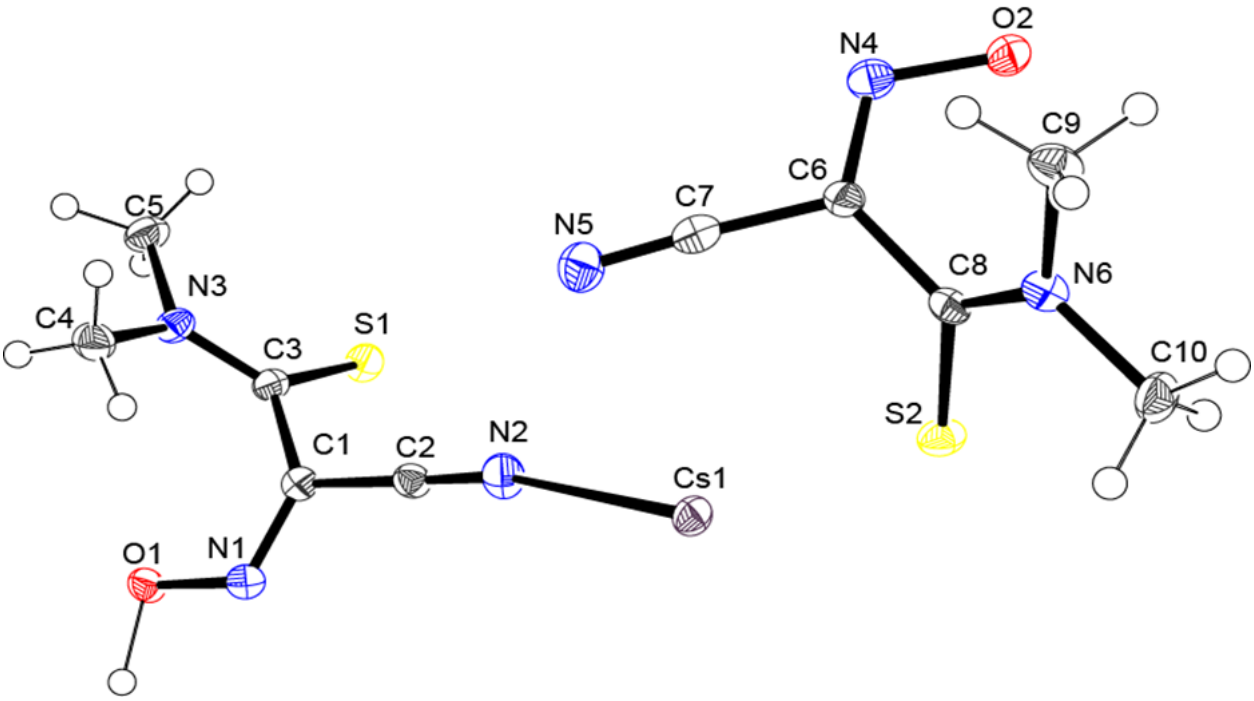

Figure 26. The ASU in the structure of Cs(TDCO)×H(TDCO) depicting the numbering scheme.

Table 6. Crystal and refinement data for the acid salt of Cs(TDCO)×H(TDCO).

Parameter	**Cs(TDCO) ×H(TDCO).**
Empirical formula	$C_5H_6CsN_3OS$
Formula weight, g/mol	223.15
Temperature, K	100.15
Wavelength, Å	0.71073
Crystal size, mm	0.117×0.105×0.091
Color	orange
Crystal system	triclinic
Space group	*P- 1*
Unit cell dimensions, Å, °	a = 6.4244(6) α = 105.1810(10)
	b = 10.2553(10) β = 101.3430(10)
	c = 13.3679(13) γ = 96.8400(10)
Unit cell volume, $Å^3$	819.74(14)
Z	4
Density (calculated), g/cm^3	1.8080
Absorption coefficient, mm^{-1}	2.525
F (000)	436.1
Θ range, °	4.18 to 56
Index ranges	$9 \leq h \leq 9$
	$-15 \leq k \leq 15$
	$-19 \leq l \leq 19$
Reflections collected	13640
Independent reflections	3932 [R_{int} = 0.0774, R_{sigma} = 0.1059]
Transmission (max and min)	0.7645 and 0.6950
Data / restraints / parameters	3932/2/193
Goodness-of-fit on F^2	0.937
Final R indices [I>2σ(I)]	R1 = 0.0411
	wR2 = 0.0948
R indices [all data]	R1 = 0.0485
	wR2 = 0.0988
Largest diff. peak and hole, $eÅ^{-3}$	1.00 and -1.05

Table 7. Selected bond lengths and valence angles of the ligand Cs(TDCO)xH(TDCO).

Cs(TDCO)xH(TDCO).			
Bond length, Å		**Valence angle,°**	
O1 - N1	1.345(4)	C1 - N1 - O1	114.3(3)
N1 - C1	1.297(5)	C2 - C1 - N1	114.0(4)
C1 - C2	1.448(6)	N1 - C1 - C3	128.0(4)
C1 - C3	1.491(5)	C3 - C1 - C2	117.3(4)
C2 - N2	1.149(5)	N2 - C2 - C1	179.1(4)
C3 - N3	1.324(5)	N3 - C3 - S1	125.0(3)
C3 - S1	1.674(4)	N3 - C3 - C1	118.6(4)
		C1 - C3 - S1	116.3(3)

V. 3. Tl- Cyanoximates.

All the Tl(I)-cyanoximates were prepared by Dr. Gerasimchuk to avoid graduate students' exposure to stench or toxic chemical compounds. These were all precursors for the antimony cyanoximates synthesized.

Crystal structure of Tl(4-Cl-PhCO). Selected bond lengths and valence angles within the molecule are presented in Table 8. The crystal and refinement data are shown in the Table 9. The asymmetric unit (ASU) structure of Tl(4-Cl-PhCO) is shown in Figure 27. All the hydrogens within the complex were identified on the electron difference map and refined to create this ASU structure. The cyanoxime anion adopts an anti-geometry with no trans or cis assignment of geometry since the chlorine atom is in the para position to the cyanoxime fragment. The two fragments present within the molecule are the chloro-aryl group and the cyanoxime group. Both fragments are planar, but the molecule is non-planar. This is due to the dihedral angle between the chloro-aryl group and the cyanoxime group which is 9.47 °. This angle was calculated using mean planes Cl1-C6-C7-C8-C3-C4-C5 and N2-C3-C1-N1-O1, respectively. This is very similar to the structure of ligand H(4-Cl-PhCO) and metal complex Tl(4-Br-PhCO).[57] The bond lengths

for N1-C1 = 1.308(7) Å and N1-O1 = 1.340(6) Å are within range of bond lengths observed for the cyanoxime group in similar classes of compounds. When compared to the ligand H(4-Cl-PhCO),[57] the bond lengths are 1.289 Å and 1.378 Å respectively, with differences between bond lengths for the ligand and the metal complex attributed to the redistribution of the electron density in the C-N-O fragment during the complexation to the metal Tl center.[57,67] Interestingly, the sum of these bond lengths in both the ligand and the metal complex are almost identical with 2.667 Å for H(4-Cl-PhCO) and 2.648 Å for Tl(4-Cl-PhCO). The π-π stacking interactions between 4-chlorophenyl rings of neighboring molecules holds the structure together in packing with the distance between the 2 closest centroids of the 4-chlorophenyl rings being 4.085 Å. Intra- and inter molecular forces, along with van-der-Waal forces are also present to stabilize the crystal structure.

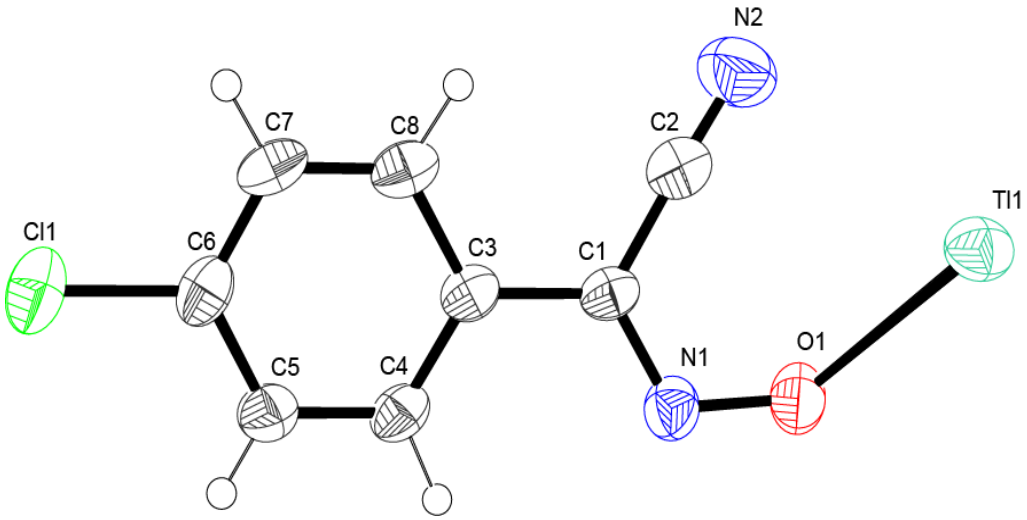

Figure 27. The ASU in the structure of one of the initial compounds Tl(4-Cl-PhCO) drawn in ORTEP representation at 50% ellipsoid probability level showing atomic numbering.

Table 8. Crystal and refinement data for Tl (4-Cl-PhCO).

Parameter	**Tl (4-Cl-PhCO)**
Empirical formula	$C_8H_4ClN_2OTl$
Formula weight, g/mol	383.95
Temperature, K	296(2)
Wavelength, Å	0.71073
Crystal size, mm	0.193×0.051×0.041
Color	lemon - yellow
Crystal system	monoclinic
Space group	*P 1 21/n 1*
Unit cell dimensions, Å, °	a = 10.951(4) α = 90 b = 4.0853(15) β = 99.041(4) c = 20.616(7) γ = 90
Unit cell volume, $Å^3$	910.9(6)
Z	4
Density (calculated), g/cm^3	2.800
Absorption coefficient, mm^{-1}	17.980
F (000)	688
Θ range, °	2.00 to 28.90
Index ranges	-14 ≤ h ≤ 14 -5 ≤ k ≤ 5 -27 ≤ l ≤ 28
Reflections collected	10544
Independent reflections	2391 [R_{int} = 0.0544]
Transmission (max and min)	0.641 and 0.327
Data / restraints / parameters	2391 / 0 / 130
Goodness-of-fit on F^2	1.025
Final R indices [I>2σ(I)]	1893 data; R1 = 0.0362 Wr2 = 0.0829
R indices [all data]	R1 = 0.0490 Wr2 = 0.0892
Largest diff. peak and hole, e $Å^{-3}$	1.857 and -2.041

Table 9. Selected bond lengths and valence angles of the ligand Tl(4-Cl-PhCO).

Tl(4-Cl-PhCO)			
Bond length, Å		**Valence angle, °**	
O1 - N1	1.340(6)	C1 - N1 - O1	115.9(4)
N1 - C1	1.308(7)	C2 - C1 - N1	119.4(5)
C1 - C2	1.440(8)	N1 - C1 - C3	120.1(5)
C1 - C3	1.474(8)	C3 - C1 - C2	120.5(5)
C2 - N2	1.133(8)	N2 - C2 - C1	177.6(7)
Cl1 - C6	1.734(6)	N1 – O1 - TlO1	90.3(3)

Crystal structure of Tl(2,4-diCl-PhCO). Selected bond lengths and valence angles can be seen in Table 10. The crystal and refinement data for Tl(2,4-diCl-PhCO) is presented in Table 11. The ASU is shown in Figure 28. All 3 hydrogens on the phenyl ring were attached and refined isotropically. The crystal specimen was an inversion twin and forms an elegant dimer (Figure 29A) when viewed with Hg with both cyanoximes on each side adopting a *trans*-anti geometry. This compound was highly non-planar with planar fragments. The dihedral angle, α, formed between mean planes of the cyanoxime group and the chloro-aryl group was 51.49 ° (Figure 29B). In comparison to the ligand H(2,4-diCl-PhCO), the dihedral angle is almost similar with 50.61 °.[81] The bonds in the cyanoxime group were N1-O1 = 1.294(12) Å and N1-C1 = 1.314(13) Å. These were within the normal ranges for cyanoxime group in similar compounds. There is no hydrogen bonding present but π-π stacking interactions between the 2,4-chlorophenyl groups at 3.869 Å contribute to the lattice formation and the overall architecture of the structure. Compared to the ligand H(2,4-diCl-PhCO) which has π-π stacking interactions at 3.695 Å,[81] the difference can be the presence of H bonding holding parallel sheets of molecules together.

Columns within the crystal structure are also held together by van-der-Waal forces between the 4-chloophenyl groups.

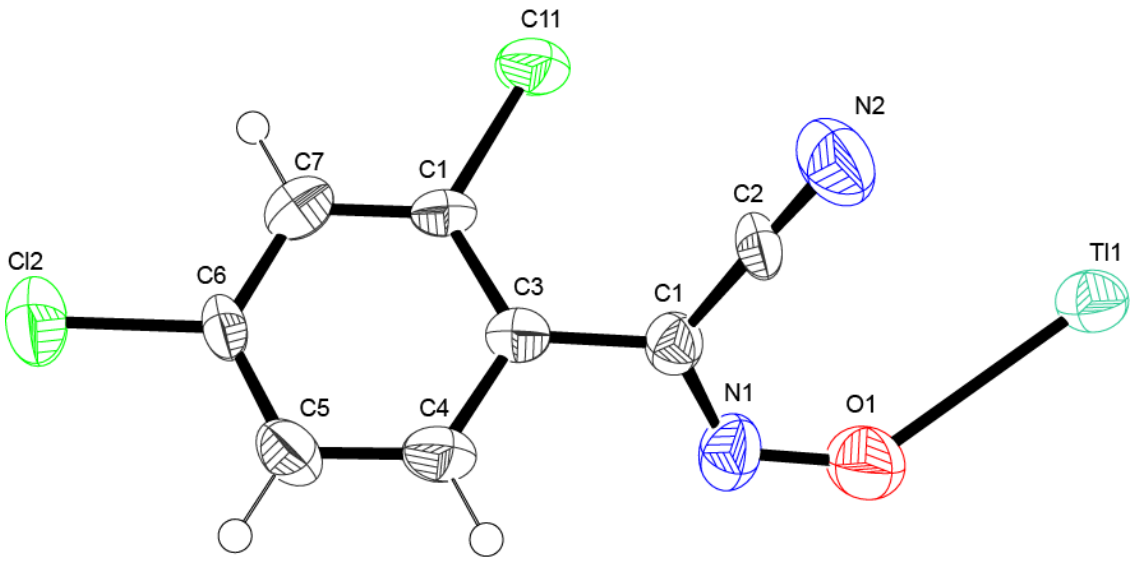

Figure 28. The ASU in the structure of one of the initial compounds Tl(2,4-diCl-PhCO) drawn in ORTEP representation and showing atomic numbering.

Table 10. Selected bond lengths and valence angles of the ligand Tl(2,4-diCl-PhCO).

Tl(2,4-diCl-PhCO)			
Bond length, Å		**Valence angle,º**	
O1 - N1	1.294(12)	C1 - N1 - O1	115.8(10)
N1 - C1	1.314(13)	C2 - C1 - N1	121.3(9)
C1 - C2	1.402(13)	N1 - C1 - C3	117.5(9)
C1 - C3	1.466(13)	C3 - C1 - C2	120.4(9)
C2 - N2	1.151(13)	N2 - C2 - C1	177(1)
Cl1 – C8	1.734(9)		
Cl2 - C6	1.756(9)		

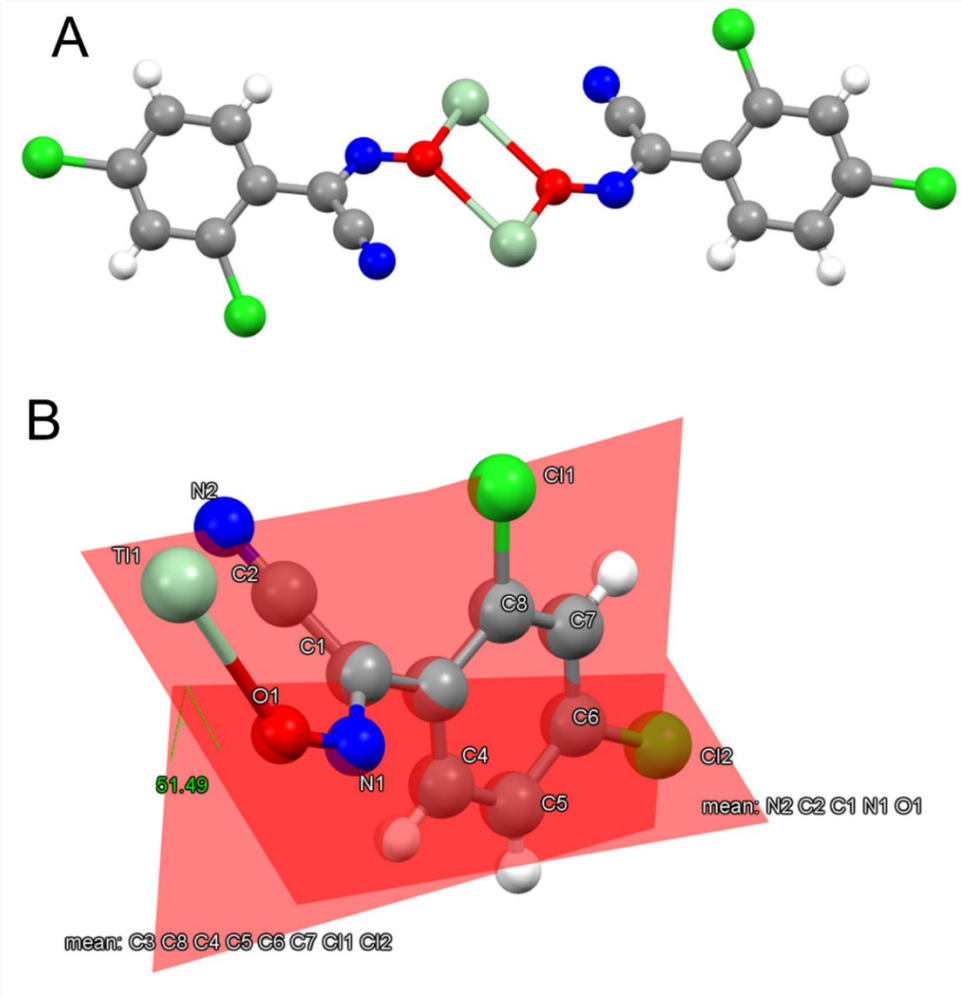

Figure 29. Molecular structure of Tl(2,4-diCl-PhCO) presented using mercury software package. **(A)** Dimeric structure of Tl(2,4-diCl-PhCO). **(B)** Dihedral angle, α, between the cyanoxime and the chloro-aryl group.

Table 11. Crystal and refinement data for Tl(2,4-diCl-PhCO).

Parameter	Tl(2,4-diCl-PhCO)
Empirical formula	$C_8H_3Cl_2N_2OTl$
Formula weight, g/mol	418.41
Temperature, K	296.15
Wavelength, Å	1.54184
Crystal size, mm	0.186×0.109×0.095
Color	Light-yellow
Crystal system	Monoclinic
Space group	*C 1 2/c 1*
Unit cell dimensions, Å, °	a = 37.013(9) α = 90 b = 3.8692(10) β = 107.072(3) c = 14.624(4) γ = 90
Unit cell volume, $Å^3$	2002.0(9)
Z	8
Density (calculated), g/cm^3	2.7761
Absorption coefficient, mm^{-1}	16.638
F (000)	1487.0
Θ range, °	4.6 to 66.02
Index ranges	-54 ≤ h ≤ 50, -5 ≤ k ≤ 5, -21 ≤ l ≤ 21
Reflections collected	10667
Independent reflections	3433 [R_{int} = 0.0437]
Transmission (max and min)	0.811 and 0.418
Data / restraints / parameters	3433 / 0 / 122
Goodness-of-fit on F^2	1.037
Final R indices [I>2σ(I)]	R1 = 0.0564 wR2 = 0.1164
R indices [all data]	R1 = 0.0822 wR2 = 0.1282
Largest diff. peak and hole, $eÅ^{-3}$	2.81 and -3.29

Crystal structure of Tl(2,6-diCl-PhCO). Important bond lengths and valence angles are shown in Table 12. The crystal data for Tl(2,6-diCl-PhCO) is shown in Table 13. The asymmetric unit for Tl(2,6-diCl-PhCO) is shown in Figure 30. Its crystalline specimen proved

difficult to work with because it was multidomain, but only main domain reflections were being used to analyze the crystalline structure. It was found to just be an overlaying of several crystals. Tl(2,6-diCl-PhCO) forms a dimer (Figure 31), and the cyanoxime adopts an anti-geometry, with all the H-atoms attached manually to their hosting C-atoms in APEX. The dihedral angle between the chloro-aryl group and the cyanoxime (Figure 31) was 57.62 ° attesting to the non-planarity of the compound. The ligand H(2,6-diCl-PhCO)[59,67] on the other hand has a dihedral angle of 77.1 °. The bond lengths for N1-C1 = 1.30(3) Å and N1-O1 = 1.35(2) Å are within the normal ranges for the cyanoxime bond lengths in similar class of compounds. These are identical to that of the bond lengths in the ligand H(2,6-diCl-PhCO) with 1.323 Å and 1.352 Å respectively. Electrostatic attractions are present to stabilize the structure. Furthermore, the presence of π–π stacking interactions between neighboring di-chloroaryl fragments and van-der-Waal forces help stabilize the crystal structure.

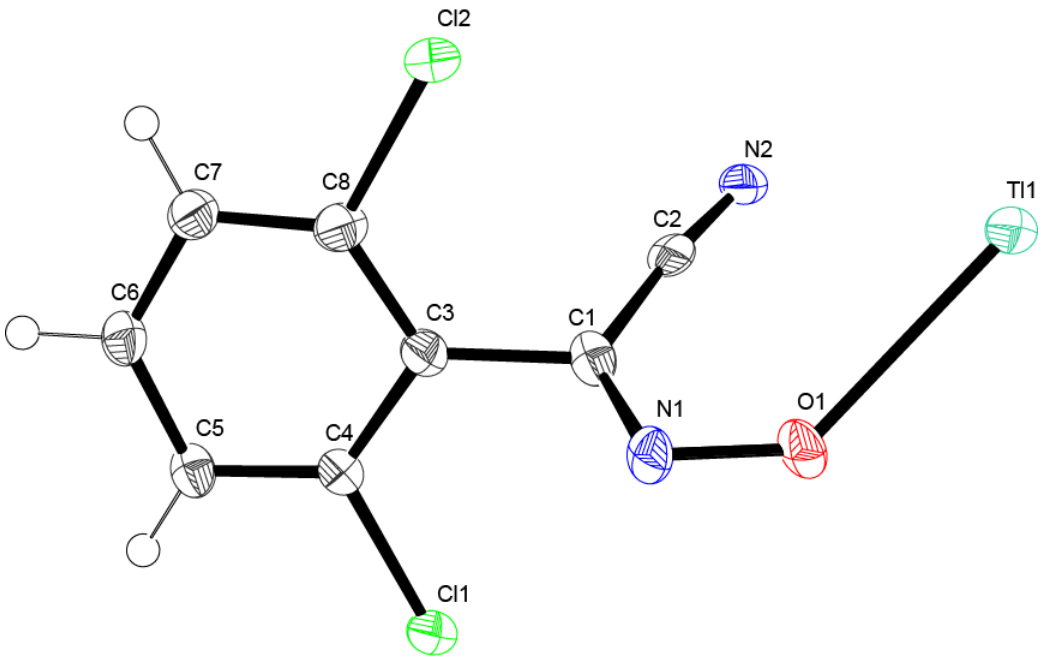

Figure 30. The ASU in the structure of one of the initial compounds Tl(2,6-diCl-PhCO) drawn in ORTEP representation showing atomic numbering.

Table 12. Selected bond lengths and valence angles of the ligand Tl(2,6-diCl-PhCO).

Tl(2,6-diCl-PhCO)			
Bond length, Å		**Valence angle,°**	
O1 - N1	1.35(2)	C1 - N1 - O1	111.2(18)
N1 - C1	1.30(3)	C2 - C1 - N1	125.0(2)
C1 - C2	1.39(3)	N1 - C1 - C3	115.6(19)
C1 - C3	1.54(3)	C3 - C1 - C2	119.0(2)
C2 - N2	1.13(3)	N2 - C2 - C1	173.0(3)
Cl1 – C4	1.77(2)		
Cl2 – C8	1.77(2)		

Table 13. Crystal and refinement data for Tl (2, 6-diCl-PhCO).

Parameter	**Tl (2, 6-diCl-PhCO)**
Empirical formula	$C_8H_4Cl_2N_2OTl$
Formula weight, g/mol	419.40
Temperature, K	150(2)
Wavelength, Å	0.71073
Crystal size, mm	0.143×0.056×0.051
Color	lemon - yellow
Crystal system	monoclinic
Space group	*P 1 21/n 1*
Unit cell dimensions, Å, °	a = 4.070(12) α = 90 b = 7.73(2) β = 91.01(5) c = 31.04(9) γ = 90
Unit cell volume, $Å^3$	976.(5)
Z	4
Density (calculated), g/cm^3	2.852
Absorption coefficient, mm^{-1}	17.047
F (000)	756
Θ range, °	2.63 to 30.52
Index ranges	$-1 \leq h \leq 5$ $-10 \leq k \leq 10$ $-31 \leq l \leq 33$
Reflections collected	3816
Independent reflections	2440 [R_{int} = 0.0966]
Transmission (max and min)	-
Data / restraints / parameters	2440 / 110 / 122
Goodness-of-fit on F^2	0.921
Final R indices [I>2σ(I)]	1275 data; R1 = 0.0796 wR2 = 0.1676
R indices [all data]	R1 = 0.1539 wR2 = 0.2004
Largest diff. peak and hole, $eÅ^{-3}$	4.768 and -3.392

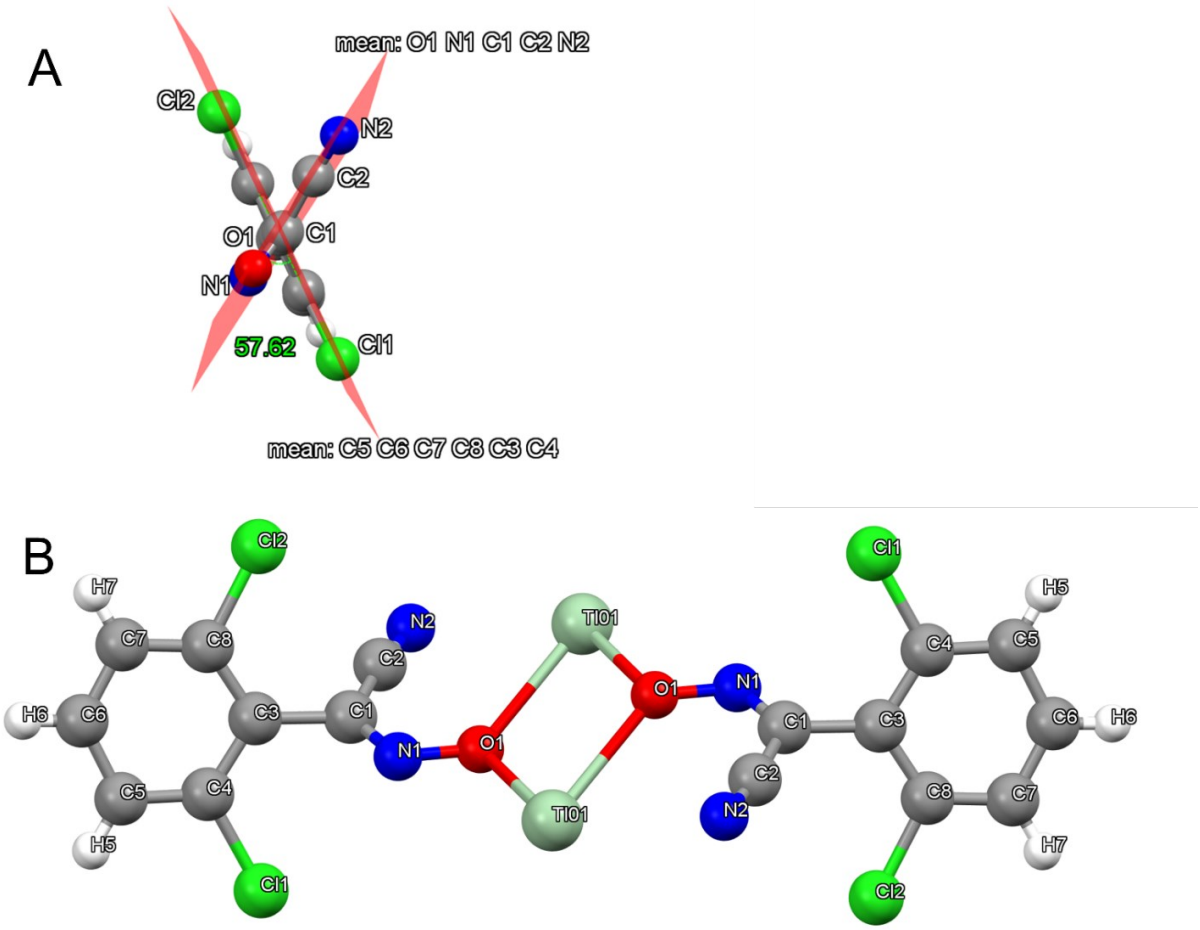

Figure 31. Molecular structure of Tl(2,6-diCl-PhCO) presented using the help of mercury program. **(A)** Dihedral angle, α, between the cyanoxime and the chloro-aryl group. **(B)** Dimeric structure of Tl(2,6-diCl-PhCO).

Crystal structure of Tl(TCO). The crystal and refinement data for Tl(TCO) are shown in Table 14. The ASU is presented in Figure 33. All H-atoms were attached to hosting N-atom within the structure. Selected bond lengths and valence angles are shown in Table 15. The cyanoxime adopts a *trans*-anti geometry. The molecule is planar with dihedral angle between the mean planes for the thioamide and the cyanoxime being around 3.51 Å. The bond lengths for N1-C1 = 1.333(6) and N1-O1 = 1.320(5) of the cyanoxime fragment are within range for the observed bond lengths in similar complexes. Intra- and inter-molecular forces present within

Tl(TCO) are highlighted in Figure 32. The hydrogen bond parameters are as follows; N3-H3B---O1 = 2.06 Å, H3B---O1 = 2.06 Å with the angle <DHA = 162.6 °; N3-H3A---N2 = 2.20, H3A---N2 = 2.856(6) with <DHA = 131.2 °. These H- bonds lead to the formation of sheets within the crystal. There are also intermolecular van-der-Waal forces and electrostatic interactions that further stabilize the crystal structure of Tl(TCO).

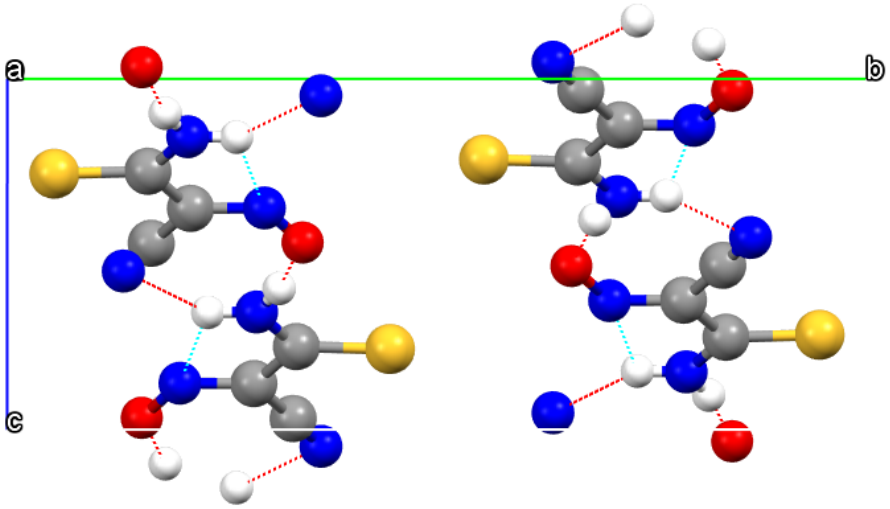

Figure 32. Hydrogen bonding within and between molecules of Tl(TCO) viewed along *a*-axis. *Tl atom is omitted from structure for clarity.

Table 14. Crystal and refinement data for Tl(TCO).

Parameter	**Tl(TCO)**
Empirical formula	$C_3H_2N_3OSTl$
Formula weight, g/mol	332.51
Temperature, K	100(2)
Wavelength, Å	0.71073
Crystal size, mm	0.164 x 0.197 x 0.231
Color	clear light orange-yellow
Crystal system	monoclinic
Space group	*P 1 21/c 1*
Unit cell dimensions, Å, °	a = 6.1861(5) α = 90
	b = 15.4823(12) β = 104.7800(10)
	c = 6.5276(5) γ = 90
Unit cell volume, $Å^3$	604.50(8)
Z	4
Density (calculated), g/cm^3	3.654
Absorption coefficient, mm^{-1}	26.971
F (000)	584
Θ range, °	2.63 to 25.99
Index ranges	-7<=h<=7
	-19<=k<=19
	-8<=l<=8
Reflections collected	6788
Independent reflections	1188 [$R_{(int)}$ = 0.0333]
Transmission (max and min)	0.0960 and 0.0620
Data / restraints / parameters	1188 / 0 / 82
Goodness-of-fit on F^2	1.124
Final R indices [I>2σ(I)]	1120 data; R1 = 0.0173
	wR2 = 0.0407
R indices [all data]	R1 = 0.0185
	wR2 = 0.0411
Largest diff. peak and hole, $eÅ^{-3}$	1.409 and -1.169 $eÅ^{-3}$

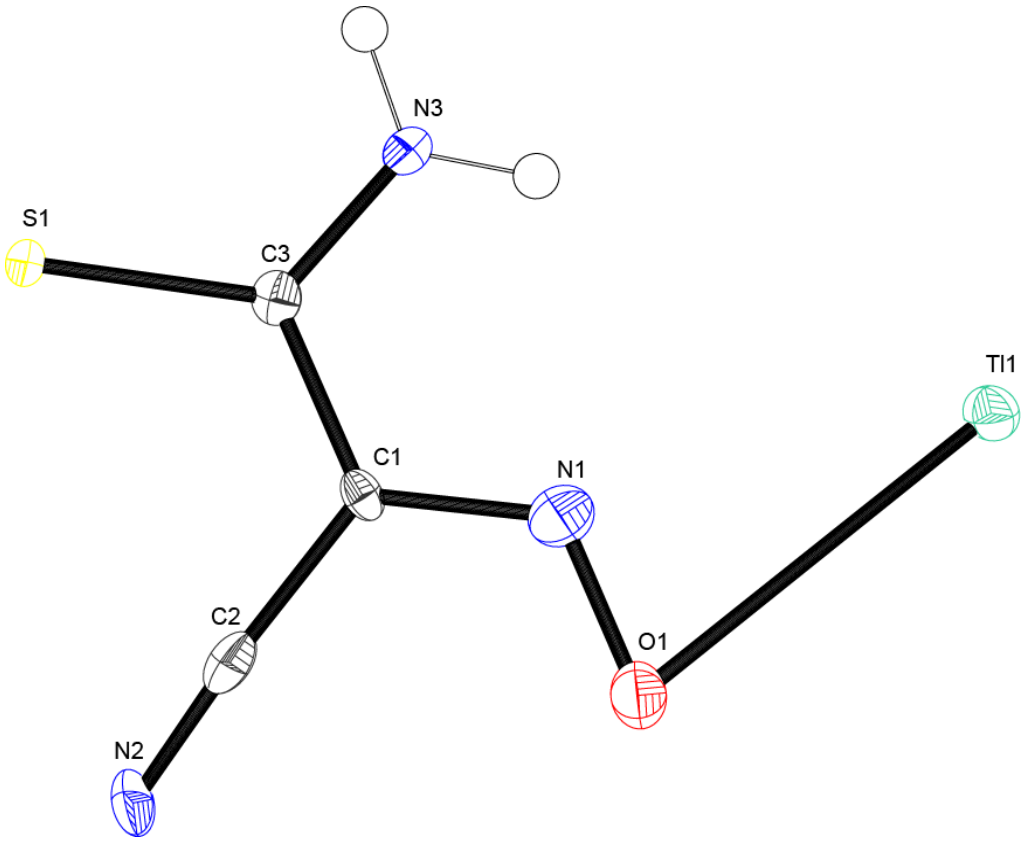

Figure 33. The ASU in the structure of one of the initial compounds Tl(TCO) drawn in ORTEP representation at 50% ellipsoid probability level.

Table 15. Selected bond lengths and valence angles of the ligand Tl(TCO).

Tl(TCO)			
Bond length, Å		**Valence angle,°**	
O1 - N1	1.320(5)	C1 - N1 - O1	119.1(4)
N1 - C1	1.333(6)	C2 - C1 - N1	121.6(4)
C1 - C2	1.446(7)	N1 - C1 - C3	119.5(4)
C1 - C3	1.457(6)	C3 - C1 - C2	119.0(4)
C2 - N2	1.160(6)	N2 - C2 - C1	176.2(5)
C3 – N3	1.333(6)	N3 - C3 - S1	123.1(4)
C3 – S1	1.687(5)	N3 - C3 - C1	115.7(4)
		C1 - C3 - S1	121.2(3)

V. 4. Antimony (V) Cyanoximates

Crystal structure of $SbMe_3(4\text{-Cl-PhCO})_2$. Crystal and refinement data for $SbMe_3(4\text{-Cl-PhCO})_2$ is presented in Table 16. Bond lengths and valence angles are summarized in Table 17. Both anions within the $SbMe_3(4\text{-Cl-PhCO})_2$ adopt an anti-geometry (Figure 34). All the H-atoms were calculated and placed onto hosting C-atoms for the structural solution. All methyl groups attached to the metal Sb center were slightly different from each other in bond lengths. The bond angle for O2-Sb1-O1 is less than 180° meaning the metal center and its bonded atoms for a slightly distorted trigonal bipyramid geometry when compared to the initial starting compound $SbMe_3Br_2$. The two anions within the molecular structure possess different planarity as shown in Figure 35. This is mostly due to the interactions within the environment of each anion. The bond lengths of the cyanoxime groups N1-C1 = 1.306(4) Å, N3-C9 = 1.284(4) Å, N1-O1 = 1.354(3) Å, and N3-O2 = 1.375(3) Å are all within the expected and previously published bond lengths. Again, differences between bond lengths for the ligand H(4-Cl-PhCO)[57,83,88] and the antimony cyanoximate can be attributed to the redistribution of the electron density in the C-N-O fragment during the complexation to the metal Sb center. The difference in the dihedral angles within the molecule can only be explained by the presence of bulkier atoms near cyanoxime 35A than 35B and hence there is less steric strain present in 15B. Tl(4-Cl-PhCO) has a larger dihedral angle than 35A and a smaller angle than 35B. The crystal structure is held together by π-π interactions and van-der-Waal forces.

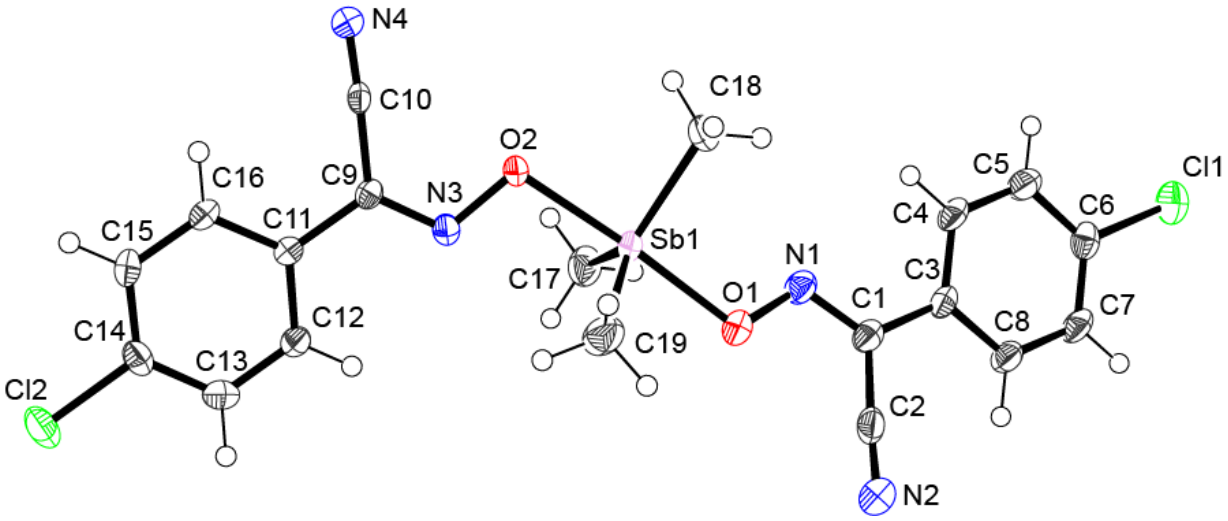

Figure 34. Molecular structure and atomic numbering of $SbMe_3(4Cl\text{-}PhCO)_2$.

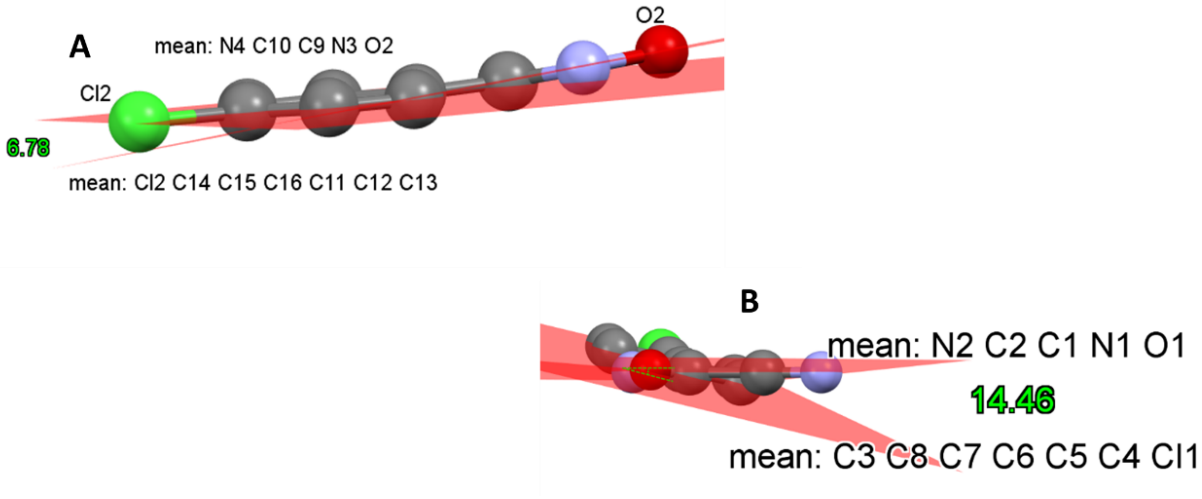

Figure 35. Planarity within the molecular structure of $SbMe_3(4Cl\text{-}PhCO)_2$. **(A)** anion with Cl2 and O2; **(B)** anion with Cl1 and O1.

Table 16. Crystal and refinement data for $SbMe_3(4\text{-Cl-PhCO})_2$.

Parameter	**$SbMe_3(4\text{-Cl-PhCO})_2$**
Empirical formula	$C_{19}H_{17}Cl_2N_4O_2Sb$
Formula weight, g/mol	526.02
Temperature, K	120(2)
Wavelength, Å	0.71073
Crystal size, mm	0.069 x 0.109 x 0.144
Color	clear light colorless block
Crystal system	monoclinic
Space group	P 2_1/n
Unit cell dimensions, Å, °	a = 11.683(3) α = 90
	b = 7.2655(18) β = 96.141(4)
	c = 25.126(6) γ = 90
Unit cell volume, $Å^3$	2120.5(9)
Z	4
Density (calculated), g/cm^3	1.648
Absorption coefficient, mm^{-1}	1.575
F (000)	1040
Θ range, °	2.01 to 26.00
Index ranges	-13<=h<=14
	-8<=k<=8
	-30<=l<=30
Reflections collected	17852
Independent reflections	4135 [R_{int} = 0.0497]
Transmission (max and min)	0.8990 and 0.8050
Data / restraints / parameters	4135 / 0 / 256
Goodness-of-fit on F^2	1.036
Final R indices [I>2σ(I)]	R1 = 0.0300
	wR2 = 0.0642
R indices (all data)	R1 = 0.0428
	wR2 = 0.0693
Largest diff. peak/hole, $eÅ^{-3}$	0.534 and -0.448

Table 17. Selected bond lengths and valence angles of $SbMe_3(4\text{-Cl-PhCO})_2$.

$SbMe_3(4\text{-Cl-PhCO})_2$			
Bond length, Å		**Valence angle,°**	
Cyanoxime:			
O1 - N1	1.354(3)	C1 - N1 - O1	112.9(3)
N1 - C1	1.306(4)	C2 - C1 - N1	120.5(3)
C1 - C2	1.456(5)	N1 - C1 - C3	121.0(3)
C1 - C3	1.472(5)	C3 - C1 - C2	118.5(3)
C2 - N2	1.135(4)	N2 - C2 - C1	176.4(4)
Cl1 - C6	1.741(4)		
Cl2 - C14	1.754(3)		
Metal Center:			
Sb1 - O1	2.093(2)	C17-Sb1-C18	120.29(15)
Sb1 - O2	2.111(2)	C18-Sb1-C19	117.01(17)
Sb1 - C17	2.087(3)	C18-Sb1-O1	95.71(12)
Sb1 - C18	2.088(3)	C17-Sb1-O2	90.43(11)
Sb1 - C19	2.092(4)	C19-Sb1-O2	91.32(12)
		C17-Sb1-C19	122.69(16)
		C17-Sb1-O1	91.06(12)
		C19-Sb1-O1	84.29(12)
		C18-Sb1-O2	87.21(11)
		O1-Sb1-O2	175.49(8)

Crystal Structure of $SbMe_3(2,4\text{-diCl-PhCO})_2$. The crystal and refinement data for $SbMe_3(2,4\text{-diCl-PhCO})_2$ is presented in Table 18. Selected bond lengths and angles are presented in Table 19. The molecular structure of $SbMe_3(2,4\text{-diCl-PhCO})_2$ can be seen in Figure 36. When co-crystallization happens within our crystals, it is normally a combination of both diastereomers attached to the same metal center. Here, we see a rare case of co-crystallization of two

diastereomers within the same molecule at a 50:50 ratio. This is the first time it has been expressed within a crystal structure. Within this complex are both *trans syn and trans anti* geometry. All H-atoms were attached to the structure, not found when solved. The crystalline specimen was a rotational twin. The bond lengths of the carbon atoms attached to the metal Sb center are all different. The dihedral angle between the mean planes N2-C2-C1-N1-O1 and Cl2-C6-C7-C8-Cl1-C3-C4-C5 is 40.83 ° for the *trans anti* stereoisomer which is around 10 ° smaller than that of Tl(2,4-diCl-PhCO). This means antimony has more of a steric effect on the cyanoxime anion than thallium. The dihedral angle for the *trans syn* isomer was 53.41 °. The bond lengths for the cyanoxime group are all within the normal expected ranges for this class of compounds. There was not a huge difference between $SbMe_3(2,4\text{-diCl-PhCO})_2$ and its thallium precursor; N1-O1 = 1.329(12), N3-O2 = 1.285(15), N1-C1 = 1.285(14), N3-C12 = 1.388(18) compared to N1-O1 =1.294(12) and N1-C1 = 1.314(13). There are no hydrogen bonds present and so the crystal lattice is supported by π-π stacking interactions between the aryl groups and inter - and intra-molecular forces such as van-der-Waal forces.

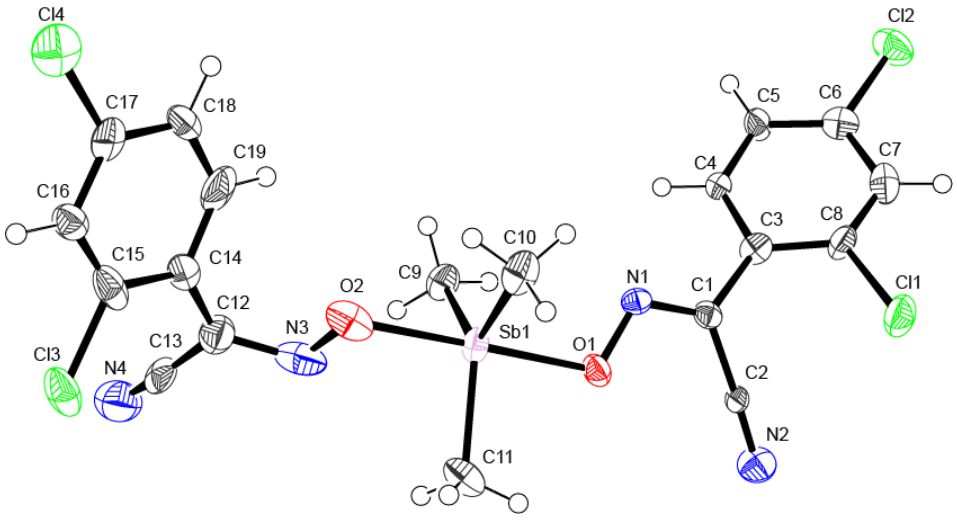

Figure 36. Molecular structure and atomic numbering of $SbMe_3(2,4\text{-diCl-PhCO})_2$ drawn in ORTEP at 50% ellipsoid probability level.

Table 18. Crystal and refinement data for $SbMe_3(2,4\text{-diCl-PhCO})_2$.

Parameter	**$SbMe_3(2,4\text{-diCl-PhCO})_2$**
Empirical formula	$C_{19}H_{15}Cl_4N_4O_2Sb$
Formula weight, g/mol	594.93
Temperature, K	120.15
Wavelength, Å	N/A
Crystal size, mm	0.212 × 0.187 × 0.143
Color	colorless
Crystal system	monoclinic
Space group	$P2_1/c$
Unit cell dimensions, Å, °	a = 7.1216(19) α = 7.1216(19) b = 23.813(6) β = 23.813(6) c = 13.847(4) γ =13.847(4)
Unit cell volume, $Å^3$	2288.4(10)
Z	4
Density (calculated), g/cm^3	1.7267
Absorption coefficient, mm^{-1}	1.696
F (000)	1168.3
Θ range, °	3.46 to 50.00
Index ranges	$-8 \le h \le 8$ $0 \le k \le 29$ $0 \le l \le 17$
Reflections collected	4666
Independent reflections	4026 [R_{int} = 0.0000, R_{sigma} = 0.1081]
Transmission (max and min)	0.791 and 0.984
Data / restraints / parameters	4026/12/274
Goodness-of-fit on F^2	1.053
Final R indices [I>2σ(I)]	R_1 = 0.0878 wR_2 = 0.1629
R indices [all data]	R_1 = 0.1459 wR_2 = 0.1867
Largest diff. peak and hole, e $Å^{-3}$	1.86 and -2.17

Table 19. Selected bond lengths and valence angles of the ligand $SbMe_3(2,4\text{-diCl-PhCO})_2$

$SbMe_3(2,4\text{-diCl-PhCO})_2$			
Bond length, Å		**Valence angle,°**	
Chloro-aryl and Cyanoxime:			
O1 - N1	1.329(12)	C1 - N1 - O1	113.5(9)
N1 - C1	1.285(14)	C2 - C1 - N1	118.9(10)
C1 - C2	1.464(17)	N1 - C1 - C3	121.3(11)
C1 - C3	1.462(16)	C3 - C1 - C2	119.7(10)
C2 - N2	1.130(15)	N2 - C2 - C1	176.0(14)
N3 - C12	1.388(18)	C12 – N3 – O2	109.8(12)
N3 - O2	1.285(15)	C13 - C12 – N3	112.5(12)
		N3 - C12 – C14	126.4(13)
		C14 - C12 – C13	121.1(11)
		N4 – C13 - C12	174.9(16)
Metal Center:			
Sb1 - O1	2.100(8)	C10 - Sb1 – C9	117.4(5)
Sb1 - O2	2.184(10)	C11 - Sb1 - C9	122.4(5)
Sb1 - C9	2.079(12)	C10 - Sb1 - O1	120.2(5)
Sb1 - C10	2.065(13)	C9 - Sb1 - O1	94.0(4)
Sb1 - C11	2.099(13)	C10 - Sb1 - O1	92.2(4)
		C11 - Sb1 - O1	84.9(5)
		C9 - Sb1 - O2	91.1(4)
		C10 - Sb1 – O2	83.9(4)
		C11 - Sb1 - O2	93.8(5)
		O1 - Sb1 - O2	174.6(3)

Crystal Structure of $SbMe_3(2,6\text{-diCl-PhCO})_2$. The crystal and refinement data are shown in Table 20. The molecular structure of $SbMe_3(2,6\text{-diCl-PhCO})_2$ is shown in Figure 37. The cyanoxime moieties within the structure adopt an *anti*-geometry like their Tl precursor

Tl(2,6-diCl-PhCO). Selected bond lengths and valence angles are presented in Table 21. This compound is completely non-planar. The dihedral angles between the cyanoxime group and the disubstituted aryl group are 69.65 ° for mean planes Cl4-Ph-Cl5 and N3-C9-C10-N4, and 83.08 ° for mean planes Cl2-Ph-Cl1 and N1-C1-C2-N2. These angles are larger than the dihedral angle in the Tl precursor which makes sense since there are bulkier atoms surrounding the cyanoxime in $SbMe_3(2,6\text{-diCl-PhCO})_2$ than in $Tl(2,6\text{-diCl-PhCO})_2$ and hence there would be a need for more space to minimize repulsion. The bonds in the cyanoxime group were N1-O1 = 1.359(7) Å, N3-O2 = 1.354(7) Å, N1-C1 = 1.282(8) Å and N3-C9 = 1.273(8) Å. These were within the normal expected ranges and when compared to their Tl precursor, the bond lengths do not differ much, with any changes attributed to the redistribution of electron density due to complexation to the metal Sb center. Slipped π-π stacking interaction is present to stabilize the crystal structure.

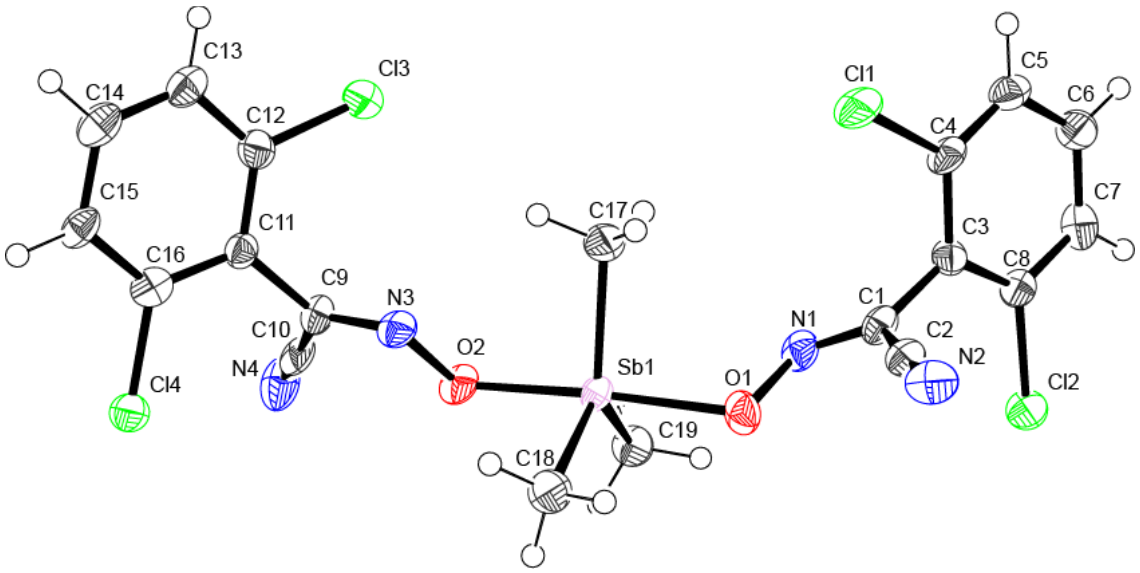

Figure 37. Molecular structure of $SbMe_3(2,6\text{-diCl-PhCO})_2$ drawn in ORTEP representation showing the numbering scheme.

Table 20. Crystal and refinement data for $SbMe_3(2,6\text{-diCl-PhCO})_2$.

Parameter	**$SbMe_3(2,6\text{-diCl-PhCO})_2$**
Empirical formula	$C_{19}H_{15}Cl_4N_4O_2Sb$
Formula weight, g/mol	594.90
Temperature, K	150(2)
Wavelength, Å	0.71073
Crystal size, mm	0.105 × 0.095 × 0.071
Color	colorless
Crystal system	triclinic
Space group	*P -1*
Unit cell dimensions, Å, °	a = 7.540(3) α = 104.891(6) b = 10.889(4) β = 93.234(6) c = 14.709(6) γ = 100.956(6)
Unit cell volume, $Å^3$	1138.8(8)
Z	2
Density (calculated), g/cm^3	1.735
Absorption coefficient, mm^{-1}	1.704
F (000)	584
Θ range, °	1.98 to 26.37°
Index ranges	-9≤ h≤ 9 -13≤ k≤ 13 -18≤ l≤ 18
Reflections collected	12471
Independent reflections	4636 [R_{int} = 0.0707]
Transmission (max and min)	0.7454 and 0.5843
Data / restraints / parameters	4636 / 0 / 274
Goodness-of-fit on F^2	0.968
Δ/σ_{max}	-
Final R indices [I>2σ(I)]	R1 = 0.0541 wR2 = 0.1233
R indices (all data)	R1 = 0.0847 wR2 = 0.1376
Largest diff. peak and hole, $eÅ^{-3}$	1.517 and -1.668
R.M.S. deviation from mean, $eÅ^{-3}$	0.168

Table 21. Selected bond lengths and valence angles of the ligand $SbMe_3(2,6\text{-diCl-PhCO})_2$.

$SbMe_3(2,6\text{-diCl-PhCO})_2$			
Bond length, Å		**Valence angle,°**	
Chloro-aryl and Cyanoxime:			
O1 - N1	1.359(7)	C1 - N1 - O1	113.1(5)
N1 - C1	1.282(8)	C2 - C1 - N1	122.2(6)
C1 - C2	1.464(9)	N1 - C1 - C3	121.2(6)
C1 - C3	1.481(9)	C3 - C1 - C2	116.5(6)
C2 - N2	1.134(9)	N2 - C2 - C1	176.3(7)
N3 - O2	1.354(7)	C9 - N3 - O2	112.7(5)
N3 - C9	1.273(8)	C11 - C9 - N3	118.0(6)
		N3 - C9 - C10	123.4(6)
		C11 - C9 - C10	118.6(5)
		N4 - C10 - C9	177.2(8)
Metal Center:			
Sb1 - O1	2.115(4)	C18 - Sb1 - O2	92.7(2)
Sb1 - O2	2.091(4)	O2 - Sb1 - C19	83.6(2)
Sb1 - C17	2.098(7)	O2 - Sb1 - C17	93.7(2)
Sb1 - C18	2.083(6)	C18 - Sb1 - O1	87.3(2)
Sb1 - C19	2.098(7)	C19 - Sb1 - O1	92.5(2)
		C18 - Sb1 - C19	120.2(3)
		C18 - Sb1 - C17	118.5(3)
		C19 - Sb1 - C17	121.3(3)
		O2 - Sb1 - O1	175.55(18)
		C17 - Sb1 - O1	90.2(2)

Crystal Structure of $SbMe_3(TCO)_2$. The crystal and refinement data are shown in Table 22. The crystal structure of $SbMe_3(TCO)_2$ showing the ASU and the grow fragment of the complex is presented in Figure 39A. Important bond lengths and valence angles have also been

included in Figure 39B. The dihedral angle between the thioamide and the cyanoxime is 8.68° which is larger than that of Tl(TCO) 3.51° attesting to the strain caused by the presence of antimony and the three methyl groups. The methyl carbons reside in a special position as shown in Figure 38, and therefore the presence of 6 hydrogens on the methyl carbons, each hydrogen with site occupancy of 0.5. The side view shows that the complex is not planar. Intermolecular hydrogen bonds are one of the important bonds that keep the lattice of $SbMe_3(TCO)_2$ intact. The parameters for the hydrogen bonds are N3-H3B---N2 = 2.19 Å, H3B---N2 = 3.016(12) Å with <DHA = 161.8°. This bond is much weaker than that of its Tl precursor which had its hydrogen donor-acceptor bond less than 3 Å. Electrostatic forces as well as van-der-Waal forces are present to further stabilize the crystal structure.

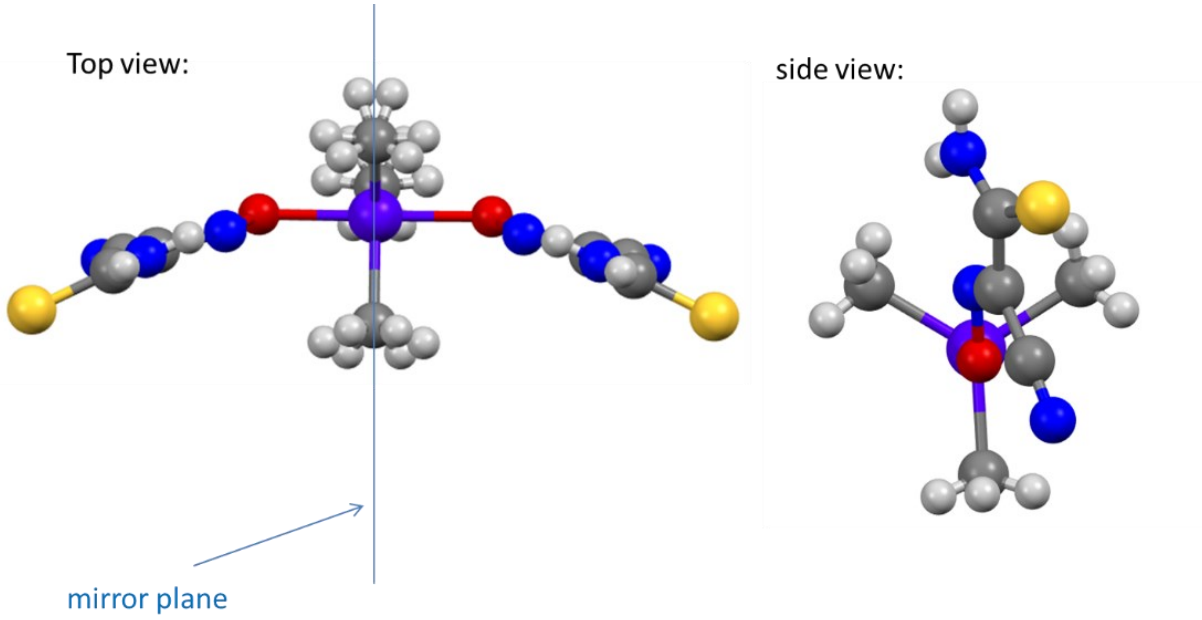

Figure 38. Two orthogonal views of the structure of $SbMe_3(TCO)_2$.

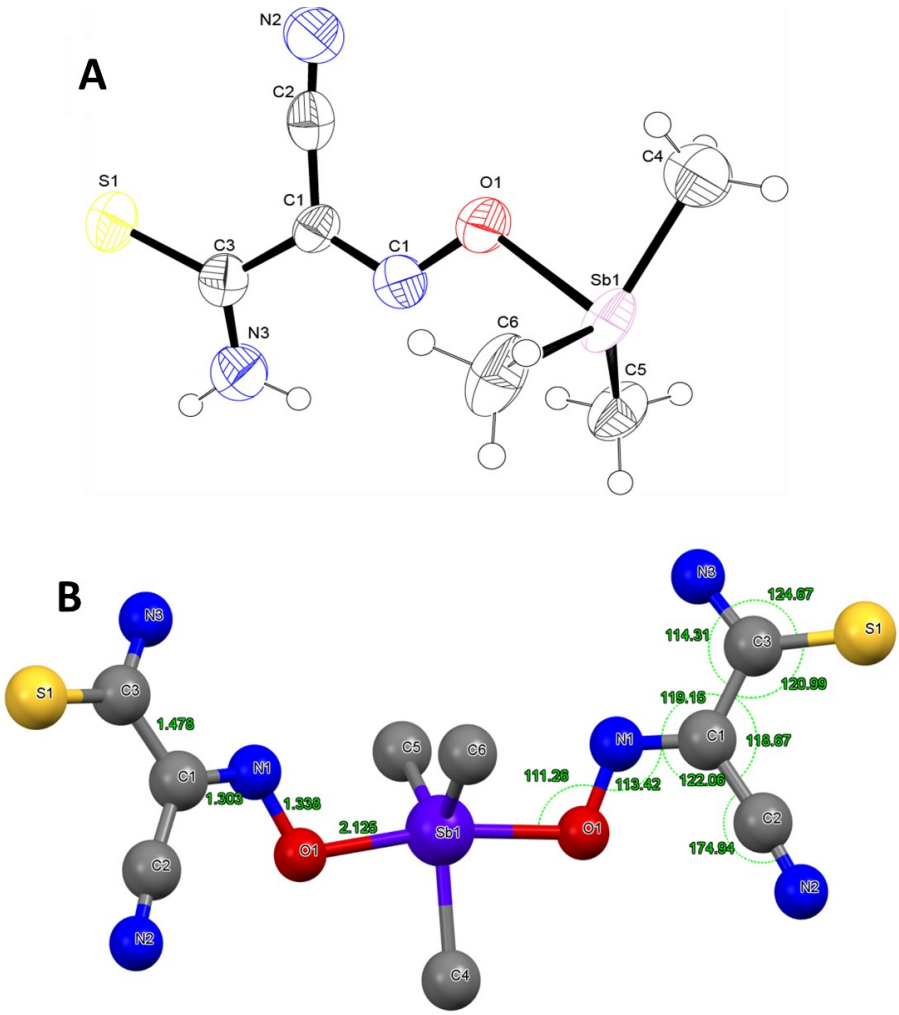

Figure 39. Crystal structure of $SbMe_3(TCO)_2$ compound: **A** – the ASU in ORTEP representation with atomic numbering; **B** – GROW fragment showing full structure with the most important bond lengths and valence angles (H-atoms are not shown for clarity).

Table 22. Crystal and refinement data for $SbMe_3(TCO)_2$.

Parameter	$SbMe_3(TCO)_2$	
Empirical formula	$C_9H_{13}N_6O_2S_2Sb$	
Formula weight, g/mol	423.12	
Temperature, K	296(2)	
Wavelength, Å	0.71073	
Crystal size, mm	0.076 x 0.103 x 0.146	
Color	clear light yellow-bronze	
Crystal system	orthorhombic	
Space group	*P 21/n*	
Unit cell dimensions, Å, °	a = 14.6202(15)	α = 90
	b = 16.0815(16)	β = 90
	c = 7.1203(7)	γ = 90
Unit cell volume, $Å^3$	1674.1(3)	
Z	4	
Density (calculated), g/cm^3	1.679	
Absorption coefficient, mm^{-1}	1.906	
F (000)	832	
Θ range, °	2.53 to 25.00	
Index ranges	$-17 \leq h \leq 17$	
	$-19 \leq k \leq 19$	
	$-8 \leq l \leq 8$	
Reflections collected	17301	
Independent reflections	1532 [$R_{(int)} = 0.0519$]	
Transmission (max and min)	0.8690 and 0.7680	
Data / restraints / parameters	1532 / 0 / 100	
Goodness-of-fit on F^2	1.141	
Final R indices [$I>2\sigma(I)$]	1139 data;	R1 = 0.0645
		wR2 = 0.1489
R indices [all data]		R1 = 0.0855
		wR2 = 0.1618
Largest diff. peak and hole, $eÅ^{-3}$	4.515 and -1.070	

Crystal Structure of $SbMe_3(TDCO)_2$. The crystal and refinement data for $SbMe_3(TDCO)_2$ is shown in Table 23. The molecular structure showing the results of co-

crystallization during the synthesis of the complex is shown in Figure 40. Important bond lengths and valence angles are presented in Table 24. This is the normal cases of co-crystallization we normally see with our crystals unlike the rare case seen with the $SbMe_3(2,4\text{-diCl-PhCO})_2$ mentioned earlier. In Figure 40 we see that one cyanoxime is totally in *trans-syn* geometry but with the second cyanoxime, there is a co-crystallized mixture of two diastereomers: *trans-syn* and *trans-anti* geometry. The *syn*-isomer is the dominant isomer with 84% while the *anti*-isomer is minor with about 16%. This is confirmed by the NMR data. The geometries of the methyl groups attached to antimony are all the same. Both acidoligands attached to the metal Sb are non-planar and the dihedral angle for the *syn*-isomer is 60.76°. The co-crystallized mixture has similar dihedral angles of 56.20° for the *syn*-isomer and 58.22° for the *trans*-isomer. The cyanoxime bond lengths for the minor *anti*-isomer is much longer than the bond lengths for the major *syn*-isomers. Van-der-Waal forces and electrostatic interactions are responsible for maintaining the structural integrity of the crystal.

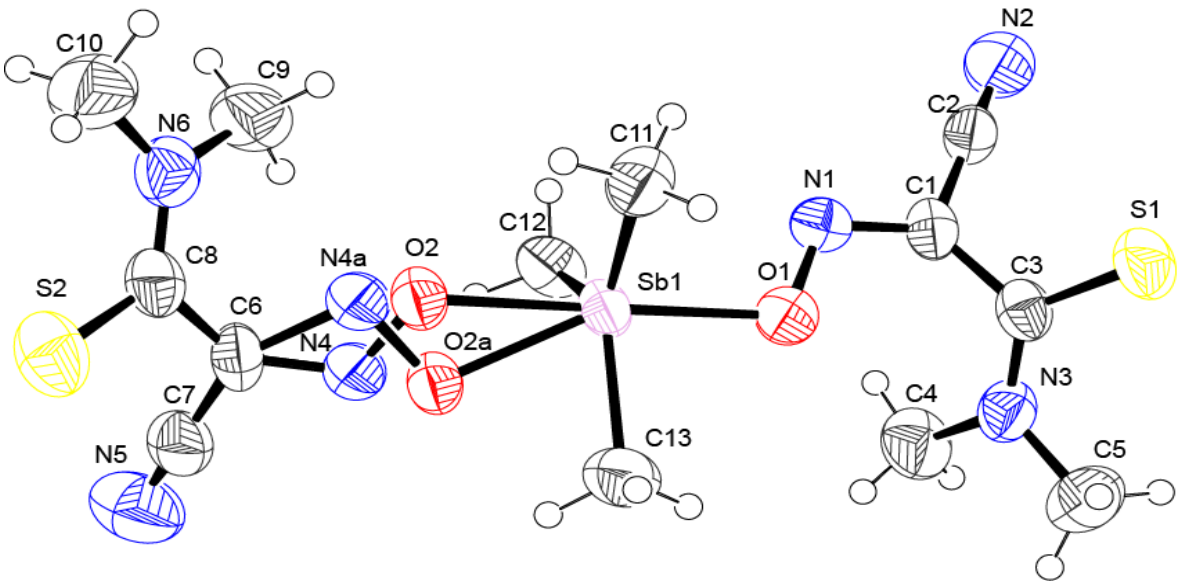

Figure 40. Molecular structure of $SbMe_3(TDCO)_2$ drawn in ORTEP showing the presence of both *syn*- and *anti*- geometrical conformations within the structure.

Table 23. Crystal and refinement data for $SbMe_3(TDCO)_2$.

Parameter	**$SbMe_3(TDCO)_2$**
Empirical formula	$C_{13}H_{21}N_6O_2S_2Sb$
Formula weight, g/mol	479.23
Temperature, K	296(2)
Wavelength, Å	0.71073
Crystal size, mm	0.211 x 0.173 x 0.149
Color	yellow
Crystal system	monoclinic
Space group	$P2_1/c$
Unit cell dimensions, Å, °	a = 7.540(3) α = 104.891(6)
	b = 10.889(4) β = 93.234(6)
	c = 14.709(6) γ = 100.956(6)
Unit cell volume, $Å^3$	2056.4(3)
Z	4
Density (calculated), g/cm^3	1.548
Absorption coefficient, mm^{-1}	1.562
F (000)	960.0
Θ range, °	3.118 to 52.834
Index ranges	$-16 \leq h \leq 16$
	$-15 \leq k \leq 14$
	$-16 \leq l \leq 16$
Reflections collected	18608
Independent reflections	4221 [R_{int} = 0.0590, R_{sigma} = 0.0542]
Transmission (max and min)	0.7456 and 0.6833
Data / restraints / parameters	4221/0/231
Goodness-of-fit on F^2	1.031
Final R indices [I>2σ(I)]	R1 = 0.0514
	wR2 = 0.1011
R indices [all data]	R1 = 0.0837
	wR2 = 0.1130
Largest diff. peak and hole, $eÅ^{-3}$	1.79 and -1.25

Table 24. Selected bond lengths and valence angles of the ligand $SbMe_3(TDCO)_2$.

$SbMe_3(TDCO)_2$			
Bond length, Å		**Valence angle,°**	
		Cyanoxime:	
O1 - N1	1.340(6)	C1 - N1 - O1	111.4(5)
N1 - C1	1.306(7)	C2 - C1 - N1	113.3(5)
C1 - C2	1.452(9)	N1 - C1 - C3	128.3(6)
C1 - C3	1.488(8)	C3 - C1 - C2	117.7(5)
C2 - N2	1.135(8)	N2 - C2 - C1	177.4(7)
S1 – C3	1.663(6)	C1 - C3 - S1	116.4(4)
S2 - C8	1.672(7)	N3 - C3 - C1	118.5(5)
C6 - N4a	1.55(4)	N3 - C3 - S1	125.1(5)
C6 - N4	1.299(9)	C4 - N3 - C5	114.3(6)
N4a - O2a	1.37(5)	C9 - N6 - C10	114.2(6)
N4 - O2	1.352(9)	N5 - C7 - C6	178.7(8)
		anti - geometrical configuration:	
		C7 - C6 - N4a	148.7(16)
		C8 - C6 - N4a	93.50(15)
		Sb1 - O2a - N4a	105.0(2)
		syn - geometrical conformation:	
		C7 - C6 - N4	117.5(5)
		C8 - C6 - N4	134.2(6)
		Sb1 - O2 - N4	106.8(4)
		Metal Center:	
Sb1 - O1	2.114(4)	O1 - Sb1 - O2	174.2(18)
Sb1 - O2	2.163(6)	O1 - Sb1 - O2a	150.1(7)
Sb1 – O2a	2.080(3)	C11 - Sb1 - C12	120.2(3)
Sb1 - C11	2.080(6)	C11 - Sb1 - C13	121.4(3)
Sb1 - C12	2.082(6)	C11 - Sb1 - O2a	114.7(7)
Sb1 - C13	2.072(6)	C11 - Sb1 - O1	92.30(2)
		C11 - Sb1 - O2	83.20(2)
		C12 - Sb1 - C13	118.4(3)
		C12 - Sb1 - O2a	84.90(8)
		C12 - Sb1 - O2	92.60(2)
		C12 - Sb1 - O1	92.70(2)
		C13 - Sb1 - O1	86.10(2)
		C13 - Sb1 - O2	93.20(3)
		C13 - Sb1 - O2a	69.30(8)

Crystal Structure of $SbMe_3(ACO)_2$. The crystal and refinement data for this structure is shown in Table 25. The molecular structure drawn in ORTEP can be seen in Figure 42. Selected bond length and valence angles are presented along with the structure of $SbMe_3(ACO)_2$ in Figure 41. The cyanoxime moieties adopt a strictly *trans-anti* geometry. This compound is non-planar with dihedral angles of 6.80° and 9.34°. The cyanoxime bond lengths are all within the expected range for this class of compounds. Complexation of the metal Sb center with two bulkier ligands leads to the slight distortion of the trigonal bipyramid geometry present in the starting compound $SbMe_3Br_2$ (Figure 43B). The amine hydrogens are responsible for the hydrogen bonding in this structure. Figure 44 shows two views of the hydrogen bonds within $SbMe_3(ACO)_2$ with bond lengths for both the inter- and intra-molecular bonding present. Intermolecular electrostatic attractions and van-der-Waal contacts help further stabilize the crystal structure of this compound (Figure 43A).

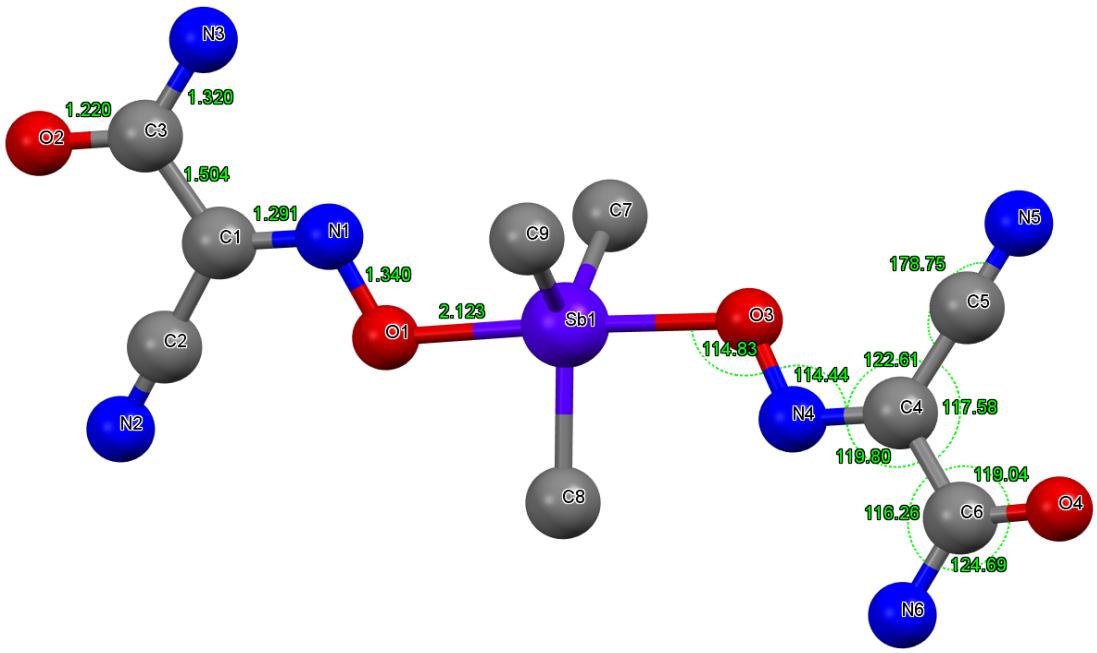

Figure 41. Crystal structure of $SbMe_3(ACO)_2$ with the most important bond lengths and valence angles (H-atoms have been omitted for clarity).

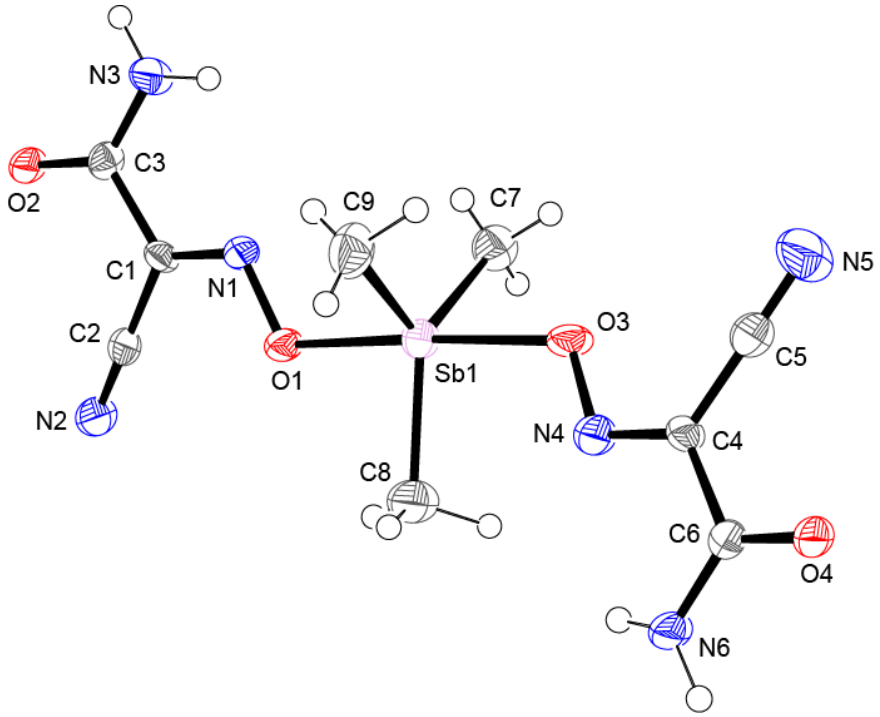

Figure 42. Molecular structure of $SbMe_3(ACO)_2$ drawn in ORTEP showing atomic numbering.

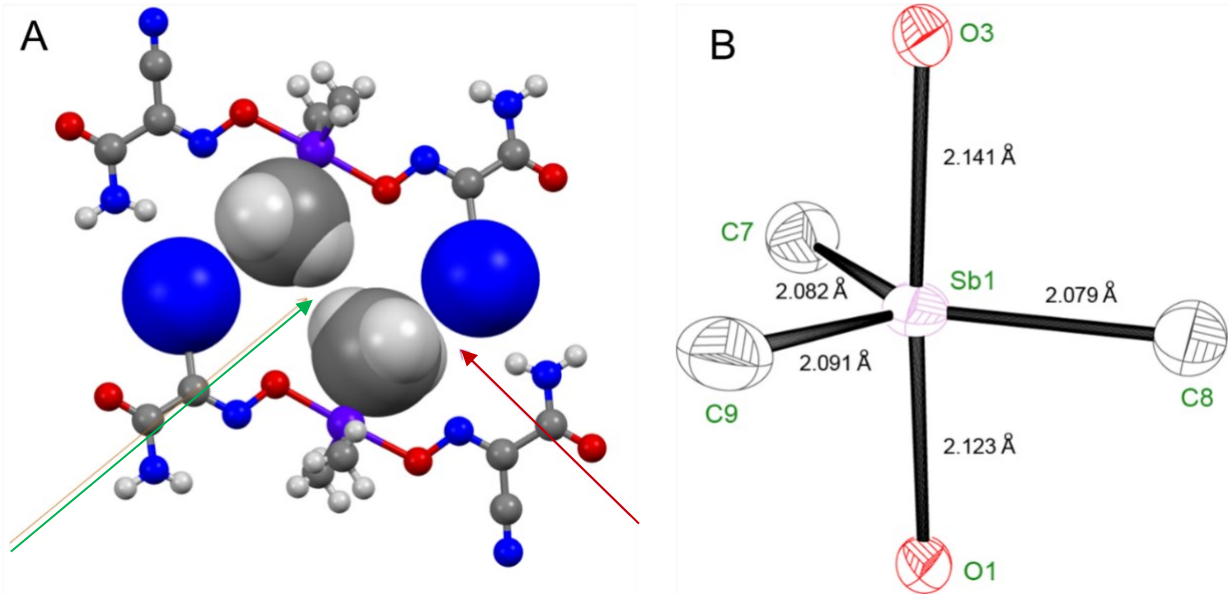

Figure 43. Details of crystal packaging in the structure $SbMe_3(ACO)_2$ **(A)** with the view of electrostatic (red arrow) and van-der-Waals (green arrow) contacts within $SbMe_3(ACO)_2$ units. **(B)** slightly distorted trigonal bipyramidal shape adopted by the antimony core metal center.

Table 25. Crystal and refinement data for $SbMe_3(ACO)_2$.

Parameter	**$SbMe_3(ACO)_2$**
Empirical formula	$C_9HN_6O_4Sb$
Formula weight, g/mol	378.91
Temperature, K	120(2)
Wavelength, Å	0.71073
Crystal size, mm	0.313 x 0.241 x 0.218
Color	N/A
Crystal system	triclinic
Space group	*P -1*
Unit cell dimensions, Å, °	a = 8.727(2) α = 92.780(4) b = 8.829(2) β = 92.045(4) c = 10.349(2) γ = 107.665(4)
Unit cell volume, $Å^3$	757.8(3)
Z	2
Density (calculated), g/cm^3	1.660
Absorption coefficient, mm^{-1}	1.840
F (000)	360
Θ range, °	1.973 to 26.430
Index ranges	$-10 \leq h \leq 10$ $-11 \leq k \leq 11$ $-12 \leq l \leq 12$
Reflections collected	7575
Independent reflections	3096 [R_{int} = 0.0585, R_{sigma} = 0.0832]
Transmission (max and min)	0.7465 and 0.5055
Data / restraints / parameters	3096 / 0 / 228
Goodness-of-fit on F^2	0.987
Final R indices [I>2σ(I)]	2373 data; R1 = 0.0446 wR2 = 0.0791
R indices [all data]	R1 = 0.0663 wR2 = 0.0891
Largest diff. peak and hole, $eÅ^{-3}$	1.507 and -0.952

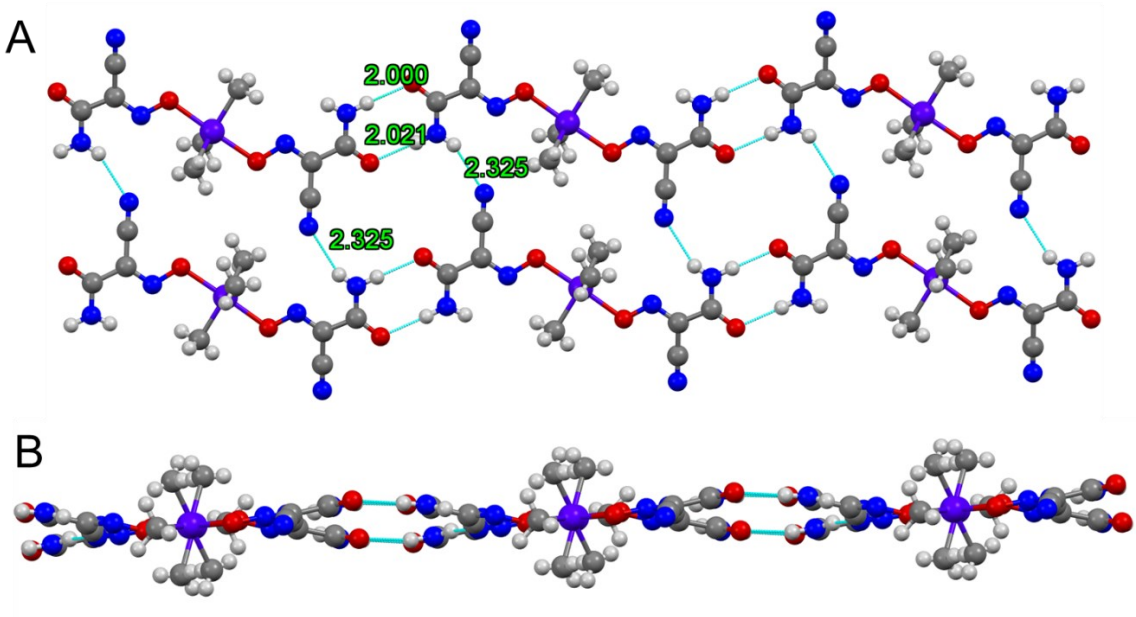

Figure 44. Details of crystal packing in the structure of $SbMe_3(ACO)_2$; two orthogonal views of sheets formed via H – bonding.

Crystal Structure of $SbMe_3(ECO)_2$. The crystal and refinement data for $SbMe_3(ECO)_2$ is shown in Table 27. The molecular structure with the numbering scheme is presented in Figure 45. The most important bond lengths and valence angles are shown in Table 28. The cyanoxime moieties adopt a *trans-anti* geometry. All H-atoms within the structure were attached in APEX and all the methyl groups around the metal Sb center are structurally and chemically equivalent. This cyanoximate is non-planar with the methyl group attached to one of the cyanoxime moieties coming out of the page. It forms an angle of <O6-C9-C10 = 105.1(6). This causes a dihedral angle of 27.01 ° between the oxo fragment and the cyanoxime fragment. The second dihedral angle is 6.05 ° for the other moiety. The bond lengths for the cyanoxime are all within the expected range. Crystal packing within the structure consists of linear sheets, non-linearly stacked on top of each other. Electrostatic forces and van-der-Waal forces present within the structure maintains it lattice.

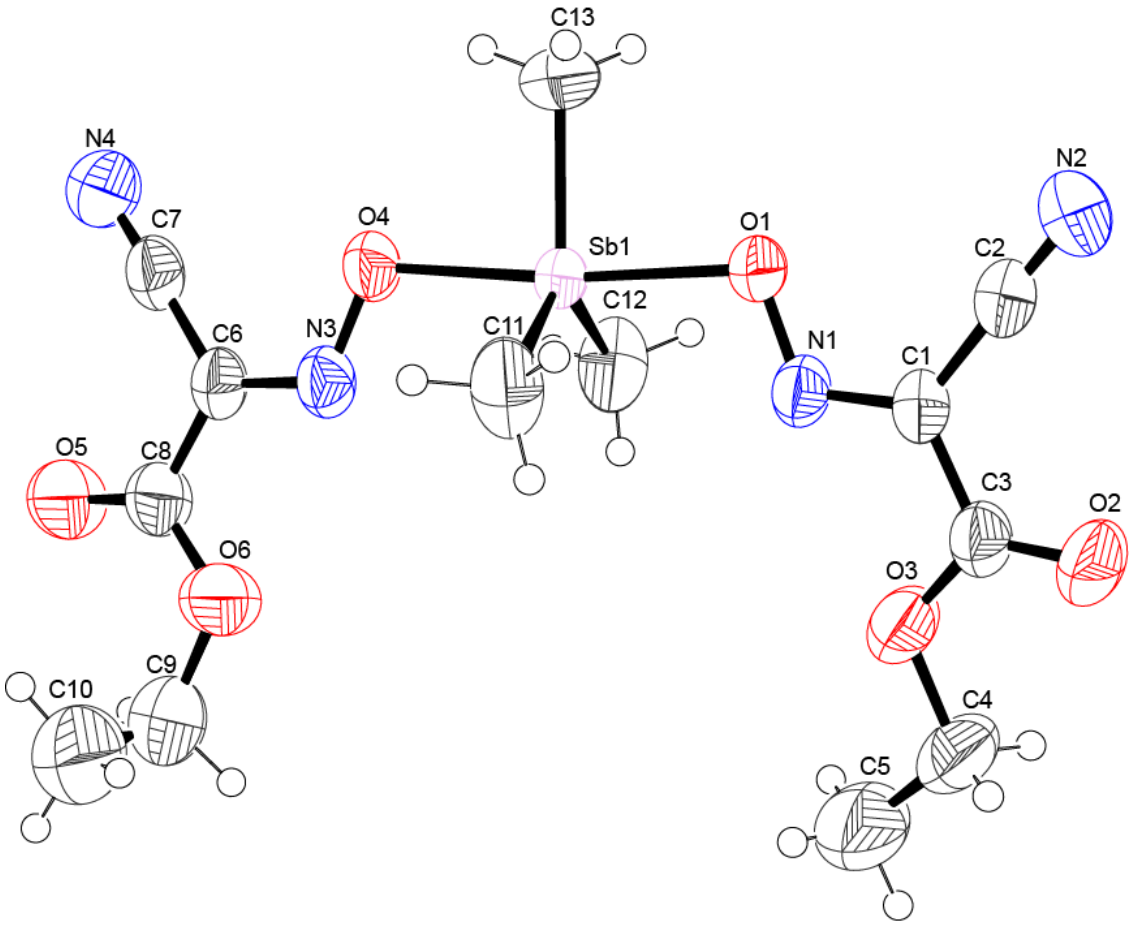

Figure 45. Molecular structure and atomic numbering for $SbMe_3(ECO)_2$.

Table 26. Crystal and refinement data for $SbMe_3(ECO)_2$.

Parameter	**$SbMe_3(ECO)_2$**
Empirical formula	$C_{13}H_{19}N_4O_6Sb$
Formula weight, g/mol	449.08
Temperature, K	296.15
Wavelength, Å	N/A
Crystal size, mm	0.276 × 0.192 × 0.183
Color	colorless
Crystal system	monoclinic
Space group	$P2_1/n$
Unit cell dimensions, Å, °	a = 9.1401(5) α = 90
	b = 16.0912(9) β = 103.1870(10)
	c = 13.4416(8) γ = 90
Unit cell volume, $Å^3$	1924.80(19)
Z	4
Density (calculated), g/cm^3	1.5496
Absorption coefficient, mm^{-1}	1.466
F (000)	894.0
Θ range, °	4.02 to 50
Index ranges	$-12 \leq h \leq 12$
	$-22 \leq k \leq 22$
	$-18 \leq l \leq 18$
Reflections collected	29353
Independent reflections	3375 [R_{int} = 0.0263, R_{sigma} = 0.0197]
Transmission (max and min)	0.7459 and 0.6738
Data / restraints / parameters	3375/0/222
Goodness-of-fit on F^2	1.076
Final R indices [I>2σ(I)]	R_1 = 0.0253
	wR_2 = 0.0654
R indices [all data]	R_1 = 0.0297
	wR_2 = 0.0705
Largest diff. peak and hole, e $Å^{-3}$	0.59/-0.31

Table 27. Selected bond lengths and valence angles of $SbMe_3(ECO)_2$.

$SbMe_3(ECO)_2$			
Bond length, Å		**Valence angle,°**	
Cyanoxime:			
O1 - N1	1.336(3)	C1 - N1 - O1	115.1(2)
N1 - C1	1.294(4)	C2 - C1 - N1	123.7(3)
C1 - C2	1.442(5)	N1 - C1 - C3	119.9(3)
C1 - C3	1.476(4)	C3 - C1 - C2	116.3(3)
C2 - N2	1.127(4)	N2 - C2 - C1	178.6(4)
N3 - O4	1.345(3)	O3 - C3 - O2	124.6(3)
N3 - C6	1.291(4)	C6 - N3 - O4	114.6(3)
		C7 - C6 - N3	122.5(3)
		N3 - C6 - C8	121.5(3)
		C7 - C6 - C8	116.0(3)
		N4 - C7 - C6	178.3(4)
		O5 - C8 - O6	121.7(4)
		O6 - C9 - C10	105.1(6)
Metal Center:			
Sb1 - O1	2.134(2)	C12 - Sb1 - C11	120.9(2)
Sb1 - O4	2.115(2)	C13 - Sb1 - C11	120.3(18)
Sb1 - C11	2.078(3)	C13 - Sb1 - C12	118.8(18)
Sb1 - C12	2.083(3)	O1 - Sb1 - C11	90.80(12)
Sb1 - C13	2.075(4)	O1 - Sb1 - C12	91.56(12)
		O1 - Sb1 - C13	87.10(12)
		O4 - Sb1 - C11	91.82(12)
		O4 - Sb1 - C12	91.65(12)
		O4 - Sb1 - C13	86.99(13)
		O4 - Sb1 - O1	174.1(8)

Crystal Structure of $SbMe_3(MCO)_2$. The crystal and refinement data are shown in Table 28. The molecular structure is shown in Figure 46. Selected bond lengths and valence angles are shown in Table 29. The six-membered ring in the MCO-cyanoxime presents in a chair conformation to minimize any steric hindrance. The cyanoxime adopts a *trans-anti* geometry and is non-planar. The dihedral angle between the mean planes for the six-membered ring and O4-N4-C8-C9-N5 is 34.11 ° compared to the mean planes involving N2-C2-C1-N1-O1 which is 59.72 °. This is mostly due to arrangements of bond around the metal Sb center and the effect it has on the cyanoxime moieties to help alleviate steric hindrance. The bond lengths for the cyanoxime group are all acceptable within this molecule. The crystal lattice is stabilized by π-π stacking interactions due to the presence of the ring. Electrostatic attractions as well as van-der-Waal forces further support the structure of $SbMe_3(MCO)_2$.

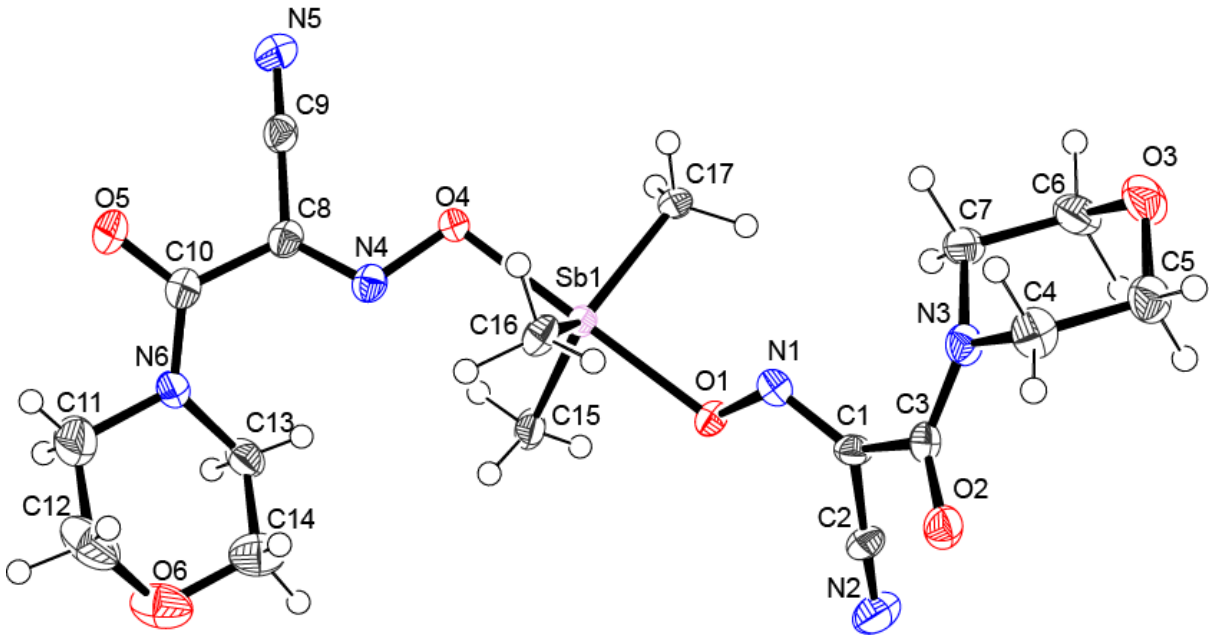

Figure 46. Molecular structure and atomic numbering for $SbMe_3(MCO)_2$.

Table 28. Crystal and refinement data for $SbMe_3(MCO)_2$.

Parameter	**$SbMe_3(MCO)_2$**	
Empirical formula	$C_{17}H_{25}N_6O_6Sb$	
Formula weight, g/mol	531.18	
Temperature, K	120(2)	
Wavelength, Å	0.71073	
Crystal size, mm	0.201 x 0.170 x 0.050	
Color	Transparent and colorless	
Crystal system	orthorhombic	
Space group	*P b c a*	
Unit cell dimensions, Å, °	a = 11.3901(19)	α = 90
	b = 12.602(2)	β = 90
	c = 31.362(5)	γ = 90
Unit cell volume, $Å^3$	4501.6(13)	
Z	8	
Density (calculated), g/cm^3	1.568	
Absorption coefficient, mm^{-1}	1.270	
F (000)	2144	
Θ range, °	1.30 to 26.43	
Index ranges	-14<=h<=14	
	-15<=k<=15	
	-39<=l<=39	
Reflections collected	52122	
Independent reflections	4621 [R_{int} = 0.1406]	
Transmission (max and min)	0.7454 and 0.644	
Data / restraints / parameters	4621 / 0 / 360	
Goodness-of-fit on F^2	1.045	
Final R indices [I>2σ(I)]	3056 data;	R1 = 0.0418
		wR2 = 0.0930
R indices [all data]		R1 = 0.0830
		wR2 = 0.1186
Largest diff. peak and hole, e $Å^{-3}$	0.598 and -1.298	

Table 29. Selected bond lengths and valence angles of $SbMe_3(MCO)_2$.

$SbMe_3(MCO)_2$			
Bond length, Å		**Valence angle,°**	
Cyanoxime:			
O1 - N1	1.350(5)	C1 - N1 - O1	114.2(4)
N1 - C1	1.285(7)	C2 - C1 - N1	120.8(5)
C1 - C2	1.453(7)	N1 - C1 - C3	122.2(5)
C1 - C3	1.494(7)	C3 - C1 - C2	116.0(5)
C2 - N2	1.139(7)	N2 - C2 - C1	178.5(6)
O4 - N4	1.353(5)	C1 - C3 - O2	116.7(5)
N4 - C8	1.282(7)	C1 - C3 - N3	119.6(5)
		O2 - C3 - N3	123.6(5)
		O4 - N4 - C8	114.8(4)
		N4 - C8 - C9	123.1(5)
		N4 - C8 - C10	122.0(5)
		C9 - C8 - C10	114.5(5)
		N5 - C9 - C8	179.0(6)
		C8 - C10 - O5	116.7(5)
		C8 - C10 - N6	120.2(5)
		N6 - C10 - O5	123.0(5)
Metal Center:			
Sb1 - O1	2.114(3)	C17 - Sb1 - C16	120.5(2)
Sb1 - O4	2.123(3)	C17 - Sb1 - C15	120.1(2)
Sb1 - C15	2.105(6)	C16 - Sb1 - C15	119.4(3)
Sb1 - C16	2.094(5)	C17 - Sb1 - O1	90.04(17)
Sb1 - C17	2.085(5)	C16 - Sb1 - O1	93.21(19)
		C15 - Sb1 - O1	85.20(2)
		C17 - Sb1 - O4	88.64(17)
		C16 - Sb1 - O4	90.83(19)
		C15 - Sb1 - O4	92.10(2)
		O1 - Sb1 - O4	175.9(13)

V. 5. Differential Scanning Calorimetry - Thermal Gravimetric Analysis (DSC/TGA)

Thermal analysis of solids provides important information about samples' thermodynamic stability. In case of investigations of biologically active compounds, it is critical to know whether they are stable at temperatures above 105 °C normally used for sterilization purposes. The most accurate way of investigating the thermal stability of new compounds is via the Thermogravimetry/ Differential Thermal Analysis (TG/DTA) method. TG/DTA measures temperatures where decomposition, reduction or oxidation occurs within a sample. This method simultaneously measures the weight changes associated with all these physical or chemical changes happening, as well as phase changes that indicate melting within the sample.

Traces of samples' weight loss and heat flow were recorded with the help of Q-600 TG/DSC analyzer from TA Instruments (Delaware, USA) in the range of 30 – 800 °C. The UHP grade argon was used as gas carrier at 100±1 mL/min flow rate and 10°/min heating rate. The brand-new alumina crucible was calcined prior to experiment using the propane torch. Data were processed and graphed using the TA Universal Analysis software package and allowed accurate determination of the melting point of a target cyanoxime. The thermogram of $SbMe_3(ECO)_2$ as a representative example is shown in Figure 47. The melting point was found to be 140.52 °C and decomposition started at X. The melting points for all the synthesized antimony (V) cyanoximates have melting points above 100 ° and decompose well beyond that. This makes it possible for use in drug development or in medical devices which aligns with our goals for this research. Additional thermograms can be found in Appendix B. All studied Sb(V) cyanoximates were found to be stable to~120 – 140 °C, which clears their application as potential active pharmaceutical ingredients (APIs).

Digimelt was used to measure the melting point of compounds that the TG/DSC analyzer could not accurately measure. Moreover, these measurements were carried out in open air.

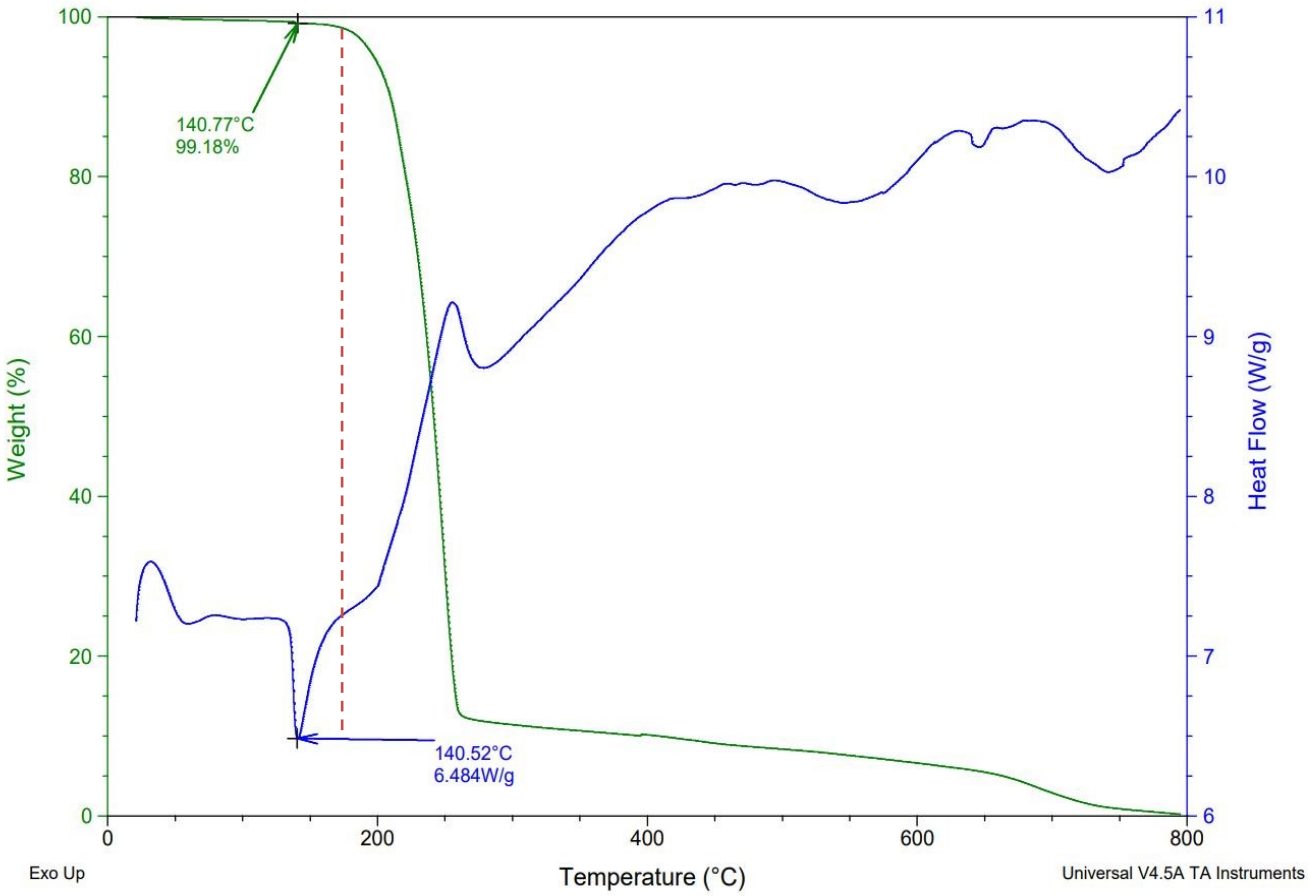

Figure 47. Thermal analysis traces for $SbMe_3(ECO)_2$: panoramic view. Melting point at 140.52 ° and decomposition~170°C. Green line indicates the weight loss and blue line indicates heat flow.

V. 6. NMR Spectroscopy

The NMR spectra for all the compounds were recorded at room temperature by Dr. Sergiy Tyukhtenko from NEU in Boston, MA using the Varian INova-400 MHz. All the assignments of chemical shifts were made based off previous work completed by Dr. Gerasimchuk and his research group. Due to low quantities and other technical difficulties with the synthesized compounds, NMR spectra were not obtained for all the newly synthesized compounds. A typical example of the spectral appearance of one of the organic ligands, *syn*-H(2,6-diCl-PhCO) is shown in Figure 48 and 49. A bulk sample of synthesized dichloro-substituted arylcyanoxime H(2,6-diCl-PhCO) demonstrates the presence of both syn- and anti-isomers in solutions. Thus, the $^{13}C\{^1H\}$ NMR spectrum of protonated arylcyanoximes HL in dmso-d_6 solutions contains a double set of signals (Figure 49). The exact assignment of the NMR signals of the individual isomers within the mixture was accomplished using HMQC and HSQC techniques. The proton NMR spectra $\{^1H\}$ of the arylcyanoximes — which represent an isomeric mixture in dry dmso-d_6 and acetone-d_6 — show the presence of two broadened signals of the N-OH group at ~14ppm at room temperature (Figure 48). Heating the dmso-d_6 solutions of this cyanoxime to +105°C did not lead to changes in the $^{13}C\{^1H\}$ NMR spectrum. Thus, there is no interconversion of isomers in the mixture:

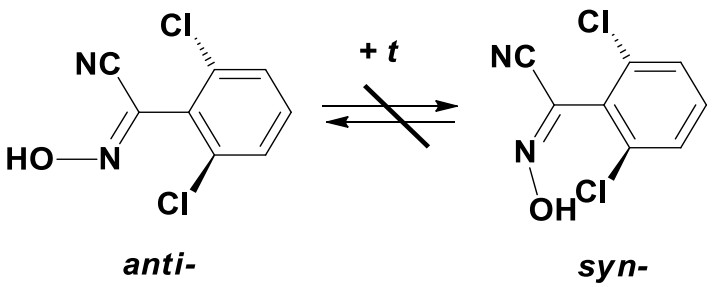

The crystal data of some synthesized Sb(V) cyanoximates also evidenced co-crystallization of two diastereomers which were confirmed by $^{13}C\{^{1}H\}$ NMR spectroscopy. Thus, $SbMe_3(TDCO)_2$ contained co-crystallized mixture of two isomers shown in its NMR spectra. The $^{13}C\{^{1}H\}$ spectra for Tl(TDCO) and $SbMe_3(TDCO)_2$ are presented in Figures 50 and 51 respectively as typical examples of spectral appearance of the mixture. In Figure 50A, the ^{1}H presents three separate hydrogen environments when there should only be two corresponding to the methyl groups in both the *syn*- and *anti*- isomer. This is caused by the charge distribution between the elements S=C-$N(Me)_2$ within the molecule. Consequently, each isomer should have two different hydrogen environments for the methyl hydrogens, but due to an accidental overlap, only three absorbance signals are seen in the ^{1}H spectra. Confirmation of this explanation is found in the integrations of each absorbance signal. The most downfield signal has an integration of about 6 compared to about 3 for the other upfield signals. The $^{13}C\{^{1}H\}$ in Figure 50B further shows the presence of two diastereomers within Tl(TDCO) with a double set of absorbance signals. In Figure 51, the $^{13}C\{^{1}H\}$ showed the presence of two diastereomers at uneven ratios within the structure of $SbMe_3(TDCO)_2$. Coupled with x-ray crystallography, we determined that the *syn* - isomer was more dominant than the *anti*- isomer, with the syn- isomer having an 84% occurrence compared to 16% for the anti- isomer.

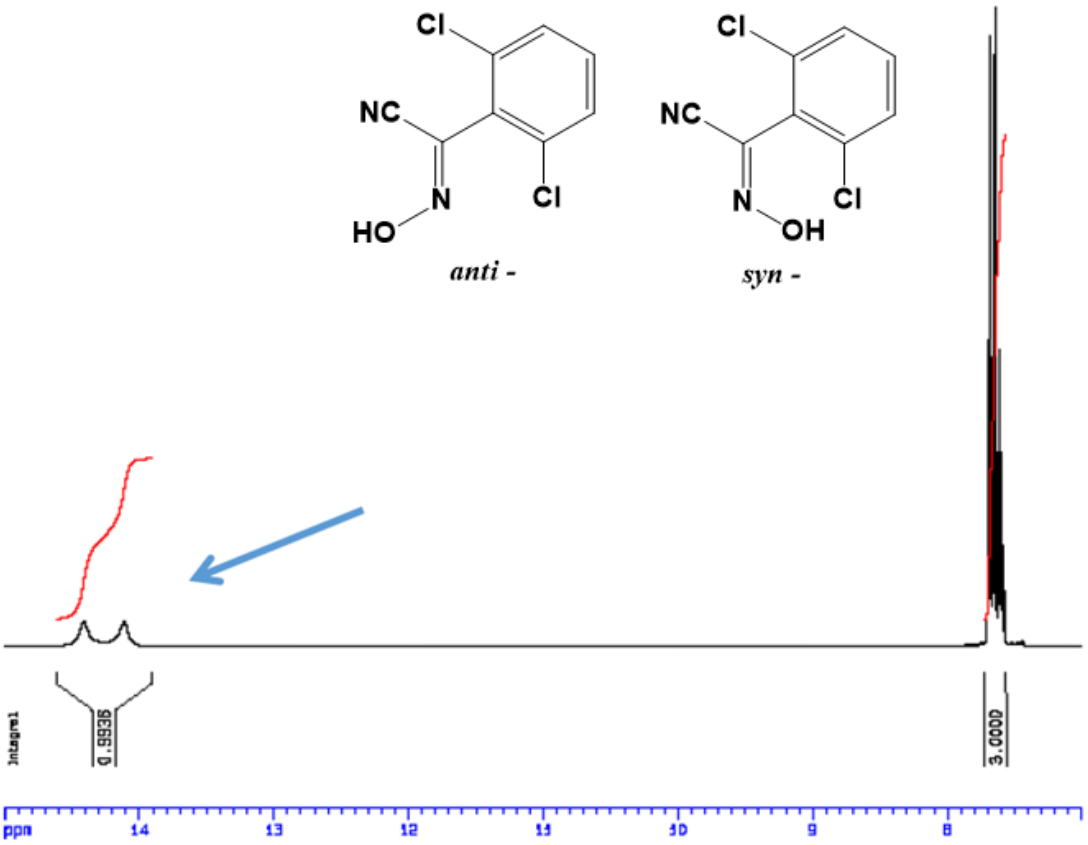

Figure 48. The ^{1}H NMR spectrum of the H(2,6-diCl-PhCO) in DMSO-d_6 at RT showing presence of two diastereomers clearly seen in the oxime-group range.

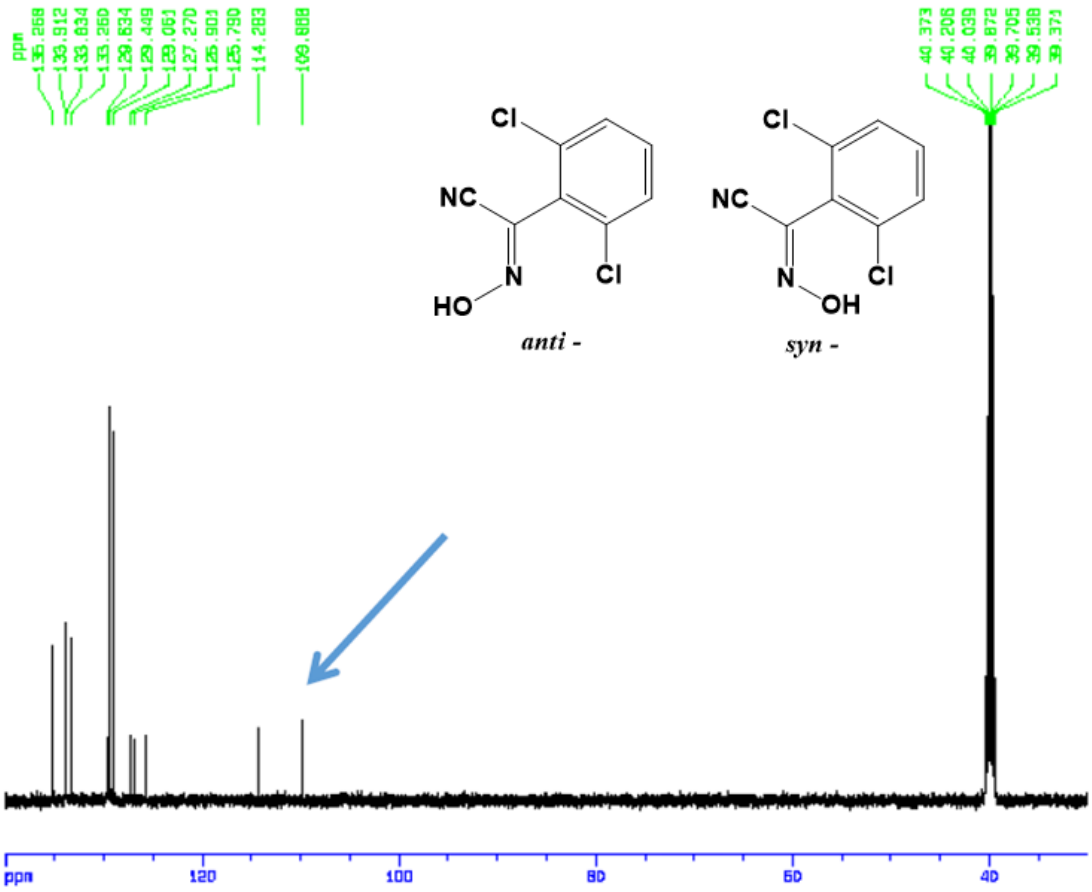

Figure 49. The $^{13}C\{^{1}H\}$ NMR spectrum of the H(2,6-diCl-PhCO) in DMSO-d_6 at RT showing presence of two diastereomers.

In summary, the use of NMR spectroscopy was crucial in the confirmation of the correctness in assignments of the presence of two diastereomers of cyanoximes in studied compounds, and that these findings were not just crystallographic disorders.

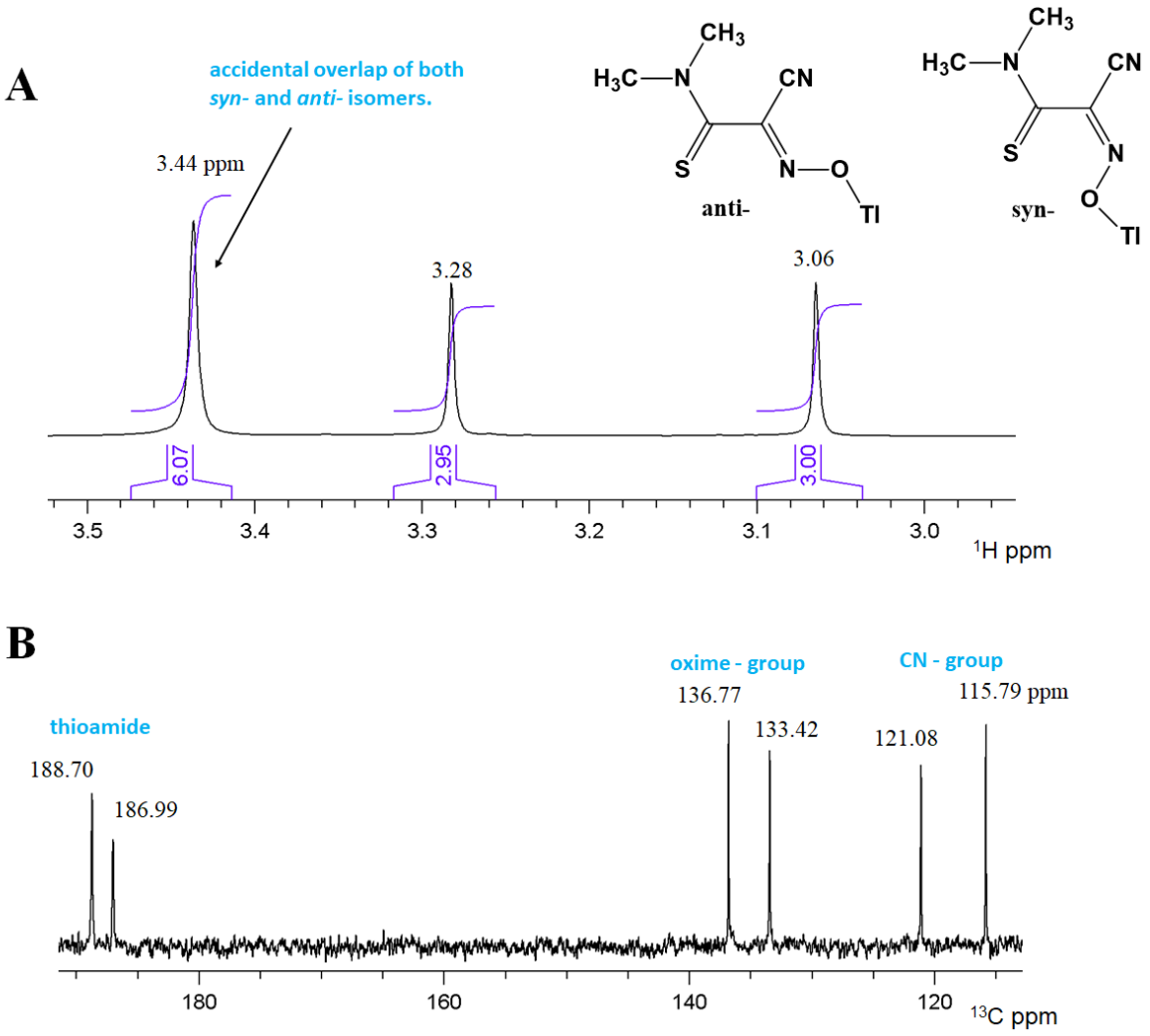

Figure 50. The RT NMR data for Tl(TDCO) in dmso-d_6 showing presence of two diastereomers: **A** – ^{1}H spectrum in which there is accidental overlap of two methyl groups (indicated with *); **B** – ^{13}C spectrum in the sp^2 carbon atoms region.

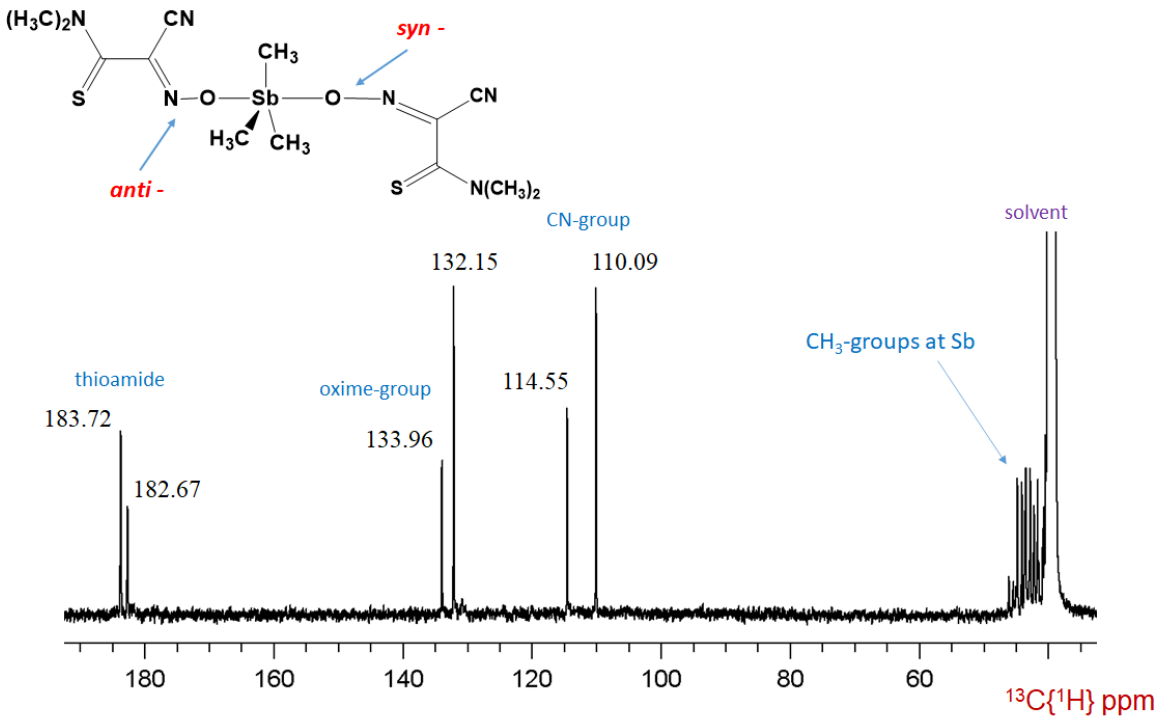

Figure 51. The $^{13}C\{^{1}H\}$ NMR spectrum of $SbMe_3(TDCO)_2$ in dmso-d_6 at RT showing presence of two diastereomers.

V. 7. Antimicrobial Studies

The biological activity studies were performed by our collaborators at Oklahoma State University in the Department of Microbiology and Molecular Genetics. These collaborators are Dr. Marianna Patrauchan and her research group (antibacterial studies), and Dr. Karen Wozniak and her research group (antifungal studies). Due to limited quantity of synthesized compounds and other technical difficulties, the biological activity data was obtained only for some of my synthesized compounds, and they will be described below. The rest of the compound sent for testing will be summarized later.

Minimum Inhibition Concentration (MIC) Tests. Minimum Inhibition Concentration (MIC) assays determine the lowest concentration of an antimicrobial agent that prevents the visible growth of a microorganism.[92] A dilution gradient of the synthesized compound is made

and tested against microbial strains. The cell growth at each concentration is measured to show the effectiveness of the compound. A total of nine newly synthesized compounds were submitted to OSU for biological testing. $SbMe_3Br_2$ and the cyanoxime ligands accompanied these compounds to OSU for biological activity testing. For these tests, the compounds had to be dissolved in DMSO. DMSO has inhibition effects at concentrations of 200 µg/mL and so that was taken into consideration when determining the effects of my newly synthesized compounds on bacteria and fungi. Antibacterial activity was assessed by testing my synthesized compounds against *P. aeruginosa, E. coli,* and *S. aureus.* The control used in all the testing was my initial compound $SbMe_3Br_2$. Unbound, free cyanoximes, HL, were also used as controls to see if there were any synergistic effect when Sb(V) source was combined with the cyanoxime. The independent variable was the concentrations of the compounds used in the MIC tests and the dependent variable was cell growth measured.

MIC Tests for the Most Effective Compounds. The $SbMe_3(MCO)_2$ was the most effective compound against *P. aeruginosa.* At~50 µg/mL, there was barely any cell growth and at subsequent concentrations afterwards indicating significant antimicrobial effect. Its ligand, H(MCO) that is in the structure, did not have the same effect when tested against the same bacterial strain. Figure 52 shows the comparison between the effects of the $SbMe_3Br_2$ (which was our control substance), H(MCO), and $SbMe_3(MCO)_2$ on *P. aeruginosa.* The control also had significant activity at~50 µg/mL but was less than that of $SbMe_3(MCO)_2$. All the other tested compounds on this strain on bacteria were not significantly effective. My compounds were also tested against *E. coli* and the cell growth analysis showed that $SbMe_3(2,6\text{-diCl-PhCO})_2$ was the most effective compound at stopping the growth of *E. coli* at a concentration of~50 µg/mL, like $SbMe_3(MCO)_2$ on *P. aeruginosa.* Figure 53 shows results of the MIC tests against *E. coli* where

$SbMe_3(2,6\text{-diCl-PhCO})_2$ was more effective than the control used. My antimony cyanoximates were not very effective against MRSA, with only the control being the compound that was able to completely stop bacterial cell growth at~100 µg/mL, with significant effect being seen at~50 µg/mL. Only the control and the ligand H(2,4-diCl-PhCO) were effective against the *S. aureus* (MRSA) strain used in the biological testing. Significant MRSA cell growth inhibition was seen at~100 µg/mL for H(2,4-diCl-PhCO), with no cell growth recorded at~150 µg/mL (Figure 54).

MIC Tests for Remaining Compounds. The graphical results for the MIC tests of compounds that were not very effective against the strains of bacteria they were tested on will be presented in this section. The MIC results for *P. aeruginosa* are shown in Figures 55 to 60. Figures 61 to 65 illustrate the MIC results for compounds tested against *E. coli*, and Figure 66 shows the results acquired from testing the free cyanoxime, H(2Cl-PhCO), and $SbMe_3(2\text{Cl-PhCO})_2$ against *MRSA*. Some of these graphs do not include the MIC test result for the free cyanoxime, which will be presented later. My research goals included assessing the effectiveness of my synthesized compounds against the most effective compounds in Kevin Pinks' research work. On comparison of the controls, ($SbMe_3Br_2$ vs $SbPh_4Br$), Figure 67 shows that $SbMe_3Br_2$ was more effective at inhibiting bacterial growth its bulkier counterpart, $SbPh_4Br$. The $SbMe_3Br_2$ had the lower MIC average of the two showing that a lower concentration of $SbMe_3Br_2$ is needed to inhibit bacterial cell growth. Lastly, Table 30 and 31 summarizes the effectiveness of each compound against the bacterial strains it was tested against. It shows the MIC (µg/mL) for an easier understanding of the results achieved in this research project.

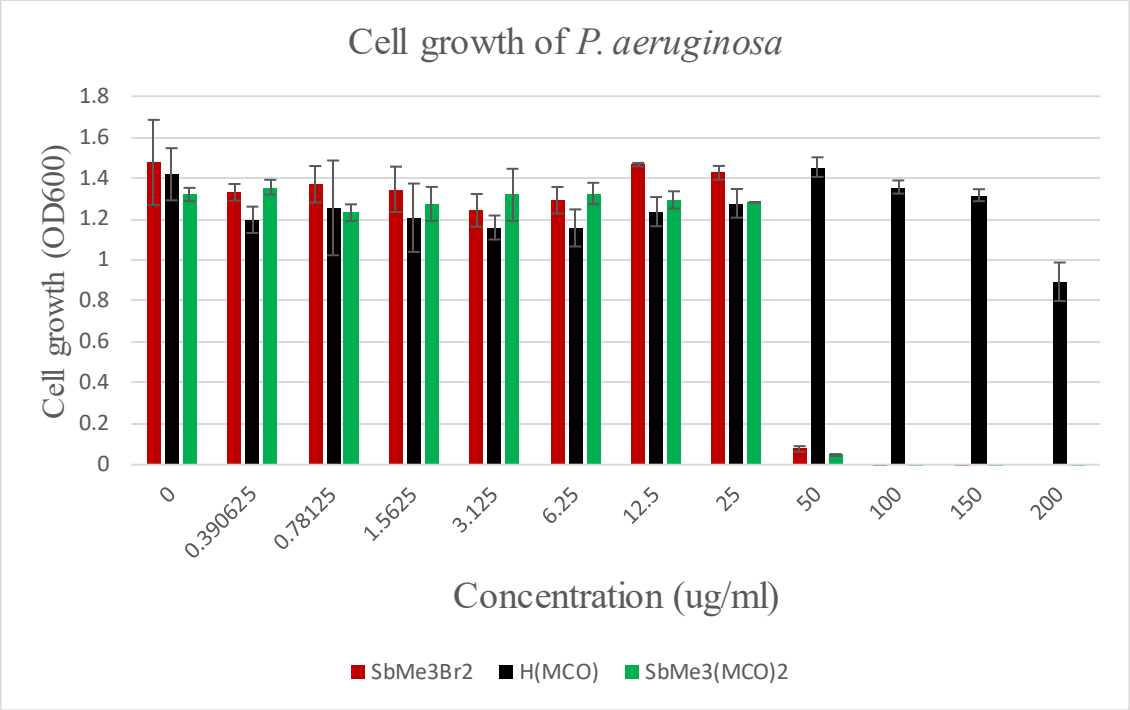

Figure 52. Results of MIC tests of $SbMe_3Br_2$, H(MCO) and $SbMe_3(MCO)_2$ against *P. aeruginosa*.

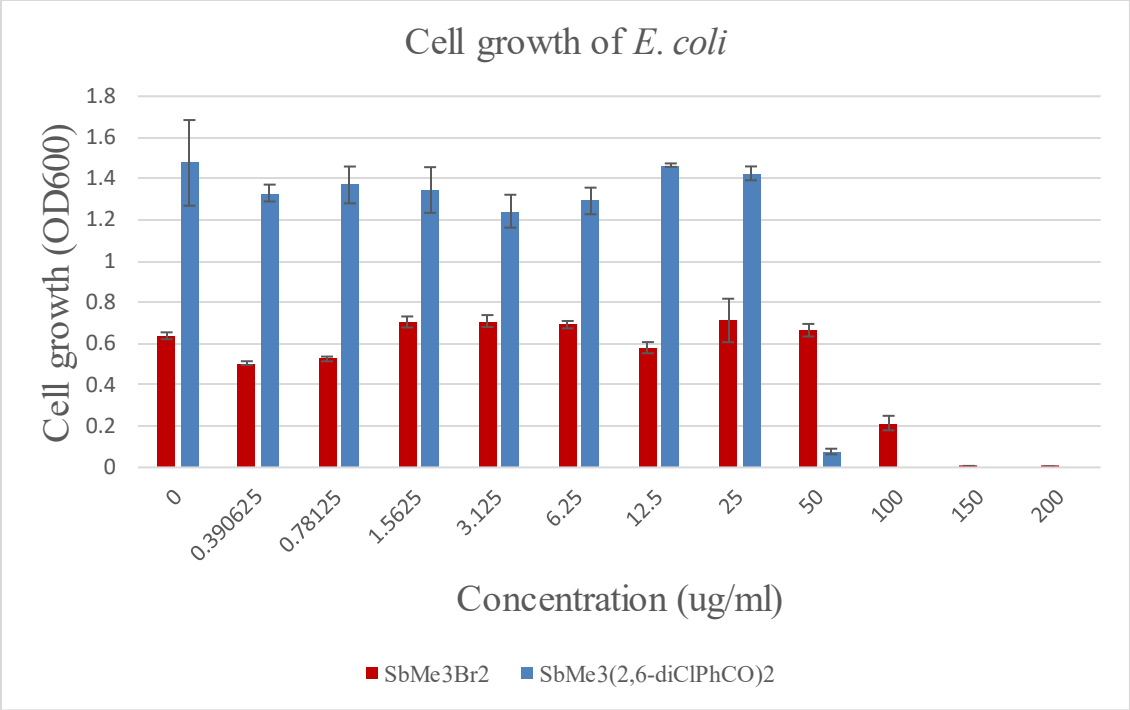

Figure 53. Results of MIC tests of $SbMe_3Br_2$, and $SbMe_3(2,6\text{-diCl-PhCO})_2$ against *E. coli*.

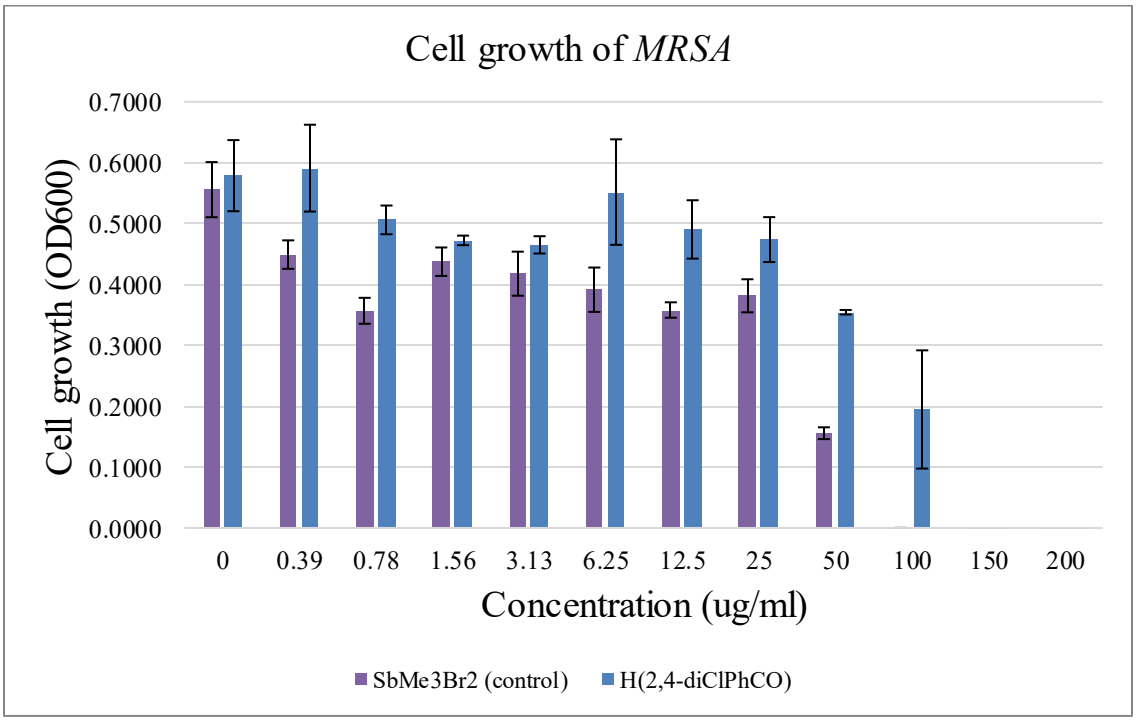

Figure 54. Results of H(2,4-diCl-PhCO) testing against MRSA, compared to $SbMe_3Br_2$ showing a downward trend for the free cyanoxime from 25 µg/mL to complete inhibition at 150 µg/mL.

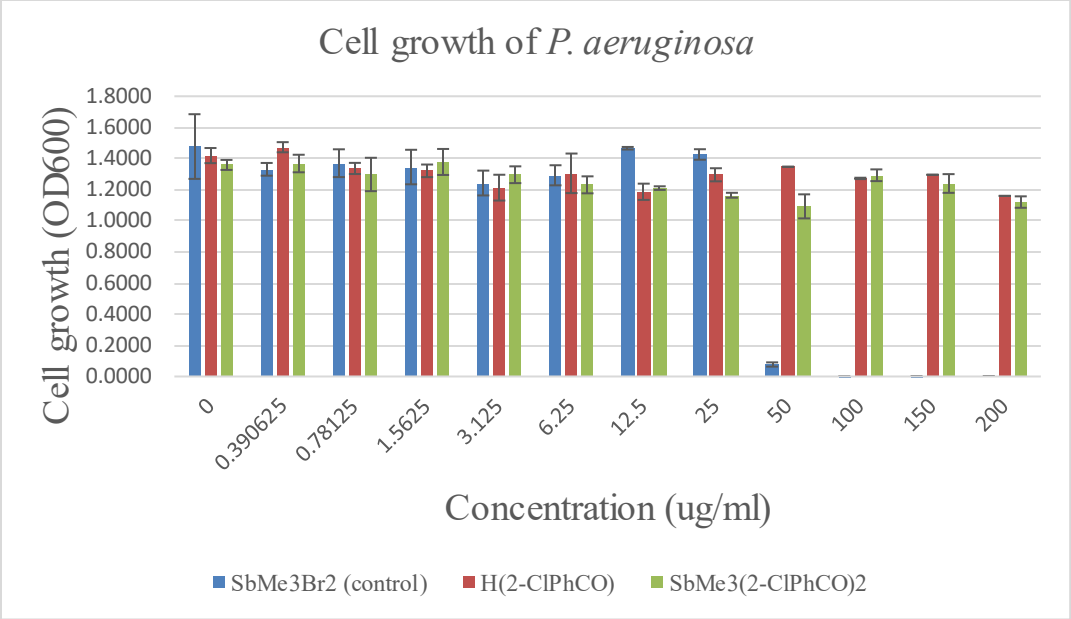

Figure 55. Results of MIC tests of $SbMe_3Br_2$, H(2-Cl-PhCO) and $SbMe_3(2\text{-Cl-PhCO})_2$ against *P. aeruginosa*.

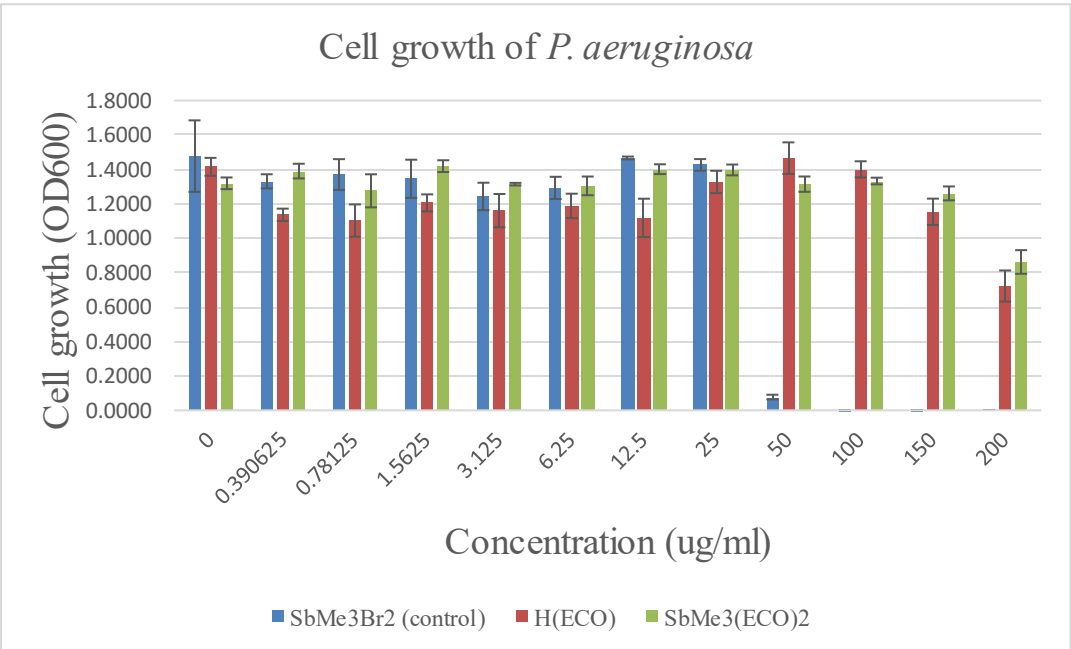

Figure 56. Results of MIC tests of $SbMe_3Br_2$, H(ECO) and $SbMe_3(ECO)_2$ against *P. aeruginosa*.

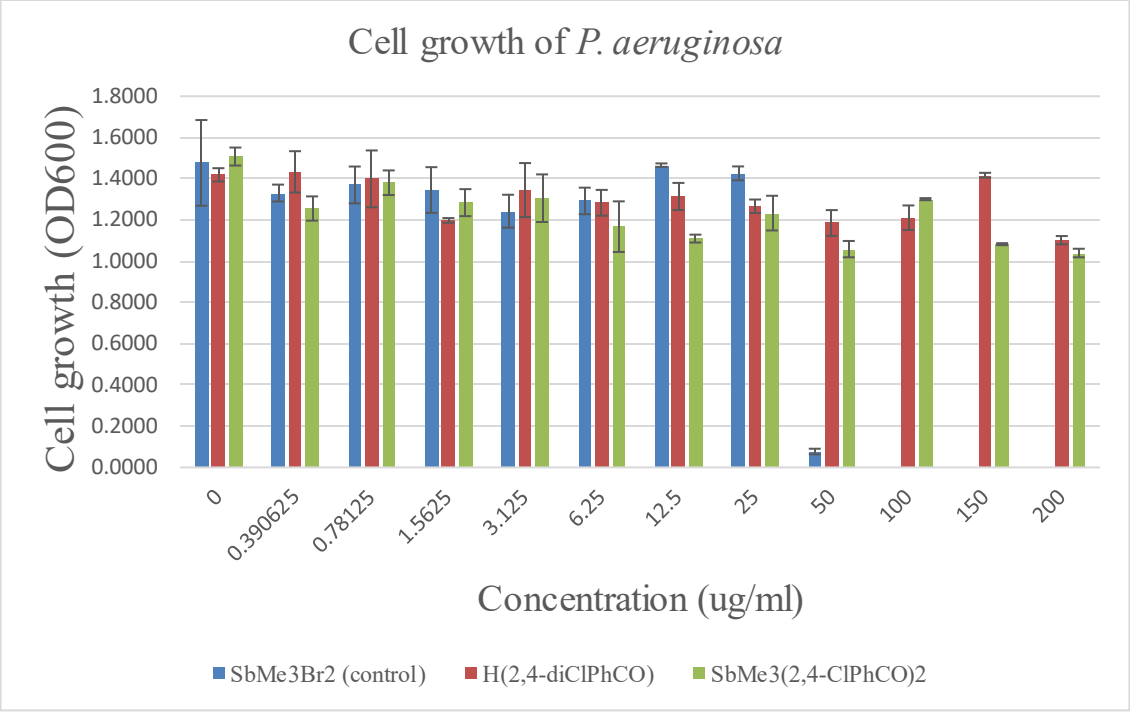

Figure 57. Results of MIC tests of $SbMe_3Br_2$, H(2,4-diCl-PhCO) and $SbMe_3(2,4\text{-diCl-PhCO})_2$ against *P. aeruginosa*.

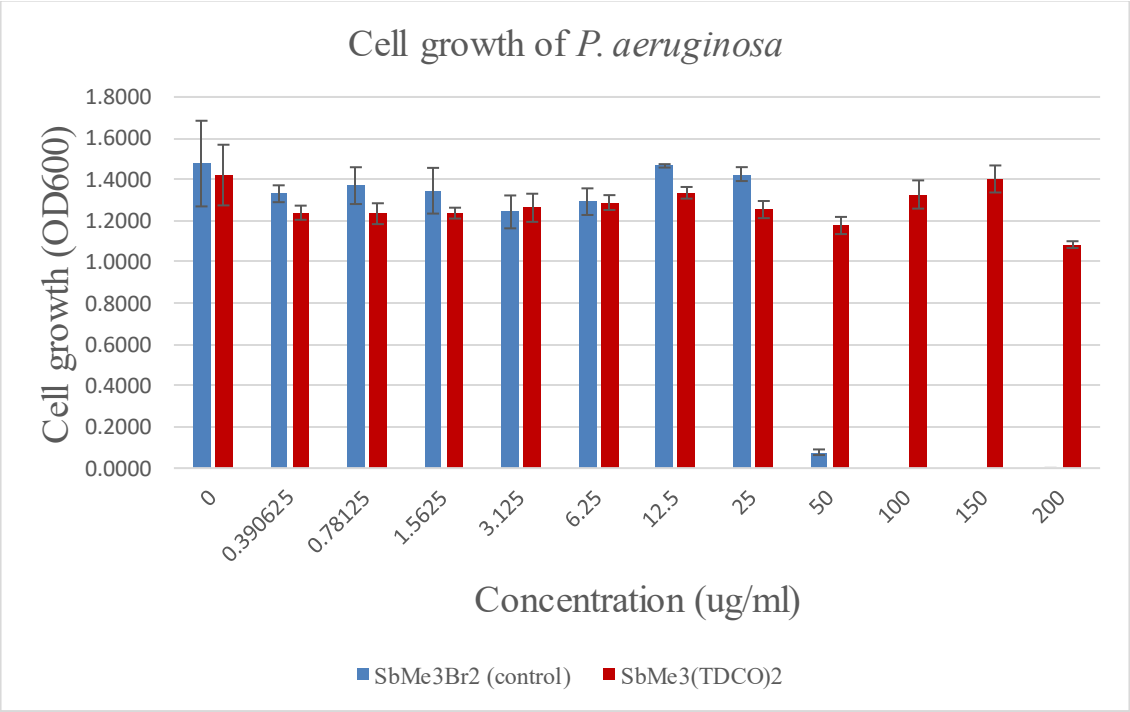

Figure 58. Results of MIC tests of $SbMe_3Br_2$, and $SbMe_3(TDCO)_2$ against *P. aeruginosa*.

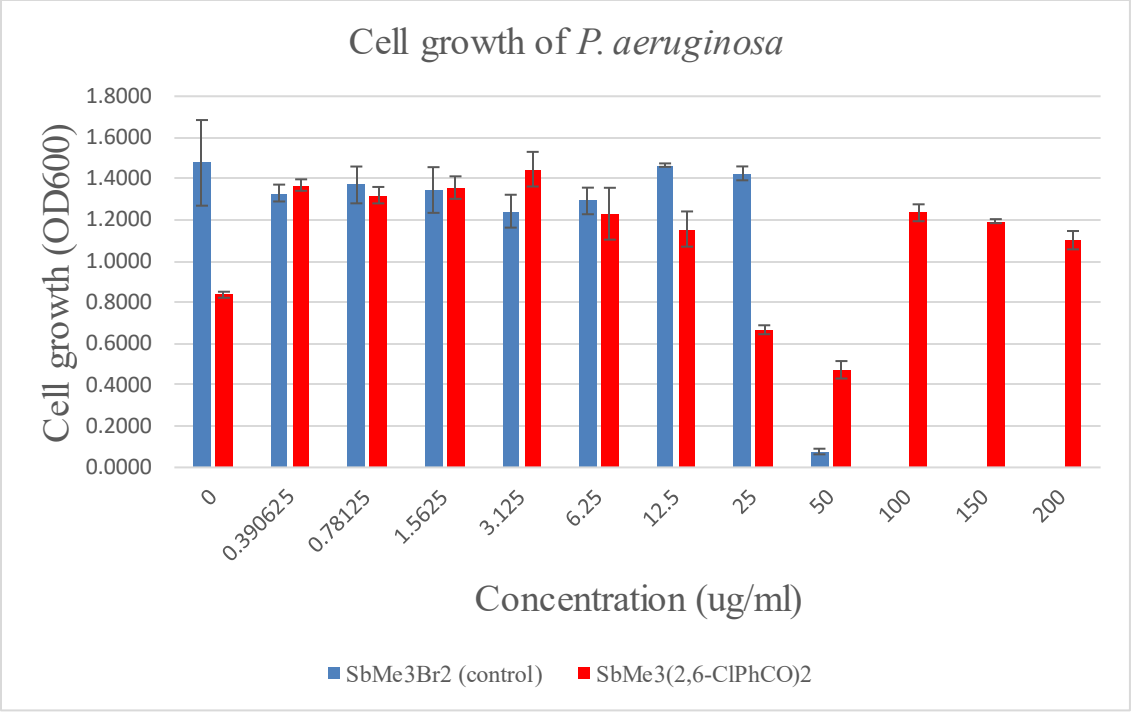

Figure 59. Results of MIC tests of $SbMe_3Br_2$, and $SbMe_3(2,6\text{-diCl-PhCO})_2$ against *P. aeruginosa*.

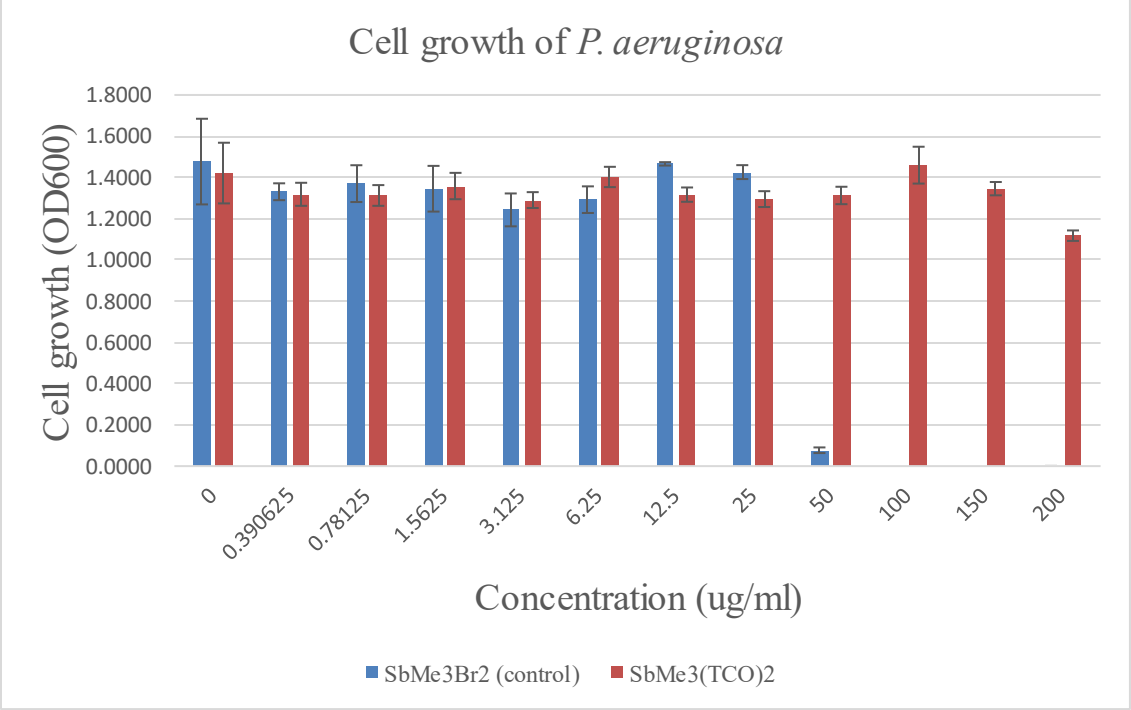

Figure 60. Results of MIC tests of $SbMe_3Br_2$, and $SbMe_3(TCO)_2$ against *P. aeruginosa*.

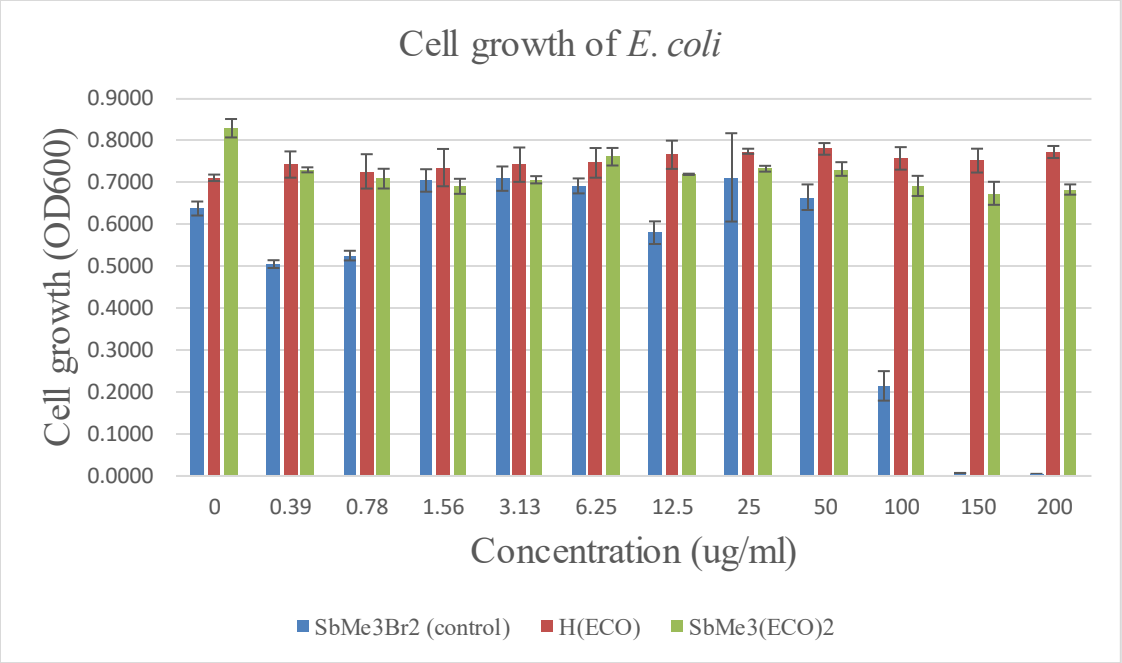

Figure 61. Results of MIC tests of $SbMe_3Br_2$, H(ECO) and $SbMe_3(ECO)_2$ against *E. coli*.

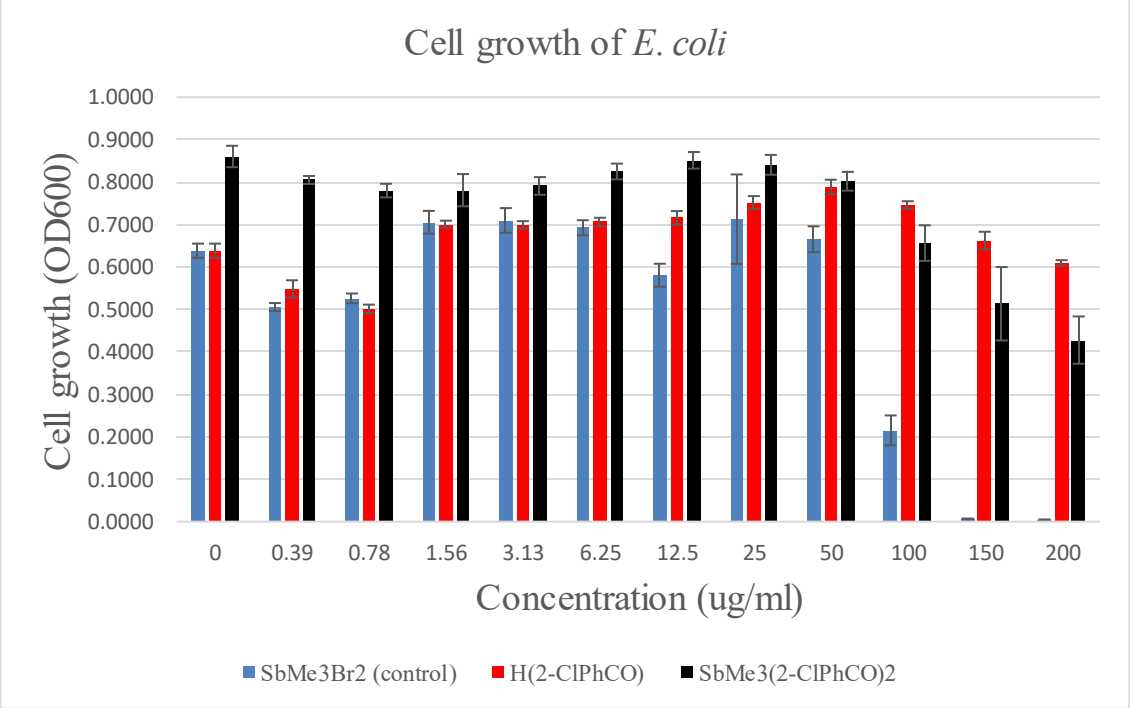

Figure 62. Results of MIC tests of $SbMe_3Br_2$, H(2-ClPhCO) and $SbMe_3(2\text{-}ClPhCO)_2$ against *E. coli*.

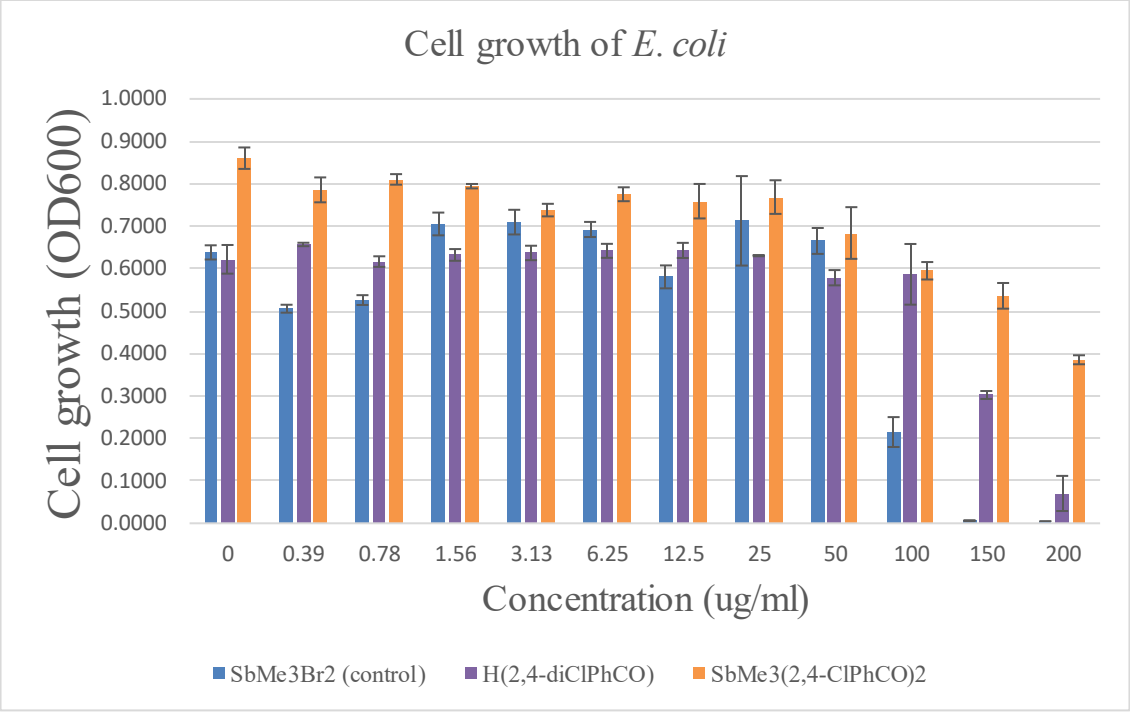

Figure 63. Results of MIC tests of $SbMe_3Br_2$, H(2,4-diCl-PhCO) and $SbMe_3(2,4\text{-diCl-PhCO})_2$ against *E. coli*.

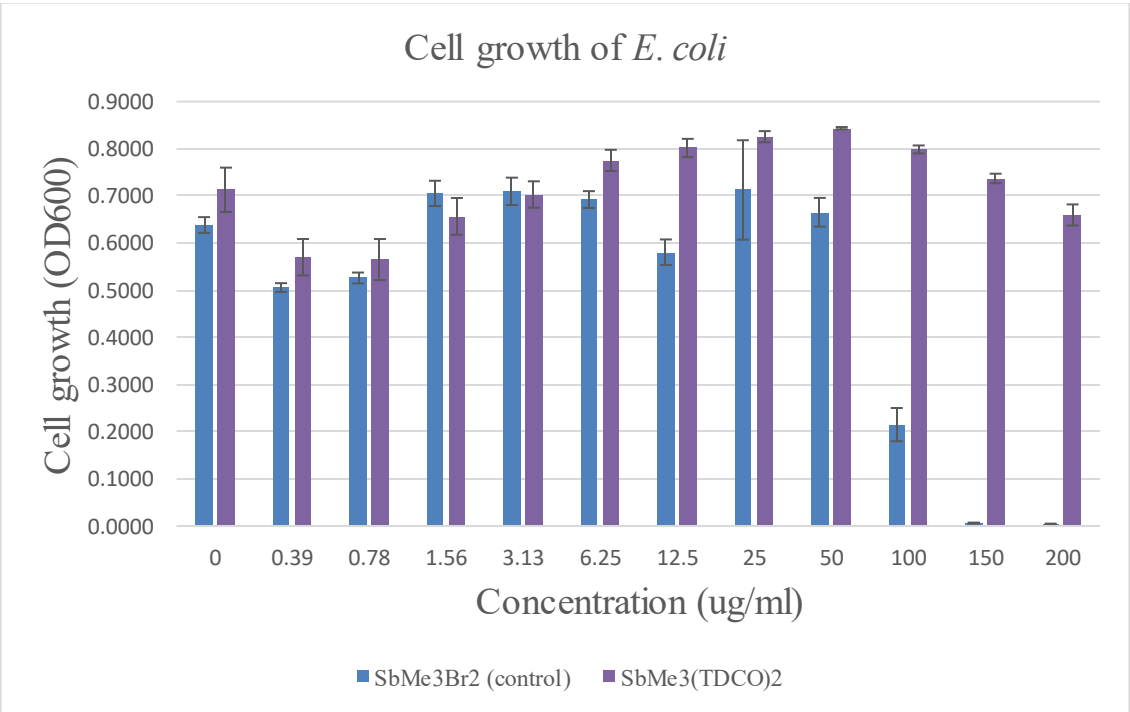

Figure 64. Results of MIC tests of $SbMe_3Br_2$, and $SbMe_3(TDCO)_2$ against *E. coli*.

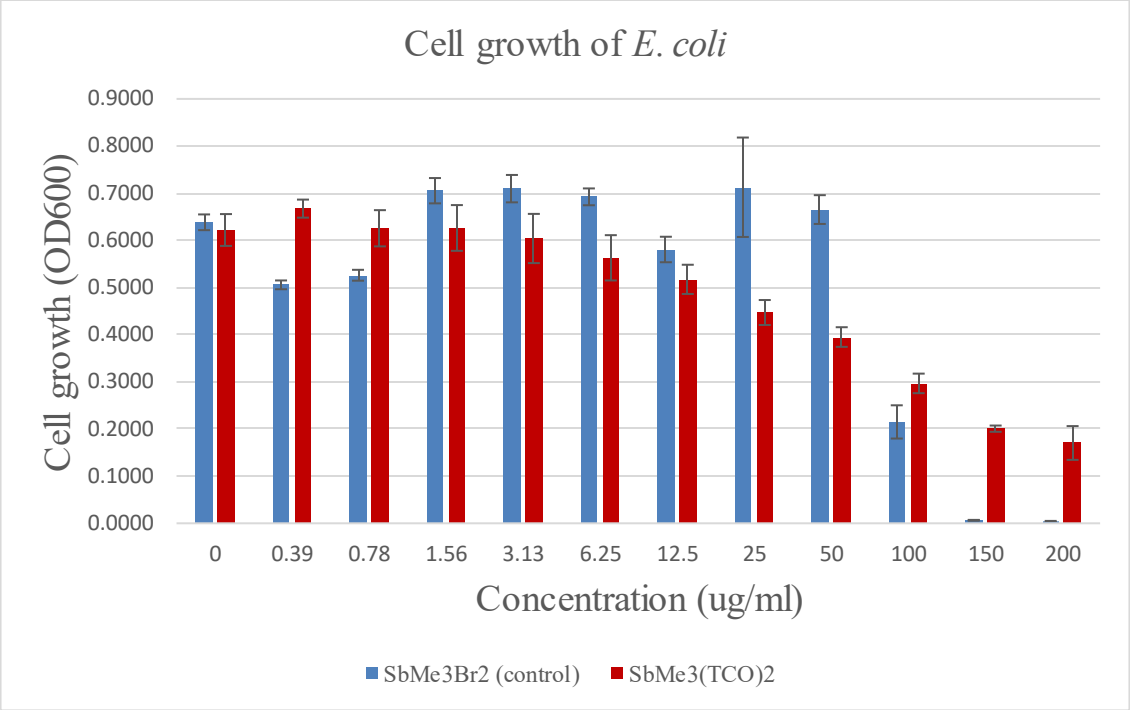

Figure 65. Results of MIC tests of $SbMe_3Br_2$, and $SbMe_3(TCO)_2$ against *E. coli*.

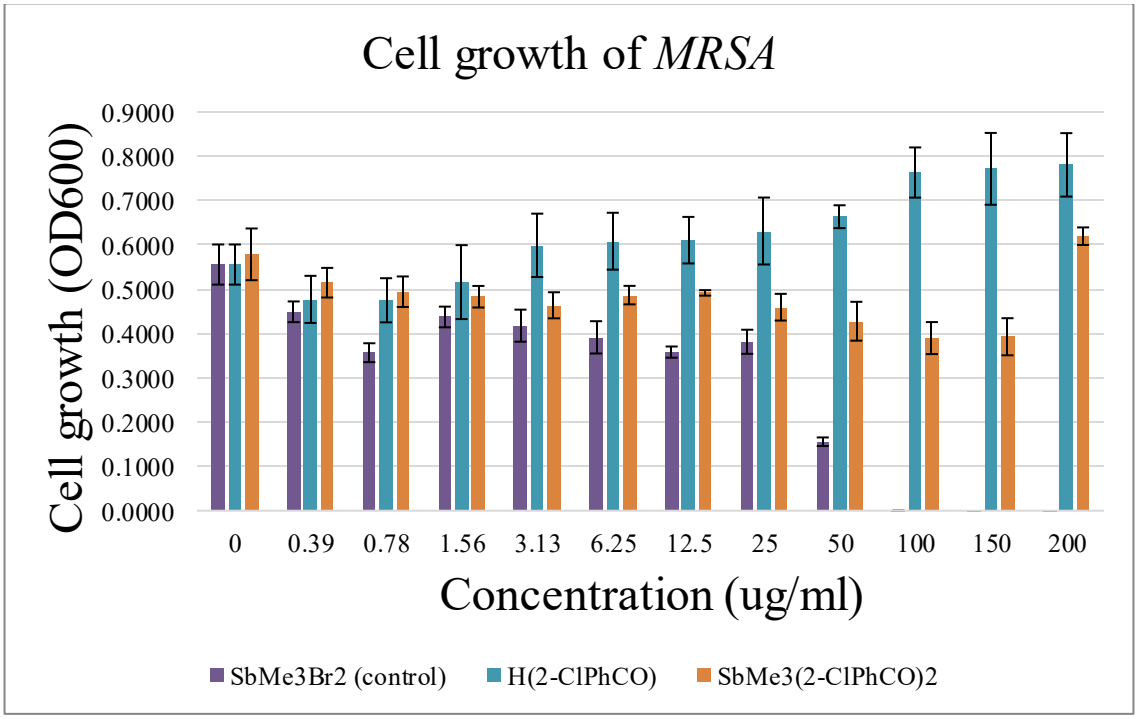

Figure 66. Results of MIC tests of $SbMe_3Br_2$, H(2-ClPhCO) and $SbMe_3(2\text{-}ClPhCO)_2$ against *MRSA*.

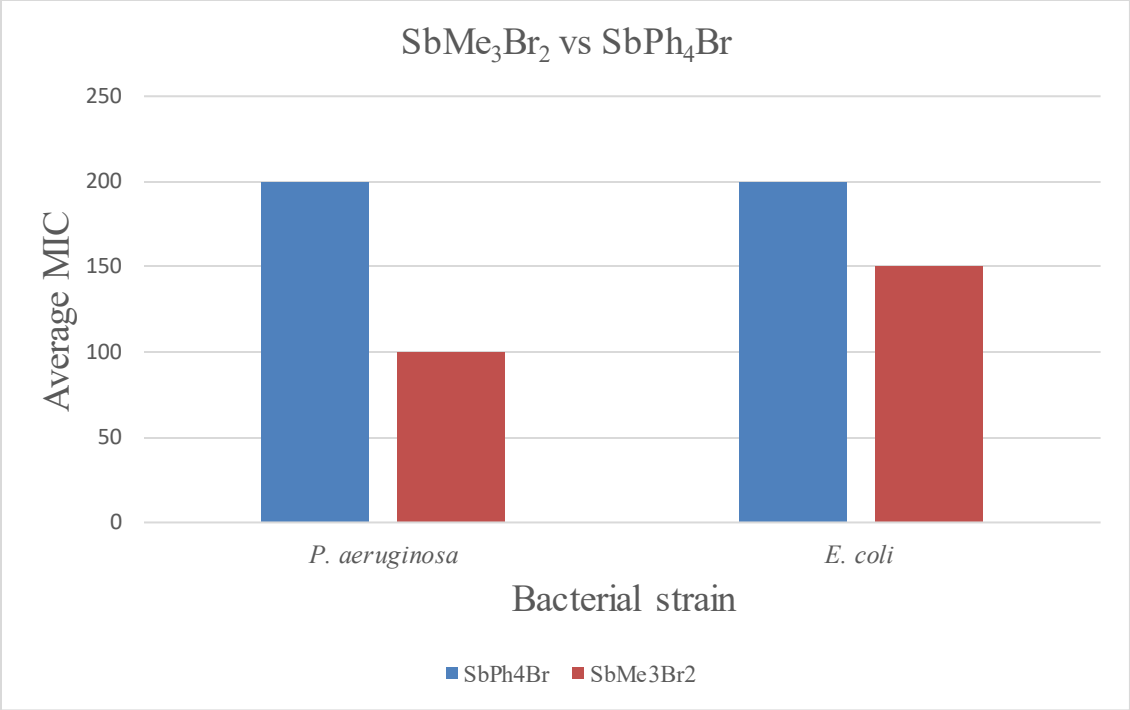

Figure 67. Comparison of the average MIC for both $SbMe_3Br_2$ and $SbPh_4Br$ against *E. coli and P. aeruginosa.*

Table 30. Summary of average MIC (μg/mL) result from biological activity tests.

Organism	**Clinical Significance**	**$SbMe_3Br_2$ (control)**	**MCO**		**ECO**		**TCO**		**TDCO**	
			HMCO	$SbMe_3(MCO)_2$	HECO	$SbMe_3(ECO)_2$	HTCO	$SbMe_3(TCO)_2$	HTDCO	$SbMe_3(TDCO)_2$
P. *aeruginosa* (PAO1)	Lab-adapted strain isolated from burn wound	100	>200	100	>200	>200	N/A	>200	N/A	>200
E. *coli* (S17 (O113:H4))	Avian Pathogenic	150	N/A	N/A	>200	>200	N/A	>200	N/A	>200
S. *aureus* (NRS70)	MRSA	100	N/A	N/A	N/A	N/A	N/A	N/A	N/A	N/A

Table 31 Contd. Summary of average MIC (μg/mL) result from biological activity tests.

Organism	**Clinical Significance**	**$SbMe_3Br_2$ (control)**	**2Cl-PhCO**		**2,4-diCl-PhCO**		**2,6-diCl-PhCO**	
			H(2Cl-PhCO)	$SbMe_3$(2Cl-PhCO)$_2$	H(2,4-diCl-PhCO)	$SbMe_3$(2,4-diCl-PhCO)$_2$	H(2,6-diCl-PhCO)	$SbMe_3$(2,6-diCl-PhCO)$_2$
P. *aeruginosa* (PAO1)	Lab-adapted strain isolated from burn wound	100	>200	>200	>200	>200	N/A	>200
E. *coli* (S17 (O113:H4))	Avian Pathogenic	150	>200	>200	>200	>200	N/A	100
S. *aureus* (NRS70)	MRSA	100	>200	>200	150	N/A	N/A	N/A

VI. CONCLUSION AND SUMMARY

The results and accomplishments made with this research project are summarized and outlined below.

1. A total of 18 compounds were synthesized in this research project: Trimethylantimony dibromide, 4 arylcyanoxime ligands, 4 thallium arylcyanoximates, and 9 methyl-antimony (V) cyanoximates.

2. Other precursors used such as Ag(I) cyanoximates, Tl(TCO) and Tl(TDCO) were previously synthesized by Dr. Gerasimchuk and his research laboratory.

3. These synthesized methyl - antimony (V) cyanoximates and their precursors were characterized using x-ray crystallography, IR, NMR and TG/DSC analysis. Crystal structures were determined for all synthesized compounds.

4. These structural characterizations of the methyl-antimony (V) cyanoximates are the first structural characterizations to be ever done in this field.

5. All the methyl-antimony (V) cyanoximates adopt a distorted trigonal bipyramid conformation around the core antimony metal center.

6. Some peculiarities and rare findings in my research include.

    - A rare case of pure *syn*- diastereomer of H(2,6-diCl-PhCO) being isolated and studied. Previously, mixtures of the two diastereomers was obtained and the pure *anti*- isomer was not characterized.

    - Sulfur- hydrogen bonding present in the structure of the ligand HTDCO to stabilize its crystal structure.

    - Co-crystallized mixture of dominant *syn*-isomer (84%) and minor *anti*- isomer (16%) within the structure of $SbMe_3(TDCO)_2$.

- 50:50 co-crystallized mixture of both *syn*- and *anti*-diastereomers in $SbMe_3(2,4\text{-diCl-PhCO})_2$. This is a new occurrence as there is always a dominant diastereomer within these mixtures like $SbMe_3(TDCO)_2$.

7. 8 of the synthesized methyl - antimony cyanoximates and their corresponding ligands were sent to OSU for biological studies including the trimethylantimony dibromide.

8. Minimum Inhibition Concentration tests were run with the synthesized cyanoximates against three different strains of bacteria: *Pseudomonas aeruginosa* PAO1, *Escherichia coli* S17, and Methicillin- resistant *Staphylococcus aureus* NRS70. The highest concentration tested was 200 μg/mL. The results are as follows.

   - $SbMe_3(MCO)_2$ was significantly effective against PAO1 at concentrations between 25 μg/mL and 50 μg/mL. Complete inhibition observed between 50 μg/mL and 100 μg/mL.

   - $SbMe_3(2,6\text{-diCl-PhCO})_2$ was significantly effective against *E. coli* at concentrations between 25 μg/mL and 50 μg/mL. Complete inhibition observed between 50 μg/mL and 100 μg/mL.

   - The ligand H(2,4-diCl-PhCO) was the only compound effective against MRSA. MRSA cell growth decline was observed at 50 μg/mL and complete inhibition was seen at 150 μg/mL.

9. Further tests must be conducted to be able to compare my results with that of my colleague Kevin Pinks. The initial compound used in my research, $SbMe_3Br_2$ was more effective against all the bacterial strains than $SbPh_4Br$, used by Kevin Pink.

VII. REFERENCES

(1) Aminov, R. I., A brief history of the antibiotic era: lessons learned and challenges for the future. *Front. in microbiol.* **2010,** *1*(134).

(2) Williams, K. J., The introduction of 'chemotherapy using arsphenamine - the first magic bullet. *J. R. Soc. Med*. **2008,** *102*(8), 343-8.

(3) Gould, K., Antibiotics: from prehistory to the present day, *Journal of Antimicrobial Chemotherapy*, **2016,** *71*(3), 572–575.

(4) Saga, T.; Yamaguchi, K., History of antimicrobial agents and resistant bacteria. *Asian Med. J.* **2009**, *52*(2), 103-108.

(5) Parker, N.; Schneegurt, M.; Thi Tu, A.; Lister, P.; Forster, B. M., History of Chemotherapy and Antimicrobial Discovery. In *Microbiology*, OpenStax, **2016**. Ch. 14.1. https://openstax.org/books/microbiology/pages/14-1-history-of-chemotherapy-and-antimicrobial-discovery (accessed March 15,2021).

(6) Parker, N.; Schneegurt, M.; Thi Tu, A.; Lister, P.; Forster, B. M., History of Chemotherapy and Antimicrobial Discovery. In *Microbiology*, OpenStax, **2016**. Ch. 14.2. https://openstax.org/books/microbiology/pages/14-2-fundamentals-of-antimicrobial-chemotherapy#0 (accessed March 15,2021).

(7) Parker, N.; Schneegurt, M.; Thi Tu, A.; Lister, P.; Forster, B. M., History of Chemotherapy and Antimicrobial Discovery. In *Microbiology*, OpenStax, **2016**. Ch. 14.3. https://openstax.org/books/microbiology/pages/14-3-mechanisms-of-antibacterial-drugs (accessed March 15,2021).

(8) CDC., Antibiotic resistance threats in the United States, 2019. U.S. Department of Health and Human Services, CDC. **2019**.

(9) World Health Organization., Antimicrobial resistance. https://www.who.int/news-room/fact-sheets/detail/antibiotic-resistance (accessed March 15, **2020**)

(10) Aslam, B.; Wang, W.; Arshad, M. I.; Khurshid, M.; Muzammil, S.; Rasool, M. H.; Nisar, M. A.; Alvi, R. F.; Aslam, M. A.; Qamar, M. U.; Salamat, M.; Baloch, Z., Antibiotic resistance: a rundown of a global crisis. *Infect. Drug Resist.* **2018,** *11*, 1645–1658.

(11) Ventola C. L., The antibiotic resistance crisis: part 1: causes and threats. *P & T: a peer-reviewed journal for formulary management,* **2015**, *40*(4), 277–283.

(12) Holmes R.K; Jobling M.G., Genetics. In: *Medical Microbiology*. 4th ed.; Baron S., Eds.; University of Texas Medical Branch: Galveston, TX, **1996**; Ch.5. https://www.ncbi.nlm.nih.gov/books/NBK7908/ (accessed March 15,2021).

(13) Parker, N.; Schneegurt, M.; Thi Tu, A.; Lister, P.; Forster, B. M., History of Chemotherapy and Antimicrobial Discovery. In *Microbiology*, OpenStax, **2016**; Ch.14.5. https://openstax.org/books/microbiology/pages/14-5-drug-resistance#0 (accessed March 15,2021).

(14) Reygaert W. C., An overview of the antimicrobial resistance mechanisms of bacteria. *AIMS microbiol.* **2018,** *4*(3), 482–501.

(15) Boucher H, W.; Talbot G.H.; Bradley J.S.; Edwards J.E.; Gilbert D.; Rice L.; Scheld M.; Spellberg B.; Bartlett J., Bad Bugs, No Drugs: No ESKAPE! An Update from the Infectious Diseases Society of America. *Clin. Infect. Dis.* **2009,** *48*(1), 1–12.

(16) Sim, W.; Barnard, R. T.; Blaskovich, M.; Ziora, Z. M., Antimicrobial Silver in Medicinal and Consumer Applications: A Patent Review of the Past Decade (2007–2017). *Antibiotics* **2018,** *7*(4), 93.

(17) Ahonkhai, I.; Pugh, W. J.; Russell, A. D., Sensitivity to antimicrobial agents of some mercury-sensitive and mercury-resistant strains of Gram-negative bacteria. *Curr. Microbiol.* **1984,** *11*, 183–185.

(18) Muhammad M.; Muhammad A. S.; Masood S.; Sidra N.; Tayyaba A.; Muhammad N. T.; Hafza M. J.; Muhammad S.; Saeed A., Crystal structure and antimicrobial properties of tetrakis(imidazole)copper (II) triiodide, [Cu(imidazole)$_4$] (I_3)$_2$, *Inorg. Nano-Met. Chem*. **2017,** *47*(1), 37-40.

(19) Jiao, L.; Lin, F.; Cao, S.; Wang, C.; Wu, H.; Shu, M., Preparation, characterization, antimicrobial and cytotoxicity studies of copper/zinc- loaded montmorillonite. *J. Anim. Sci. Biotechnol.* **2017,** *8*, 27.

(20) Veenstra D. L.; Saint S.; Saha S. ; Lumley, T. ; Sullivan, S. D., Efficacy of antiseptic-impregnated central venous catheters in preventing catheter-related bloodstream infection: a meta-analysis. In: *Database of Abstracts of Reviews of Effects (DARE): Quality-assessed Reviews* [Internet]; Centre for Reviews and Dissemination: York, UK, **1995**. https://www.ncbi.nlm.nih.gov/books/NBK67835/ (accessed March 16, 2021)

(21) Saint S.; Elmore J. G.; Sullivan S. D.; Emerson S. S.; Koepsell T. D., The efficacy of silver alloy-coated urinary catheters in preventing urinary tract infection: a meta-analysis. *Am J Med.* **1998,** *105*(3), 236-41.

(22) Rupp, M. E.; Lisco, S. J.; Lipsett, P. A.; Perl, T. M.; Keating, K.; Civetta, J. M.; Mermel, L. A.; Lee, D.; Dellinger, E. P.; Donahoe, M.; Giles, D.; Pfaller, M. A.; Maki, D. G.; Sherertz, R., Effect of a second-generation venous catheter impregnated with chlorhexidine and silver sulfadiazine on central catheter-related infections: a randomized, controlled trial. *Ann. Intern. Med.* **2005,** *143*(8), 570–580.

(23) USA. Department of Health and Human Services., Toxicological profile for Antimony and compounds, 2019. https://www.atsdr.cdc.gov/toxprofiles/tp23.pdf. Toxicology profile antimony .2019.

(24) Freedman L, D.; Doak G. O.; Long G. G.; Mahmood, T.; Lindhal, C. B., Antimony compounds. In: *Kirk-Othmer Encyclopedia of Chemical Technology*[Online], 3rd Ed.; John Wiley and Sons, Inc: New York, NY, **2003,** 105-128.

(25) Ugal, J. R.; Mohammad, I. F.; Ali, K. Z., Synthesis and Evaluation of Biological Activity of New Antimony Compounds with Methotrexate and Benzothiazole. *Int. J. Chemtech Res*. **2017**, *10*(6), 805–814.

(26) Carmalt, C. J.; Norman, C. N., Arsenic, Antimony and Bismuth: Some General Properties and Aspects of Periodicity. In *Chem. of Arsenic, Antimony and Bismuth* [Online], Norman, N. C, Ed; Springer Science & Business Media: London, UK. **1998**. 1-41. https://books.google.com/books?hl=en&lr=&id=vVhpurkfeN4C&oi=fnd&pg=PR9&dq=antimony&ots=sJkq9zvpUo&sig=fU_IEeLzzCvhdw4qi-1bNuCsqGk#v=onepage&q=antimony&f=false

(27) Domasevitch, K. V.; Gerasimchuk, N. N.; Mokhir, A., Organoantimony(V) Cyanoximates: Synthesis, Spectra and Crystal Structures. *Inorg. Chem.* **2000**, *39*(6), 1227-1237.

(28) Yin, H.; Wen, L.; Cui, J.; Li, W., Synthesis, Characterizations and Crystal Structures if New Organoantimony (V) Complexes with carious Isomers of Fluoromethylbenzoate Ligands. *Polyhedron*. **2009**, *28*, 2919-2926.

(29) Haldar, A. K.; Sen. P.; Roy. S., Use of Antimony in the Treatment of Leishmaniasis: Current status and Future Directions. *Mol. Bio. Int.* **2011**, 1-24.

(30) Thomas Jefferson National Accelerator Facility - Office of Science Education., It's Elemental - The Periodic Table of Elements, **2019**. (accessed Nov 2, 2019)

(31) Goodwin, L.G., Pentostam (sodium stibogluconate); a 50- year personal reminiscence. *Trans. R. Soc. Trop. Med. Hyg.* **1995**, *89*, 339-341.

(32) Frézard, F.; Demicheli, C.; Ferreira, C. S.; Costa, M.A.P., Glutathione-induced conversion of pentavalent antimony to trivalent antimony in meglumine antimoniate. *Antimicrob. Agents Chemother.* **2001**, 45, 913-916.

(33) Singh, R. V.; Mahajan, K.; Swami, M.; Dawara, L., Microwave Assisted Synthesis, Spectroscopic Characterizations In-Vitro Antibacterial and Antifungal Properties Of Some Antimony and Bismuth Complexes Derived From Nno and NnS Donor Imines. *Int. J. Pharm. Sci. Res.* **2010**, *33,* 141-156.

(34) Sharma, P.K.; Rehwani, H.; Rai, A.K.; Gupta, R.S.; Singh, Y.P., Antispermatogenic Activity of the Benzothiazoline Ligand and Corresponding Organoantimony(V) Derivative in Male Albino Rats. Bioinorganic Chemistry & its Applications. **2006**, *2006*(3), 1-6.

(35) Oliveira, L. G. D.; Silva, M. M.; Paula, F. C. S. D.; Pereira-Maia, E. C.; Donnici, C. L.; Simone, C. A. D.; Frézard, F.; Júnior, E. N. D. S.; Demicheli, C., Antimony(V) and Bismuth(V) Complexes of Lapachol: Synthesis, Crystal Structure and Cytotoxic Activity. *Molecules.* **2011**, *16*(12), 10314-10323.

(36) Gasser, G.; Ott, I.; Metzler-Nolte, Nils., Organometallic Anticancer Compounds. *J. Med. Chem*. **2011**, *54*(1), 3-25.

(37) Khan, N. U. H.; Sultana, K.; Nadeem. H., Synthesis, Characterization and Antibacterial Activity of New Antimony (III) Complexes of Some Tosyl-Sulfonamide Derivatives. *Middle East J. Sci. Res.* **2013**, *17*(6), 705-711.

(38) Agrawal, R.; Sharma, J.; Nandani, D.; Batra, A.; Singh, Y., Triphenylarsenic(V) and antimony(V) derivatives of multidentate Schiff bases: Synthesis, characterization, and antimicrobial activities. *J. Coord. Chem*. **2011**, *64*(3), 554-563.

(39) Silvestru, C.; Silaghi-Dumitrescu, L.; Haiduc, I.; Begley, M. J.; Nunn, M.; Sowerby, D. B., Synthesis of diphenylantimony (III) dialkyldithio- and diaryldithio-phosphinates and arsinates; Crystal structures of $Ph_2SbS_2MPh_2$ (M = P or As). *J. Chem. Soc. Dalton Trans*. **1986,** *1986*(5), 1031-1034.

(40) Silvestru, C.; Curtui, M.; Haiduc, I.; Begley, M. J.; Sowerby, D. B., Phenylantimony (III) diorganophosphorodithioates: the crystal structure of diphenylantimony (III) di-isopropyl phosphorodithioate, Ph2SbS2P(OiPr)2; unsusual polymerization through semibonding. *J. Organomet. Chem*. **1992**, *426*(1), 49-58.

(41) Silvestru, C.; Haiduc, I.; Tiekink, E.; De Vos, D.; Biesemans, M.; Willem, P.; Gielen, M., Synthesis, structural characterization, and in vitro antitumor properties of triorganoantimony(V) disalicylates: Crystal and molecular structures of $[5\text{-}Y\text{-}2\text{-}(ho)\text{-}C_6H_3COO]_2SbMe_3$ (Y=H, Me, MeO*). Appl. Organomet. Chem.* **1995**, *9*(7), 597-607.

(42) Ulrich, N., An Essay on Antimony. *Chem. Eng. News*. **2003,** *97*(31) 42-43.

(43) Shaked-Mishan, P.; Ulrich, N.; Ephros, M.; Zilberstein, D., Novel intracellular SbV reducing activity correlates with antimony susceptibility in Leishmania donovani. *J. Biol. Chem*. **2001**, *276*(6), 3971-3976.

(44) Lopez S.; Aguilar L.; Mercado L.; Bravo, M.; Quiroz, W., Sb(V) reactivity with human blood components: Redox effects. *PLoS One*, **2015,** *10*(1).

(45) Vasquez L.; Dagert J. V. S.; Scorza J.V.; et al., Pharmacokinetics of experimental pentavalent antimony after intramuscular administration in adult volunteers. *Curr. Ther. Res.* **2006,** *67*(3), 193-203.

(46) Friedrich K.; Vieira F. A.; Porrozzi R.; et al., Disposition of antimony in rhesus monkeys infected with Leishmania braziliensis and treated with meglumine antimoniate. *J. Toxicol. Environ. Health.* **2012,** *75*(2), 63-75.

(47) Neves D. B.; Caldas E. D.; Sampaio R. N., Antimony in plasma and skin of patients with cutaneous leishmaniasis--relationship with side effects after treatment with meglumine antimoniate. *Trop. Med. Int. Health* **2009***, 14*(12), 1515-1522.

(48) Lawn S, D.; Armstrong M.; Chilton D, et al., Electrocardiographic and biochemical adverse effects of sodium stibogluconate during treatment of cutaneous and mucosal leishmaniasis among returned travelers. *Trans. R. Soc. Trop. Med. Hyg.* **2006,** *100*(3), 264-269.

(49) Andersen E, M.; Cruz-Saldarriaga M.; Llanos-Cuentas A.; et al., Comparison of meglumine antimoniate and pentamidine for Peruvian cutaneous leishmaniasis. *Am. J. Trop. Med. Hyg.* **2005,** *72*(2):133- 137.

(50) Kaufmann, G. B.; Halpern, J., Coordination compound. *Encyc. Brit.* [Online]. **2018**. https://www.britannica.com/science/coordination-compound/History-of-coordination-compounds (accessed Nov 2, 2019).

(51) The Editors of Encyclopedia Britannica.; Chelate. *Encycl. Brit.* [Online]. **2007**. https://www.britannica.com/science/chelate (accessed Nov 2, 2019).

(52) Robinson, W. R.; Langley, R.; Theopold, K., Chemistry: Coordination Chemistry of Transition Metals [Online]. OpenStax Chem. **2012**. Ch. 19.2. https://opentextbc.ca/chemistry/chapter/19-2-coordination-chemistry-of-transition-metals/ (accessed Nov 3, 2019).

(53) Madhu., Difference between Bidentate and Ambidentate Ligands. [Online] https://www.differencebetween.com/difference-between-bidentate-and-vs-ambidentate-ligands/ (accessed Nov 1, 2019).

(54) Shakhashiri, B. Z.; Chelates and Chlorophyll [Online]. http://www.scifun.org/CHEMWEEK/ChelatesChlorophyll2017.pdf (accessed Nov 2, 2019)

(55) Gerasimchuk, N. N., Chemistry and Applications of Cyanoximes and their Metal Complexes. *Dal. Trans*. **2019**, *48*(23), 7985-8013.

(56) Ilkun. O. T.; Archibald, S. J.; Barnes, C. L.; Gerasimchuk, N. N.; Biagioni, R.; Silchenko, S.; Gerasimchuk, O.A.; Nemykin, V. N., Benz(2-heteroaryl) cyanoximes and their TI(I) complexes: New Room Temperature Blue Emitters. *Dalton Trans*. **2008**, (42), 5715-5729.

(57) Robertson, D. R.; Cannon, J. F.; Gerasimchuk, N. N., Double-Stranded Metal-Organic Networks for One dimensional Mixed Valence Coordination Polymers. *Inorg. Chem*. **2005**, *44*(23), 8326–8342.

(58) Gerasimchuk, N. N.; Kuzmann, E.; Buki, A.; Vertes, A.; Nagy, L.; Burger, K., Synthesis, IR-, Mossbauer studies of Eu (III) complexes formed with cyanoxime anions. *Inorg. Chim. Acta*. **1991**, *188*(1), 45-50.

(59) Goeden, L. J., *The Synthesis, Characterization, and Biological Activity Studies of Pt (II) and Pd (II) Disubstituted Arylcyanoximates*. M.S. Thesis, Missouri State University (USA), **2005**.

(60) Pinks, K. A., *Synthesis, Characterization, and Biological Studies of Novel Organoantimony (V) Cyanoximates.* M.S. Thesis, Missouri State University (USA), **2020.**

(61) Davidson, S. H., 2-Cyano-2-hydroximinoacetamides as plant disease control agents. Patent of the USA #3957847, **1978**. (b) Skopenko, V. V.; Palii, G. K.; Gerasimchuk, N. N.; Makats, E. F.; Domashevskaya, O. A.; Rakovskaya, R. V., Nitrosothiocarbamylcyanmethanid of potassium or sodium which show antimicrobial activity. Patent of the USSR #1405281, **1988**. (c) Palii, G. K.; Skopenko, V. V.; Gerasimchuk, N. N.; Makats, E. F.; Domashevskaya, O. A.; Rakovskaya, R. V., Bis-(Nitrosothiocarbamylcyanmethanid) copper (II) or nickel (II) which exhibit antimicrobial activity. Patent of the USSR, #1405282, **1988**.

(62) Skopenko, V. V.; Palii, G. K.; Gerasimchuk, N. N.; Domashevskaya, O. A.; Makats, E. F., Di (Nitrosothiocarbamylcyanmethanid)-di-(pyridine)-copper which shows bacteriostatic activity towards *Staphylococcus Aureus*, and method of preparation of the complex. Patent of the USSR, #1487422, **1989**.

(63) Lin, K., Process for making 2-cyano-2-hydroximinoacetamide salts. Patent of the USA #3919284, **1976**. (b) Kuhne, A.; Hubele, A. Method for the cultivation of plants employing R-cyanohydroximinoacetamide derivatives. Patent of the USA #4063921, **1978.**

(64) Ciba Geigy A.G., Srodek ochrony Roslin przed dzialaniem agresywnych chemikalii rolniczych. Patent of Poland #127786, **1985**. (b) Ciba Geigy AG. Mittel zum Schutz von Kulturpflanzen von agressiven Herbiziden. Patent of Austria #367268, **1982.**

(65) Eddings, D.; Barnes, C.; Gerasimchuk, N. N.; Durham, P.; Domasevich, K., First Bivalent Palladium and Platinum Cyanoximates: Synthesis, Characterization, and Biological Activity. *Inorg. Chem*. **2004**. *43*(13), 3894-3909.

(66) Gerasimchuk, N.; Maher, T.; Durham, P.; Domasevitch, K.; Wilking, J.; Mokhir, A., Tin (IV) Cyanoximates: Synthesis, Characterization and Cytotoxicity. *Inorg. Chem*. **2007**, *46*(18), 7268–7284.

(67) Gerasimchuk, N.; Goeden, L.; Durham, P.; Barnes, C. L.; Cannon, J. F.; Silchenko, S.; Hidalgo, I., Synthesis and Characterization of disubstituted arylcyanoximes and their several metal complexes. *Inorg. Chim. Acta* **2008**, *361*(7), 1983-2001.

(68) Life Science Staff., Facts about Antimony. **2013**. https://www.livescience.com/37390-antimony.html (accessed Nov 3, 2019)

(69) Reglinski, J., Environmental and Medicinal Chemistry of Arsenic, Antimony and Bismuth. In Chem. of Arsenic, Antimony and Bismuth [Online], Norman, N. C, Ed. Springer Science & Business Media: London, UK. **1998**. 403. https://books.google.com/books?hl=en&lr=&id=vVhpurkfeN4C&oi=fnd&pg=PR9&dq=antimony&ots=sJkq9zvpUo&sig=fU_IEeLzzCvhdw4qi-1bNuCsqGk#v=onepage&q=antimony&f=false

(70) Frézard, F.; Demicheli, C.; Ribeiro, R. R., Pentavalent antimonials: new perspectives for old drugs. *Molecules*, **2009,** *14*(7), 2317–2336. https://doi.org/10.3390/molecules14072317

(71) Riddles, C. N.; Whited, M.; Lotlikar, S. R.; Still, K.; Patrauchan, M.; Silchenko, S.; Gerasimchuk, N., Synthesis and Characterization of Two Cyanoxime Ligands, Their Precursors, and Light Insensitive Antimicrobial Silver(I) Cyanoximates. *Inorg. Chim. Acta* **2014**, *412*, 94–103.

(72) Centers for Disease Control and Prevention., Methicillin-resistant Staphylococcus aureus (MRSA). **2019** https://www.cdc.gov/mrsa/healthcare/index.html (accessed Nov 30, 2019).

(73) Palii, G. K.; Skopenko, V. V.; Gerasimchuk, N. N.; Domashevskaya, O. A.; Makats, E. F.; Rakovskaya, R. V., Patent of the USSR #1405281, **1988**.

(74) Gerasimchuk, N.; Gamian, A.; Glover G.; Szponar B., Light Insensitive Silver(I) Cyanoximates as Antimicrobial Agents for Indwelling Medical Devices, *Inorg. Chem*. **2010**, *49*(21), 9863-9874.

(75) Halford, B., An emerging antiviral takes aim at COVID-19. *Chem. Eng. News*, **2020**, 22-23.

(76) Marcano, D., *Pyridylcyanoximes and Their Metal Complexes* M.S. Thesis, Missouri State University (USA), **2007**.

(77) Morton, J.; Dennison, R.; Nemykin, V.; Gerasimchuk, N., Planochromism of cyanoxime anions: Computational and mechanistic studies in solid state and solutions. *Inorg. Chim. Acta*. **2020**, 507.

(78) Doak, G. O.; Long, G. G.; Key, M. E.; Bush, W. D.; Allred, A. L., Trimethylantimony Dihalides. *Inorg. Syntheses* **2009**, *9*, 92-97.

(79) Urgut, O. S.; Ozturk, I. I.; Banti, C. N.; Kourkoumelis, N.; Manoli, M.; Tasiopoulos, A. J.; Hadjikakou, S. K., Addition of Tetraethylthiuram Disulfide to Antimony (III) Iodide; Synthesis, Characterization and Biological Activity. *Inorg. Chim. Acta.* **2016**, *443*, 141-150.

(80) Gerasimchuk, N. N., Missouri State University (USA). Personal communication, **2020**.

(81) Hilton, M., Gerasimchuk, N., Silchenko, S. et al., Synthesis, Properties and Crystal Structure of the 2,4-Dichlorophenyl-cyanoxime: A Powerful Carbonyl Reductase Inhibitor. *J. Chem. Crystallogr.* **2013**. *43*, 157–164 https://doi.org/10.1007/s10870-013-0401-6

(82) Morton, J., *Further investigations of silver (1) cyanoximates.* M.S Thesis, Missouri State University (USA), **2010**.

(83) Robertson, D., Barnes, C., Gerasimchuk, N., Synthesis of the Monosubstituted Arylcyanoximes and its Na, Tl(I) and Ag(I) Compounds. *J. Coord. Chem*. **2004**, *57* (14), 1205-1216.

(84) SHELXTL, Crystallographic Software Package, version 5.1.

(85) Sheldrick, G. M., **2002**. TWINABS. Bruker-AXS, Madison, Wisconsin, USA.

(86) Burnett, M.N., & Johnson, C.K., **1996**. OR TEP-III: Oak Ridge Thermal Ellipsoid Plot Program for Crystal Structure Illustration, Oak Ridge National Laboratory Report ORNL 6895.

(87) Macrae, C.F, Edginton, P.R., McCabe, P., Pidcock, E., van de Streek, J, Bruno, I.J., Taylor, R., Chisholm, J.A., & Wood, P.A., **2008**. Mercury CSD 2.0 - New Features for the Visualization and Investigation of Crystal Structures. *J. Appl. Crystallogr. 41*, 466 – 470.

(88) Robertson, D., *Thallium(I) Coordination Polymers based on Monosubstituted Arylcyanoximes.* M.S. Thesis, Missouri State University (USA), **2006**.

(89) Gerasimchuk, N.; Guzei, I.; Sipos, P., Structural Peculiarities of Cyanoximes and their Anions: Co-crystallization of Two Diastereomers and Formation of Acid-salts. *Curr. Inorg. Chem*., **2015**, *5* (1), 38-63.

(90) Charlier, H.; Gerasimchuk, N., Cyanoxime Inhibitors of Carbonyl Reductase and methods of Using Said Inhibitors in Treatments Involving Anthracyclines. USA patent # 7,727,967 B2, **2010**.

(91) Domashevskaya, O.A.; Mazus, M.D.; Gerasimchuk, N.N.; Dvorkin, A.A.; Simonov, Y. A., Crystal and molecular structure of Cesium and Rubidium nitrosocarbamoyl-cyan methanides. Russ. *J. Inorg. Chem*. **1989**, *34* (7), 1656-1660.

(92) Emery Pharma., Minimum Inhibitory Concentration (MIC). https://emerypharma.com/biology/minimum-inhibitory-concentration/ (accessed September 2021).

(93) Domasevitch, K. V.; Skopenko, V. V.; Gerasimchuk. N. N., 2-Nitroso-2-cyan-N, N dimethylacetamide-ion: $ONC(CN)C(O)N(CH_3)_2^-$ - a new non-planar methanide-type acidoligand. *Doklady Akademii Nauk Ukrainskoi RSR*. **1989**, *part B* (5), 26-31.

(94) Gerasimchuk, N. N.; Domasevitch, K. V.; Kapshuk, A. A.; Tchernega. A. N., Coordination compounds of N, N-dimethylthioamidocyanoxime. *Russ. J. Inorg. Chem*. **1993**, *38* (11), 1718-1722.

(95) Domasevich, K. V.; Gerasimchuk, N. N.; Rusanov, E. B.; Gerasimchuk. O. A., Synthesis and crystal structures of 2-quinolyl- and 2-benzthiazolylcyanoximates of Cesium. *Russ. J. Gen. Chem*. **1996**, *66* (4), 635-640.

(96) Domashevskaya, O. A.; Mazus, M. D.; Dvorkin, A. A.; Simonov, Yu. A.; Gerasimchuk. N. N., Structure of potassium salt of $ONC(CN)C(O)NH_2^-$ ion. *Russ. J. Inorg. Chem*. **1988**, *33* (12), 3026-3030.

(97) Alavijeh, M. S.; Chishty, M.; Qaiser, M. Z.; Palmer, A. M., Drug metabolism and pharmacokinetics, the blood-brain barrier, and central nervous system drug discovery. *NeuroTherapeutics*. **2005,** *2* (4), 554–571. https://doi.org/10.1602/neurorx.2.4.554

(98) Long, G. G.; Doak, G. O.; Freedman, L. D., The Infrared Spectra of Some Alkyl-Substituted Pentavalent Antimony Compounds. *J. Amer. Chem. Soc.* **1964,** *86*, 209-213.